

Regulation and Mutation of Voltage-Gated Sodium Channel *SCN8A* (Na_v1.6)

by

Janelle Elizabeth O'Brien

A dissertation submitted in partial fulfillment
of the requirements for the degree of
Doctor of Philosophy
(Human Genetics)
in the University of Michigan
2013

Doctoral Committee:

Professor Miriam H. Meisler, Chair
Assistant Professor Anthony Antonellis
Professor Sally A. Camper
Assistant Professor Raymond C. Chan
Professor Lori L. Isom

“If I have seen further, it is by standing on the shoulders of giants.”

Sir Isaac Newton

© Janelle Elizabeth O'Brien

2013

To my parents,
for their love, support, and genetic material.

Acknowledgements

Many people have contributed to this work and my success in graduate school. First and foremost, I'd like to thank my advisor, Dr. Miriam Meisler, for her extensive advice and support, for demonstrating that mediocrity is unacceptable when one is capable of excellence, and for reminding me that "the" is often (but not always) a superfluous word. Miriam has served as an amazing role model for the rest of my scientific career, and her perfectionism has made me a better scientist and communicator.

Thanks to my thesis committee, Ray Chan, Sally Camper, Lori Isom, and Tony Antonellis, for all their input, wisdom, and guidance. I would also like to acknowledge my collaborators at the University of Michigan and beyond: Lori Isom and her lab, specifically Luis Lopez-Santiago, Lauren Gehman and Doug Black at UCLA, Ben Barres and Jason Dugas at Stanford, Sulayman Dib-Hajj and Stephen Waxman at Yale, Vikram Shattokai at U of M, and Krishna Veeramah and Michael Hammer at the University of Arizona.

Many thanks to all my colleagues in the Meisler Lab for their social and technical support, and for putting up with my shenanigans: Dr. Guy Lenk, my partner in copious coffee consumption and experimental pessimism, Christina Vallianatos, an essential domain in Team VGNa and inspiration for many a lab rage comic (double acknowledgement!), and Christen Frei, for taking over my role as cloner of

all things sodium channel. Thanks to Julie Jones for her extensive assistance- whether it be with finding that obscure reagent no one had used since 1987, knowing exactly who ran what experiment and where the results can be found, mulling over sodium channel hypotheses, or nicely pointing out (for the hundredth time) that, actually, we get that specific reagent from the core.

I'd also like to thank previous lab members Dr. Cole Ferguson, Dr. Lisa Sharkey, Adrienne Grant, Julie Blossom, and the Antonellis lab for their intellectual and technical input.

I'd like to thank my friends for their support, for keeping me sane, and for forcing me to get out of the basement and be social every once in a while. Last, but certainly not least, I'd like to thank my family-Mom, Dad, Steven, Molly, and Monica- for their constant support and encouragement. Thank you for encouraging me to do what I love to do... or at least not making fun of me for doing it.

Table of Contents

Dedication	ii
Acknowledgements	iii
List of Figures	vi
List of Tables	viii
Abstract	ix
Chapter I: A Resurgence in Channel Activity	1
Chapter II: Rbfox proteins regulate alternative splicing of neuronal sodium channel SCN8A	33
Chapter III: Interaction of voltage-gated sodium channel Na_v1.6 (SCN8A) with microtubule-associated protein Map1b	56
Chapter IV: <i>De novo</i> pathogenic mutation of SCN8A identified by whole genome sequencing of a family quartet with infantile epileptic encephalopathy and SUDEP	84
Chapter V: Generation of Na_v1.6 cDNA constructs for electrophysiology and intracellular trafficking experiments	106
Chapter VI: Conclusions	122
References	137

List of Figures

1.1	Structure of the α subunit of the voltage-gated sodium channel.....	2
1.2	Mutations of mouse <i>Scn8a</i>	9
1.3	Mutations of human <i>SCN8A</i>	10
1.4	Examples of persistent and resurgent current.....	13
1.5	Proposed model for the evolutionary origin of exons 5N/5A and 18N/18A.....	23
1.6	Locations of protein interactions with Na _v 1.6.....	25
2.1	Alternative splicing of <i>SCN8A</i>	36
2.2	Splicing of an <i>Scn8a</i> minigene.....	42
2.3	Splicing of endogenous <i>SCN8A</i> transcripts in HEK cells.....	44
2.4	Treatment with cycloheximide increases the abundance of <i>SCN8A</i> transcripts containing exon 18N.....	46
2.5	<i>SCN8A</i> expression in purified neurons and human brain.....	48
2.6	Model for restriction of active Na _v 1.6 channels to neurons.....	53
3.1	The N-terminus and first transmembrane segment of Na _v 1.6 are sufficient to direct a reporter protein to the cell surface.....	66
3.2	Yeast two-hybrid screen using the N-terminus of Na _v 1.6 as bait identified Map1b as an interactant.....	67
3.3	Interaction of Na _v 1.6 with Map1b.....	69
3.4	Map1b does not bind the N-terminus of Na _v 1.1 with high affinity.....	71
3.5	Localization of Map1b interaction site within the N-terminus of Na _v 1.6.....	73

3.6. Co-expression of Map1b increases Na _v 1.6 peak current density in ND7/23 cells transfected with Na _v 1.6 _R	75
3.7. The light chain of Map1b is expressed endogenously in ND7/23 cells.....	77
3.8. Mutation of the Map1b binding site of Na _v 1.6 _R prevents generation of sodium current in transfected ND7/23 cells.....	78
3.9. Potential role of interaction between Na _v 1.6 and Map1b in trafficking of Na _v 1.6 to the cell membrane.....	83
4.1. The <i>de novo</i> proband substitution p.Asn1768Asp in sodium channel SCN8A.....	92
4.2. Effect of the <i>de novo</i> SCN8A substitution p.Asn1768Asp on biophysical properties of the channel.....	94
4.3. Effect of the <i>de novo</i> SCN8A Substitution p.Asn1768Asp on hippocampal neuronal excitability.....	97
5.1. Na _v 1.6 cDNA constructs (A) pcDNA3Na _v 1.6 _R and (B) pcDNA3Na _v 1.6 _R -GFP.....	107
5.2. QuikChange mutagenesis and miniprep screening protocol for Na _v 1.6 cDNA.....	111
5.3. Maxiprep preparation and screening protocol for Na _v 1.6 cDNA.....	112
5.4. Wild-type restriction digest fragment patterns for pcDNA3Na _v 1.6 _R	114
5.5. <i>De novo</i> patient mutations in SCN8A.....	117
5.6. p.Arg223Gly is less stable than wild type channel in HEK cells.....	119
6.1. Proposed model of haploinsufficiency.....	134

List of Tables

1.1. The mammalian voltage-gated sodium channel family.....	6
1.2. Reduced activity of neurons from <i>Scn8a</i> null mice.....	15
2.1. Primers used in cloning and RT-PCR reactions.....	39
3.1. Alanine scanning Quikchange forward primer sequences.....	61
3.2. Map1b increases the amplitude of Na _v 1.6 current in ND7/23 Cells.....	76
4.1. Biophysical effects of the <i>SCN8A</i> p.Asn1768Asp substitution.....	95
4.2. Candidate variants under a homozygote recessive disease model.....	102
5.1. Mutated Na _v 1.6 cDNA clones generated during this thesis research.....	109
5.2. Sequencing primers for the coding sequence of pcDNA3Na _v 1.6 _R and pcDNA3Na _v 1.6 _R -GFP.....	115
5.3. <i>SCN8A</i> p.Arg223Gly: Functional effects of corresponding mutations in other sodium channels.....	118
6.1. Recurrent missense variants in <i>SCN8A</i> identified in patients with heart, lung, and blood disorders.....	124

Chapter I

A Resurgence in Channel Activity

Introduction. Voltage-gated sodium channels are critical for action potential initiation and propagation in a variety of cell types. Mammalian voltage-gated channel proteins were first purified in 1981 (Hartshorne and Catterall, 1981; Tamkun and Catterall, 1981), and the sodium channel gene cDNAs *Scn1a* and *Scn2a* were cloned in 1986 (Noda et al., 1986). The *Scn8a* gene, which encodes voltage-gated sodium channel Na_v1.6, was identified in 1995 by positional cloning of a mouse neurological mutant in the Meisler lab (Burgess et al., 1995b) and by isolation of a novel rat cDNA in the Caldwell lab (Schaller et al., 1995). The human gene was mapped to chromosome 12q13 in 1998 (Plummer et al., 1998). My thesis is focused on three aspects of the biology of sodium channel Na_v1.6: the neuron-specific alternative splicing of exons 18A and 18N (Chapter II), the protein interaction with Map1b involved in trafficking (Chapter III), and the discovery of human mutations in patients with severe epileptic encephalopathy (Chapters IV and V). In this introduction, I describe the biology of Na_v1.6 as context for my work.

Voltage-gated sodium channels. The α subunits of voltage-gated sodium channels are large, ~2000 residue proteins comprised of 4 homologous domains,

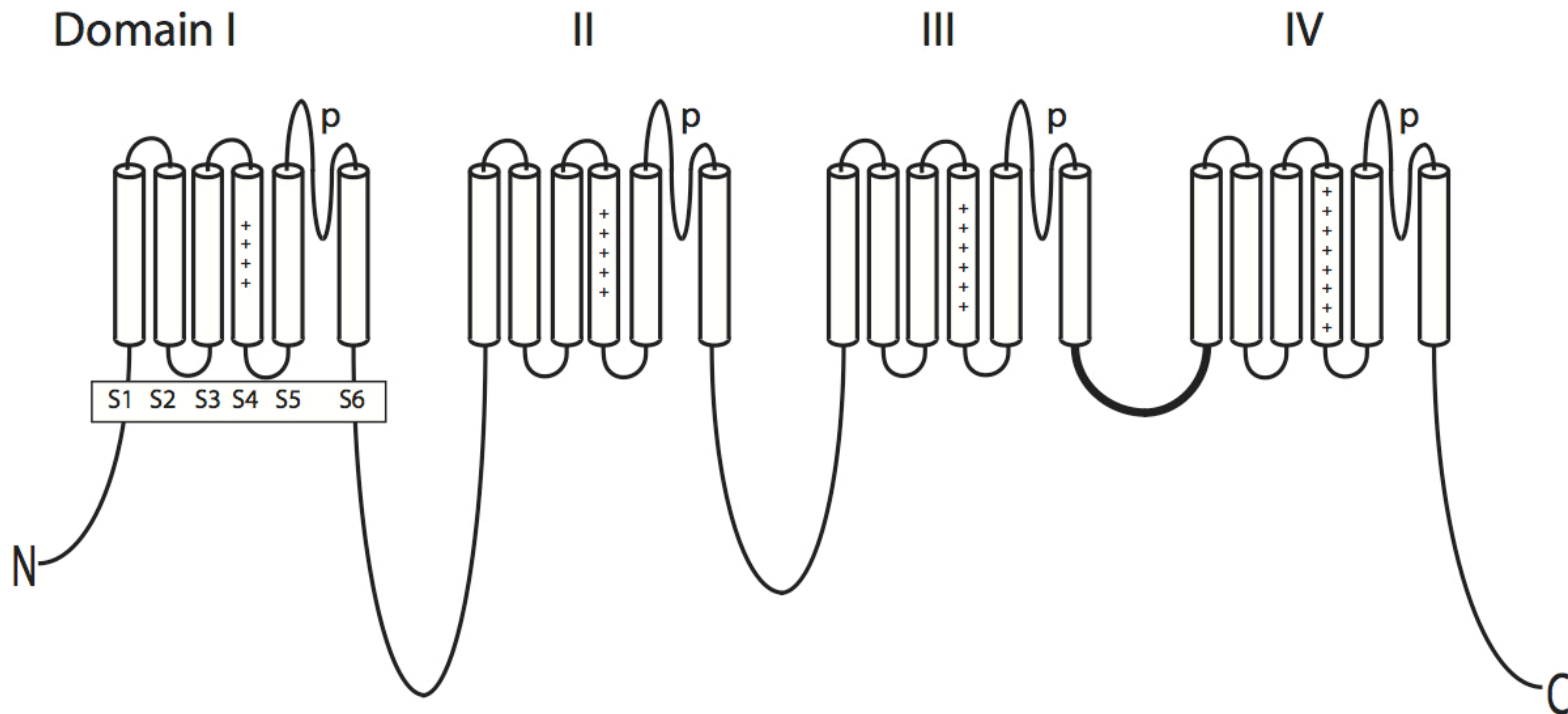


Figure 1.1. Structure of the α subunit of the voltage-gated sodium channel. Domains are labeled in Roman numerals; transmembrane segments are labeled in Arabic numerals (boxed). p, pore domain.

each consisting of 6 transmembrane segments as well as cytoplasmic N-terminal and C-terminal domains, and 3 large intracellular loops (**Figure 1.1**). Voltage-gated sodium channels open in response to membrane depolarization, allowing an influx of sodium down the concentration gradient from extracellular to intracellular. α subunits interact with small β subunits that function as cell adhesion molecules and modulate the electrophysiological properties of α subunits (Isom et al., 1994; Isom, 2001; Patino and Isom, 2010).

Voltage-gated channels are dependent on changes in membrane potential for function. Transmembrane segment S4 of each domain contains 3-5 positively charged residues that are essential for the channel response to changes in membrane potential. In response to membrane depolarization, electrostatic interactions between positively charged residues and the depolarized cytoplasm force S4 towards the extracellular surface. This results in a conformational change in S5-S6 that opens the channel pore and allows sodium influx (Yarov-Yarovoy et al., 2012). After approximately 0.5 ms (Ulbricht, 2005), the intracellular loop between domains 3 and 4, called the inactivation gate, moves into the pore region. This prevents any additional current flow and inactivates the channel. The channel then transitions from an inactive state to one of several closed states. The closed channel can respond to further changes in membrane potential (Hille, 1992).

Evolution of the voltage-gated sodium channel gene family. Voltage-gated channels evolved before the development of nervous systems, as evidenced by discovery of voltage-gated channel-like proteins in bacteria, multicellular choanoflagellates, and placozoans (e.g., NaChBac and Na_vAb) (Zakon, 2012).

These bacterial single-domain sodium channels show high levels of homology to mammalian channels, especially in transmembrane domains. Like voltage-gated potassium channels, bacterial sodium channels tetramerize to form a functional channel. The bacterial homotetramer lacks the intracellular domains present in vertebrate four-domain channels, including the inactivation gate (Payandeh et al., 2012) which renders the bacterial channel incapable of fast inactivation. The bacterial channel Na_vAb, has been crystallized in open and inactivated states (Payandeh et al., 2011; Payandeh et al., 2012). Crystallization of the channel provides a model for channel structure and the intramolecular interactions critical to pore opening and closing in mammalian channels, including the identification of hydrophilic interactions critical for stabilization of open and closed states (Payandeh et al., 2011; Payandeh et al., 2012). One unanticipated finding was the identification of membrane fatty acids that penetrate into the pore (Payandeh et al., 2011). It is likely that these fatty acids facilitate drug entry into this domain.

The four-domain cation channel is likely to have evolved through a series of tandem duplications, from a one-domain channel to a two-domain channel, similar to the TPC1/TPC2 channel, that later duplicated to generate the current four-domain channel (Hille, 2001). The sodium channel α subunit appears to have evolved from the homologous four-domain calcium channel α subunit through mutations in the pore loop. Calcium selectivity is conferred by presence of residues E/E/E/E or E/E/D/D at critical locations in the pore loops of domains I-IV, respectively. Mutation to the sodium-selective pore sequence D/E/E/A occurred in metazoans, and later evolved to the D/E/K/A sequence of tetrapod voltage-gated sodium channels

(Zakon, 2012). Evolution of the ability to use sodium as a “signal” allowed a portion of neuronal communication to become independent of the extensive calcium-based intracellular signaling (Zakon et al., 2011). It has been hypothesized that sodium channel NaChBac is the one-domain ancestor of sodium and calcium channels, since it can, under certain circumstances, permit calcium influx as well as sodium influx (Payandeh et al., 2011).

Duplication of the voltage-gated sodium channel genes in the vertebrate lineage occurred coincidentally with duplication of the HOX gene clusters in tetrapods (Lundin, 1993; Plummer and Meisler, 1999). Invertebrate genomes such as *Drosophila* contain one voltage-gated sodium channel, *para*, linked to one HOX gene cluster. The pufferfish genome contains four sodium channel genes orthologous to *Scn1a*, *Scn4a*, *Scn5a*, and *Scn8a*, each linked to one HOX gene cluster. Further tandem duplication events within two of these chromosome regions generated the *Scn3a/Scn2a/Scn1a/Scn9a* cluster and the *Scn5a/Scn10a/Scn11a* cluster in mammals. In eutherian mammals, an additional duplication within the *Scn3a/Scn2a/Scn1a/Scn9a* cluster generated the sodium channel-related gene *Scn7a/Nax* (Widmark et al., 2011).

Expansion of gene families allows for specialization of the properties and subcellular localization of individual family members. Voltage-gated sodium channels have diverged with respect to tissue-specificity in their major expression patterns (**Table 1.1**). *Scn4a* predominates in skeletal muscle and *Scn5a* is the

Table 1.1. The mammalian voltage-gated sodium channel family. TTX, tetrodotoxin. TTX-S (sensitive), binding affinity between 5 and 15 nM. TTX-R (resistant), binding affinity in the micromolar range

Gene	<i>Scn1a</i>	<i>Scn2a</i>	<i>Scn3a</i>	<i>Scn4a</i>	<i>Scn5a</i>	<i>Scn8a</i>	<i>Scn9a</i>	<i>Scn10a</i>	<i>Scn11a</i>
Protein	Na _v 1.1	Na _v 1.2	Na _v 1.3	Na _v 1.4	Na _v 1.5	Na _v 1.6	Na _v 1.7	Na _v 1.8	Na _v 1.9
Major Expression	CNS/ PNS	CNS/ PNS	CNS/ PNS	Skeletal muscle	Heart	CNS/ PNS	PNS	PNS	PNS
Mouse chromosome band	2qC1.3	2qC1.3	2qC1.3	11qE1	9qF3	15qF1	2qC1.3	9qF3	9qF3
Human chromosome band	2q24.3	2q24.3	2q24.3	17q23.3	3p22.2	12q13.13	2q24.3	3p22.2	3p22.2
TTX sensitivity	S	S	S	S	R	S	S	R	R

major channel in cardiac tissue. The other seven channels are predominantly expressed in neuronal subpopulations of the CNS and PNS. The neuronal voltage-gated sodium channel *Scn8a*, which is highly expressed in the CNS and PNS, is the focus of the remainder of this chapter.

Scn8a, a neuronal sodium channel. The gene *SCN8A* encodes the voltage-gated sodium channel Na_v1.6, which is essential for axon potential initiation and propagation in the central and peripheral nervous systems. The *Scn8a* gene is located on distal chromosome 15 in mouse (Burgess et al., 1995b) and on chromosome 12q13.13 in human (Plummer et al., 1998). *Scn8a* is a large gene, with 27 exons, and encodes a 1980 residue protein.

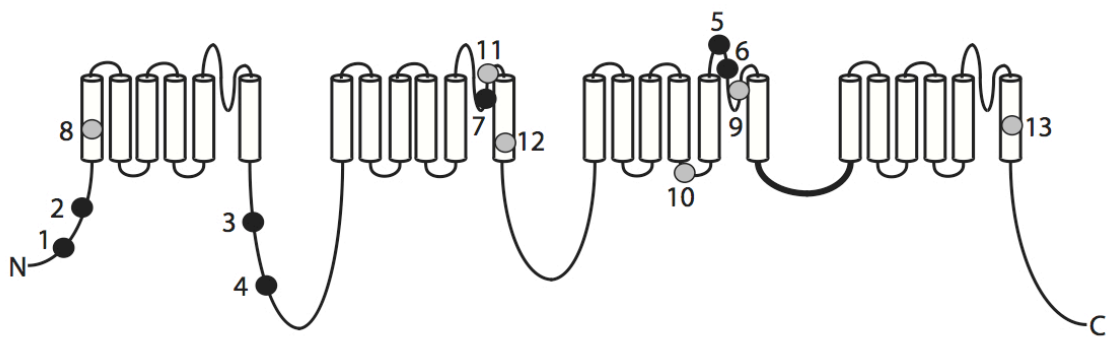
Na_v1.6 is concentrated at the axon initial segment and nodes of Ranvier in myelinated axons (Schaller and Caldwell, 2000; Boiko et al., 2001; Boiko et al., 2003; Van Wart and Matthews, 2006; Van Wart et al., 2007; Lorincz and Nusser, 2008, 2010), and is also found at lower abundance in neuronal soma and dendrites (Krzemien et al., 2000; Lorincz and Nusser, 2010). The full-length *SCN8A* transcript is highly expressed in mouse and human brain, and undergoes neuron-specific alternative splicing (Plummer et al., 1997; O'Brien et al., 2012a).

Murine Na_v1.6 mutations. Complete inactivation of mouse *Scn8a* results in ataxia, tremor (Burgess et al., 1995b; Kohrman et al., 1996), prolonged cardiac action potentials (Noujaim et al, 2012), and early lethality (Burgess et al., 1995b; Kohrman et al., 1996). Six spontaneous alleles, eight ENU-induced alleles, and one transgenic insertion allele of mouse *Scn8a* have been characterized (**Figure 1.2**). All of these mutant alleles result in recessive phenotypes. Half are null alleles (*med*,

med-tg, dmu, nmf2, nmf5, ataxia3, 8J), and homozygotes do not survive past 3 weeks of age. Two severe hypomorphic alleles (*medJ, nmf58*) cause minor tremor, severe dystonia, ataxia, muscle weakness and wasting, but mice survive past P21. The other 5 hypomorphic alleles (*medjo, jolting2J, tremorD, Clth, 9J*) produce tremor, ataxia and reduced body size, and no juvenile lethality. Phenotype severity in hypomorphs appears to depend on the extent of functional impairment of the allele.

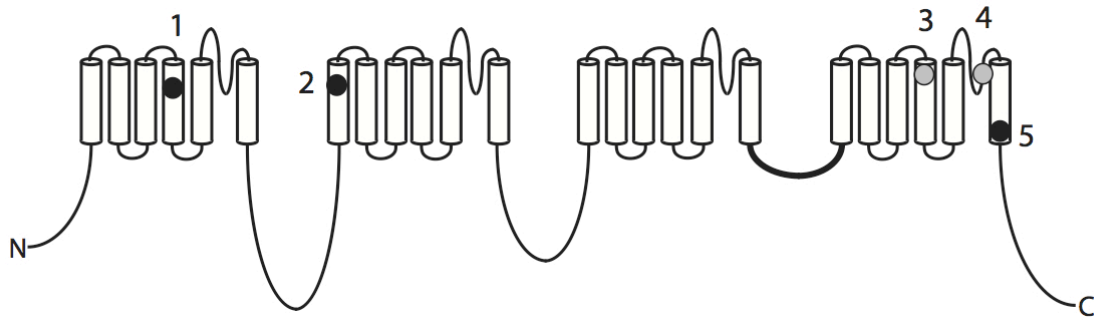
Heterozygous null mice are grossly normal, but exhibit spike-wave discharges indicative of absence epilepsy (Papale et al., 2009), disrupted sleep architecture (Papale et al., 2010), resistance to induced seizures (Martin et al., 2010), and behavioral deficits including anxiety (McKinney et al., 2008). These observations suggest that haploinsufficiency of the human channel could cause similar problems.

Human *Na_v1.6* mutations. Five potentially pathogenic mutations have been identified in *Na_v1.6* (**Figure 1.3**). In 2006, we first described a heterozygous null allele, P1719RfsX1724, that segregated with cognitive deficits in one pedigree (Trudeau et al., 2006). The haploinsufficient phenotype in these patients is consistent with observations in heterozygous null mice. The second human mutation was discovered in 2011 by whole genome sequencing. This dominant *de novo* gain of function mutation, p.Asn1768Asp, was identified in a patient with a severe epileptic encephalopathy that included features of autism, intellectual disability and ataxia, with sudden unexplained death at age 15 (Veeramah et al., 2012). Characterization of this mutation is described in Chapter IV.



	Allele	Phenotype of homozygotes	Mutation	Comments	Reference
1	ataxia3	null	S21P	Trafficking mutant	(Sharkey et al., 2009a)
2	med	null	LINE insertion into exon 2		(Kohrman et al., 1996)
3	med-tg	null	20 kb deletion at transgene insertion site		(Kohrman et al., 1995)
4	dmu	null	single nucleotide deletion in exon 10A		(De Repentigny et al., 2001)
5	nmf2	null	N1370T		(Buchner et al., 2004)
6	nmf5	null	I1392F		(Buchner et al., 2004)
7	8J	null	V929F	Spike wave discharge in heterozygotes	(Papale et al., 2009)
8	med-J	Severe hypomorph	4 base pair deletion in 5' donor site of exon 3	5-10% wt splicing, strain dependent	(Kohrman et al., 1996)
9	nmf58	Severe hypomorph	L1404H		(Buchner et al., 2004)
10	med-jo	Mild hypomorph	A1319T	10 mV positive shift in voltage dependence of activation	(Smith and Goldin, 1999)
11	tremorD	Mild hypomorph	W935L		Timms H; Smart NG; Beutler B 2008 (JAX, unpublished)
12	Clth	Mild hypomorph	D981V	Hearing tested, defective	(Mackenzie et al., 2009)
13	9J	Mild hypomorph	dell1757		(Jones et al., 2013)
	jolting2J	Mild hypomorph	Not sequenced		Thompson... Davis et al 2004 (JAX, unpublished)

Figure 1.2. Mutations of mouse *Scn8a*. Filled circles, null alleles. Grey circles, hypomorphic alleles.



	Mutation	Genetics	Pathology	Mechanism	Reference
1	R223G	<i>de novo</i>	Epileptic encephalopathy	In progress	unpublished
2	T767I	<i>de novo</i>	Epileptic encephalopathy	In progress	unpublished
3	R1617Q	<i>de novo</i>	Intellectual disability	In progress	(Rauch et al., 2012)
4	P1719RfsX6	dominant	Intellectual disability, ataxia	haploinsufficiency	(Trudeau et al., 2006)
5	N1768D	<i>de novo</i>	Epileptic encephalopathy + SUDEP	Increased persistent current	(Veeramah et al., 2012)

Figure 1.3. Mutations of human SCN8A. Filled circles, mutations identified in patients with epilepsy. Grey circles, mutations identified in patients with cognitive deficits.

In 2012, the *de novo* mutation p.Arg1617Gln was identified in a single patient by exome sequencing of patients with IQ <50, supporting the hypothesis that mutations in Na_v1.6 may be associated with intellectual disability (Rauch et al., 2012). Two additional dominant *de novo* mutations in *SCN8A*, p.Arg223Gly and p.Thr767Ile, were subsequently identified in other patients with severe epileptic encephalopathy. These mutations are described in Chapter V. Three other mutations in *SCN8A* have been recently identified by exome sequencing of patients with epilepsy (M. Hammer, personal communication). The availability of sensitive electrophysiological assays of sodium channel function permits functional analysis of putative pathogenic mutations identified in patients more efficiently than for many other genes.

Electrophysiological properties of Na_v1.6. The electrophysiological properties of Na_v1.6 have been characterized in cultured cells and in neurons from mouse. Cell culture studies allow Na_v1.6 to be studied in isolation from other channels, which is important for understanding its specific electrophysiological properties. *In vivo* studies of Na_v1.6 have focused on using null mouse mutants to remove this channel in the context of the entire neuron, and provide critical insight into the role of this channel in the complex regulation of neuronal firing.

Persistent current (**Figure 1.4A**) is a steady-state sodium current (Smith et al., 1998; Rush et al., 2005; Osorio et al., 2010) that is involved in action potential initiation at membrane voltages near the threshold of firing (Crill, 1996). Persistent current is important for populations of neurons that undergo repetitive firing.

Abnormally high levels of persistent Na_v1.6 current causes neuronal hyperexcitability

and leads to epilepsy (Veeramah et al., 2012). The magnitude of persistent current depends on the specific cell type (Rush et al., 2005; Chen et al., 2008), suggesting that this property can be modulated by other factors.

Resurgent current is a voltage- and time-dependent property of $\text{Na}_v1.6$ in which depolarization after the initial event elicits a small, transient current (**Figure 1.4B**). It has been hypothesized that resurgent current contributes to increased excitability in cerebellar Purkinje cells, leading to spontaneous firing and multi-peaked action potentials. However, resurgent current does not occur in all neurons that express $\text{Na}_v1.6$. For example, wild type hippocampal CA3 neurons have minimal resurgent current (Raman and Bean, 1997).

Resurgent current may be caused by a temporary block of the channel by an open-state channel blocker that prevents entry of $\text{Na}_v1.6$ into the true inactive state. Blocking the entry of the inactivation gate into the pore results in a temporarily inactive state that is easily reversed by minor hyperpolarization of the cell (Aman and Raman, 2010). This rapidly reversible form of inactivation allows neurons to fire rapidly and repetitively. In cerebellar Purkinje neurons (Grieco et al., 2005) and cerebellar granule cell neurons (Bant and Raman, 2010), the channel blocker for $\text{Na}_v1.6$ may be the $\beta 4$ sodium channel subunit, but the blocking peptide may vary by neuron type (Raman and Bean, 2001).

Larger relative levels of persistent and resurgent current render membranes containing $\text{Na}_v1.6$ more excitable than membranes containing the neuronal channels $\text{Na}_v1.1$ and $\text{Na}_v1.2$. This increased excitability, combined with subcellular

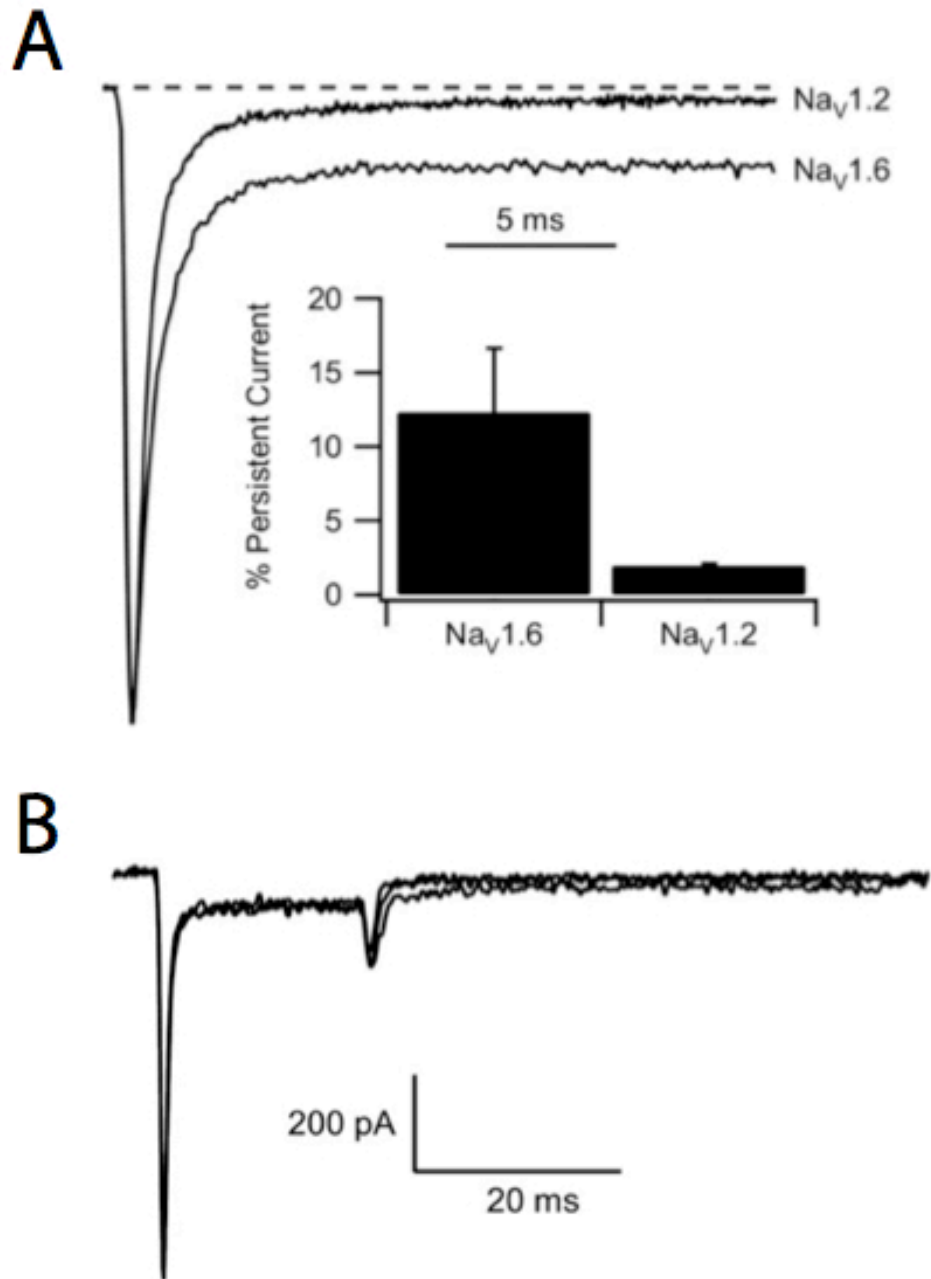


Figure 1.4. Examples of persistent and resurgent current. (A) Persistent current is a steady-state sodium current that is involved in action potential initiation at membrane voltages near the threshold of firing. Na_v1.6 has higher levels of persistent current than Na_v1.2. (B) Resurgent current is a voltage- and time-dependent property of Na_v1.6 in which depolarization after an initial event elicits a small, transient current. Adapted from Chen et al., 2008.

localization at the AIS and nodes, accounts for the role of Na_v1.6 as an action potential initiator and propagator *in vivo*.

Na_v1.6 electrophysiology in cultured cells. Direct comparison of Na_v1.6 to Na_v1.2 in HEK-tsA-201 cells did not detect a significant difference in voltage dependence of activation or inactivation (Chen et al., 2008). Na_v1.6 displayed a more positive voltage dependence of slow inactivation in this system, passing ~10% more current in the -35 mV to -25 mV range than Na_v1.2. In tsA-201 cells, Na_v1.6 also displayed persistent currents which amounted to ~12% of total current in Na_v1.6, compared with ~2% in Na_v1.2 (**Figure 1.4A**) (Chen et al., 2008).

The electrophysiological properties of Na_v1.6 and Na_v1.2 have also been studied in transfected cultured neurons and neuron-derived cell lines. Na_v1.6 has a ~10 mV depolarizing shift in voltage dependence of fast activation and fast inactivation compared to Na_v1.2 in transfected cultured DRG neurons (Rush et al., 2005). Na_v1.6 is also less likely to inactivate at higher stimulation frequencies (20-100 Hz) but inactivates more quickly from a single 40 ms depolarizing stimulus in transfected cells (Rush et al., 2005). Persistent Na_v1.6 current is ~2% of maximal current in transfected ND7/23 cells (Veeramah et al., 2012), compared to 12% in tsA-201 cells (Chen et al., 2008). These differences demonstrate the importance of neuronal factors in determining the functional properties of Na_v1.6.

Effects of loss of Na_v1.6 on neuronal excitability *in vivo*. After the description of *Scn8a* null mice in 1995 (Burgess et al., 1995b), several groups used this model to evaluate the effects of Na_v1.6 deficiency *in vivo* (**Table 1.2**). Neurons from *Scn8a* null mice consistently display defects in repetitive firing

Table 1.2. Reduced activity of neurons from *Scn8a* null mice.

	Neuron type	Reduced neuronal activity in null mice	Reference
1	Cerebellar Purkinje cells	Reduced repetitive firing, reduced resurgent current (-70%), reduced transient current (-50%) (<i>med-tg, med</i>)	(Raman et al., 1997; Aman and Raman, 2007)
2	Cerebellar nucleus	No significant changes (<i>med</i>)	(Aman and Raman, 2007)
3	Cerebellar granule cells	Reduced persistent current, reduced firing rate (<i>flox/flox; BAC-α6 CRE</i>)	(Osorio et al., 2010)
4	DRG large and small diameter	Reduced resurgent current (-100%) (<i>med</i>)	(Cummins et al., 2005)
5	Trigeminal-mesencephalic	Reduced resurgent current (-40%), reduced persistent current (-75%), reduced repetitive firing (like Purkinje) (<i>med</i>)	(Enomoto et al., 2007)
6	Subthallamic	Reduced resurgent current, altered firing (<i>med</i>)	(Do and Bean, 2004)
7	Retinal ganglion	Reduced repetitive firing (<i>med</i>)	(Van Wart and Matthews, 2006)
8	Prefrontal cortical pyramidal	Reduced resurgent current (<i>med</i>)	(Maurice et al., 2001)
9	Hippocampal CA1	Reduced persistent, reduced resurgent, significant elevation of spike threshold, altered spike initiation, reduced spike gain (<i>med</i>)	(Royeck et al., 2008)
10	Motor neurons	Reduced conduction velocity (<i>med-J</i>)	(Kearney et al., 2002)
11	Globus pallidus neurons	Impaired pacemaking, impaired capacity for fast spiking (<i>med-tg</i>)	(Mercer et al., 2007)

(Raman and Bean, 1997; Raman et al., 1997; Van Wart and Matthews, 2006; Aman and Raman, 2007), suggesting that Na_v1.6 is required for this process. In Purkinje cells isolated from *Scn8a* null mice, persistent current was reduced by ~100 pA (70%) compared to wild type (Raman et al., 1997). In *Scn8a* floxed mice crossed with the cerebellar granule neuron-specific BAC α 6-Cre, overall sodium current and resurgent current were unaffected in cerebellar granule neurons, but there was a significant decrease in persistent current from ~2% of total current in wild type to 1.2% in the null (Osorio et al., 2010). There was also an 85% reduction in resurgent current in *Scn8a* null cerebellar Purkinje cells compared to wild type, suggesting that Na_v1.6 is the major source of resurgent current in these neurons (**Table 1.2**) (Raman et al., 1997). Thus, Na_v1.6 has an essential role in generating persistent and resurgent current in mouse cerebellum, and is consequently essential for repetitive firing.

Na_v1.6 function at the axon initial segment. A large part of the overall decrease in neuronal excitability in *Scn8a* null mice can be attributed to the role of Na_v1.6 at the axon initial segment (AIS). The AIS is the membrane region at the proximal end of the axon where sodium channels are concentrated and electrical signals from the soma and dendrites are summed (and the threshold for action potential initiation is lowest) (Royeck et al., 2008). The channel composition of the AIS differs between neurons (Lorincz and Nusser, 2008), and determines the firing threshold of the AIS. Na_v1.6 is localized at the AIS and has a critical role in axon potential initiation and modulation of neuronal excitability. The decreased excitability observed in *Scn8a* null neurons (**Table 1.2**) would affect neuronal signaling within

the brain and to the periphery, resulting in the muscle atrophy, weakness, tremor, and paralysis observed in *Scn8a* null mice.

Na_v1.6 is highly concentrated in the distal half of the AIS in many types of neurons, including cerebellar granule cells and cerebellar Purkinje cells (Van Wart and Matthews, 2006; Lorincz and Nusser, 2008; Royeck et al., 2008). Van Wart and Matthews investigated the role of Na_v1.6 in action potential initiation in cerebellar granule cells. The threshold for action potential initiation in null *Scn8a*^{medtg} granule cells was 4.2 mV more positive than in wild type cells (Van Wart and Matthews, 2006), demonstrating that neurons lacking Na_v1.6 are less excitable than wild type neurons. Immunohistochemistry revealed that in the AIS of null cerebellar granule cells, Na_v1.1 and Na_v1.2 replace Na_v1.6 (Van Wart and Matthews, 2006). The change in channel composition is likely to explain the observed decrease in excitability.

Royeck and colleagues investigated the role of Na_v1.6 in AIS excitability of cultured hippocampal cells. *Scn8a*-null hippocampal CA1 pyramidal cells had a ~5 mV positive shift in the voltage dependence of activation compared to wild type (Royeck et al., 2008), making null cells less sensitive to depolarizing stimuli. Null neurons also had a 58% reduction in persistent current and approximately a 75% reduction in resurgent current (Royeck et al., 2008). This combination of more positive voltage for activation, decreased persistent current, and reduced resurgent current, renders *Scn8a* null neurons less excitable than their wild type counterparts. This is reflected in an 8 mV depolarizing (rightward) shift in the spike threshold of null CA1 neurons (Royeck et al., 2008), consistent with the previous study.

Studies of cortical pyramidal neurons revealed that action potentials tend to initiate at the distal part of the AIS, where sodium channel concentrations are highest (Van Wart et al., 2007; Kole et al., 2008; Kole and Stuart, 2008). Immunohistochemistry of the AIS of cortical pyramidal neurons demonstrated that the proximal AIS contains predominantly $\text{Na}_v1.2$, while the distal AIS contains predominantly $\text{Na}_v1.6$ (Hu et al., 2009). Consistent with this channel distribution, step-depolarizations of patched neurons revealed that the activation threshold in the distal AIS was -55 mV, while the activation threshold in the proximal AIS closest to the soma was -43 mV (Hu et al., 2009). These results support the role of $\text{Na}_v1.6$ in lowering the threshold of action potential initiation.

Action potentials are primarily directed away from the soma and down the axon. However, backpropagation, i.e., an action potential from the AIS into the soma, occurs at low frequency (Hu et al., 2009). To investigate the roles of $\text{Na}_v1.2$ and $\text{Na}_v1.6$ in backpropagation, rat cortical neurons were isolated and the axon was removed to produce a cell with a soma and an “axonal bleb” that retains the AIS (Hu et al., 2009). Current was injected into different locations in the axonal bleb, and action potentials were recorded from the soma to detect backpropagation. Injecting current into the distal AIS, containing predominately $\text{Na}_v1.6$, did not result in backpropagation, while current injection at the proximal AIS, containing predominantly $\text{Na}_v1.1$ and $\text{Na}_v1.2$, resulted in detectable action potentials in the soma (Hu et al., 2009).

Taken together, these data support the view that localization of Na_v1.6 to the distal AIS results in a lower threshold for action potential initiation and also directs the action potential down the axon and away from the soma.

Proposed roles of Na_v1.6 in non-neuronal cells. In addition to its well-characterized role in neurons, some recent studies have presented preliminary evidence consistent with novel activity of Na_v1.6 in other cell types.

Cardiac myocytes. Na_v1.5 is the predominant voltage-gated sodium channel in cardiomyocytes, but Na_v1.6 is present in low quantities (Maier et al., 2003; Maier et al., 2004; Du et al., 2007; Noujaim et al., 2012). The functional role of Na_v1.6 in cardiac myocytes is unclear. Na_v1.6 colocalizes by immunostaining with markers for transverse tubules, invaginations of the sarcolemma that are essential for excitation-contraction coupling. Cardiomyocytes cultured from the null mutant *Scn8a^{ataxia3}* displayed decreased current amplitudes (~3.5 pA, vs. ~9 pA in wild type) (Noujaim et al., 2012). The decrease in current amplitude in null cardiomyocytes was partially mimicked by addition of tetrodotoxin to wild type cells, consistent with the contribution of a tetrodotoxin-sensitive channel, such as Na_v1.6. Action potential duration was prolonged in Na_v1.6 null heart, suggesting that Na_v1.6 has an essential function in excitation-contraction coupling and cardiac function (Noujaim et al., 2012).

Vas deferens. Patch-clamp studies of smooth muscle myocytes of the mouse vas deferens identified a TTX-sensitive current that was not detectable in null *Scn8a^{med}* mice (Zhu et al., 2008). Electrophysiological studies comparing wild type and null myocytes attributed the resurgent-like currents in these cells to Na_v1.6,

consistent with its contribution to resurgent current in neuronal populations (Zhu et al., 2010; Teramoto et al., 2012).

Cellular invasion in macrophages. It has been reported that Na_v1.6 regulates podosome formation in macrophages (Carrithers et al., 2009). Podosomes are actin-rich structures located on the extracellular membrane that are important for macrophage adhesion, migration, and invasion. RT-PCR of macrophage RNA identified only the Δ 18 transcript of *Scn8a*, which splices directly from exon 17 to exon 19 (Carrithers et al., 2009). The protein product of this transcript is not predicted to function as a voltage-gated sodium channel (Plummer et al., 1997). Localization of Δ 18-Na_v1.6 protein to the podosome was observed by immunocytochemistry using polyclonal anti-Na_v1.6 (Alomone) in the human monocyte-macrophage cell line THP-1. Inhibition of Na_v1.6 by TTX, siRNA, and the *med* mutation all resulted in reduced macrophage invasion in cultured cell assays, suggesting that Na_v1.6 may function in macrophage biology.

Cancer. Voltage-gated channels may also enhance the migration of cancer cells. qRT-PCR of cervical biopsies demonstrated that ectopic expression of Na_v1.6 was increased 40-fold in tumor samples compared to normal samples (Hernandez-Plata et al., 2012). Na_v1.7 (*Scn9a*) was also upregulated 20-fold. Blocking Na_v1.6 activity with the Na_v1.6-specific β -scorpion toxin Cn2 (Schiavon et al., 2006) reduced the invasive capability of cervical cancer primary cultures in a cell culture migration assay, suggesting that Na_v1.6 may contribute to cellular migration in tumors (Hernandez-Plata 2011).

Conserved noncoding exons and the 5' UTR of the Scn8a transcript.

Previous work from our lab identified the transcription start site of *Scn8a* approximately 70 kb upstream of the translation initiation site (Drews et al., 2005). The 5'UTR is encoded by four closely spaced noncoding exons designated 1a-1d that are conserved between mouse and human (Drews et al., 2005). A 4.8-kb genomic fragment containing exons 1a-d flanked by 1.5 kb of sequence upstream and 1.5kb of downstream sequence was sufficient to drive luciferase activity in motor neuron-derived cell lines (Drews et al., 2005).

Exon 1c is highly conserved in all vertebrates, suggesting that it was the ancestral noncoding exon and that exons 1a, 1b, and 1d result from a mammal-specific duplication (Drews et al., 2007). Exon 1c contains four sequence elements with approximately 75% nucleotide conservation between mammals and fish: A (22 bp), B (20 bp), DR1 (18 bp) and DR2 (18 bp). This unusually high level of conservation for noncoding sequence is suggestive of conserved function (Drews et al., 2007). *In silico* analysis of the four sequence elements identified potential binding sites for transcription factors Pou6f1/Brn5, YY1, and REST/NRSF (Drews et al., 2007), factors implicated in regulation of neuronal genes. In transgenic mice, exon 1c was sufficient to drive LacZ expression in neurons throughout the brain, with highest expression in hippocampal and Purkinje neurons (Drews et al., 2007), consistent with the endogenous expression patterns of *Scn8a*.

Mutually exclusive alternatively spliced exons. *Scn8a* contains two pairs of mutually exclusive alternative exons, 5N/5A and 18N/18A. These pairs encode the S3-S4 transmembrane segments in domain I and domain III (Plummer et al.,

1997). Exons 5N/5A and 18N/18A are thought to have a common evolutionary origin, with exons 5A and 5N resulting from duplication of a single exon followed by duplication of the two-domain channel (**Figure 1.5**) (Plummer et al., 1997).

We demonstrated that transcripts containing exon 18A are restricted to mature neurons (O'Brien et al., 2012). Transcripts containing exon 18N have an in-frame stop codon (Plummer et al., 1997) and are subject to nonsense-mediated decay (O'Brien et al., 2012). Thus, alternative splicing of exon18 provides temporal and spatial regulation of Na_v1.6 and serves as an on/off switch for the active channel. The molecular mechanism of this alternative splicing is the subject of Chapter II of this thesis.

Alternative polyadenylation sites. 3' RACE was used to identify two alternative polyadenylation sites in *Scn8a* that are conserved through chicken and are located 4 kb and 6.5 kb downstream from the termination codon (Drews et al., 2005). Northern blot of mouse brain poly-A RNA detected the short and long 3'UTR in transcripts of 9 kb and 12 kb, respectively (Drews et al., 2005). The functional consequences of the alternate polyadenylation sites have not been investigated.

Protein interactions of Na_v1.6. Voltage-gated sodium channels are part of large, multi-protein complexes that are cell-type and subdomain specific. The known sites of interaction of Na_v1.6 with other proteins are represented in **Figure 1.6**.

Map1b. A novel interaction between the N-terminus of Na_v1.6 and the light chain of the microtubule-associated protein Map1b (residues 77-80) is described in Chapter III.

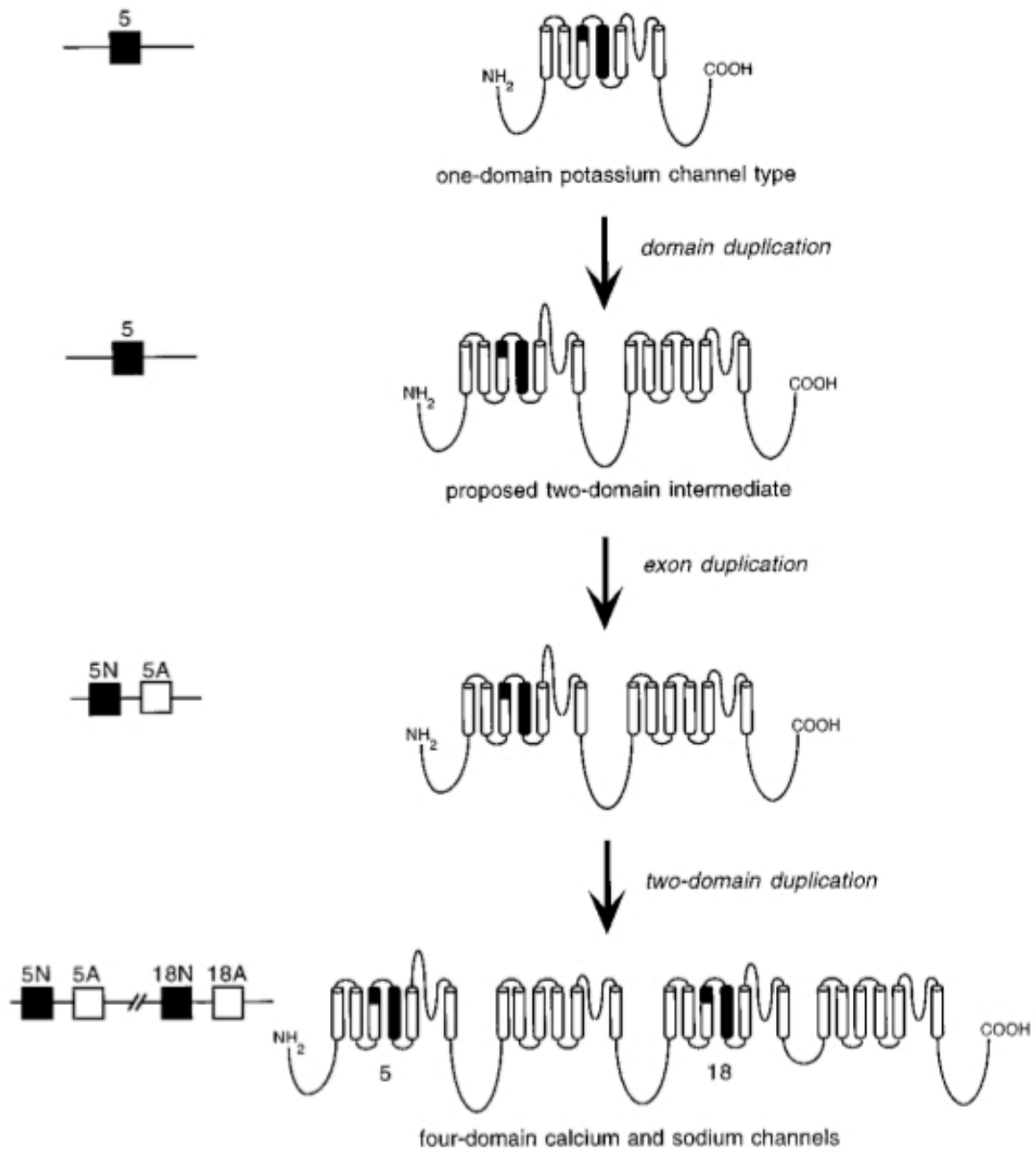


Figure 1.5. Proposed model for the evolutionary origin of exons 5N/5A and 18N/18A. From Plummer et al., 1997.

Protein kinases. Immunohistochemistry of hippocampal neurons demonstrated that the MAP kinase p38 co-localizes with Na_v1.6 (Gasser et al., 2010). This stress-activated kinase phosphorylates Na_v1.6 at serine 553 in an *in vitro* kinase assay using the first intracellular loop as a substrate (Wittmack et al., 2005). This phosphorylation creates a PXP/TP motif (residues 551-554) that facilitates binding of E3 ubiquitin ligases (Sudol and Hunter, 2000; Zarrinpar and Lim, 2000). Thus, phosphorylation by p38 indirectly results in ubiquitination and degradation of Na_v1.6 (Gasser et al., 2010). Activation of p38 by anisomycin reduced Na_v1.6 current amplitude from 95 to 52 pA in the ND7/23 cell line (Wittmack et al., 2005) and from ~1200 pA to ~800 pA in hippocampal neurons (Gasser et al., 2010). No effect of p38 on sodium current was observed in *Scn8a* null (*med*) hippocampal neurons, suggesting that Na_v1.6 is the predominant sodium channel target of activated p38 (Gasser et al., 2010).

The neuronal voltage gated sodium channel Na_v1.2 is modulated by the kinases PKA and PKC *in vitro*. Phosphorylation of Na_v1.2 reduces the mean peak sodium current by 35% for PKC and 22% for PKA (Chen et al., 2008). In contrast, the reduction of Na_v1.6 current is only 7% by PKC and 8% by PKA, despite multiple predicted PKA and PKC phosphorylation sites (Chen et al., 2008).

Ankyrin. Ankyrins are adaptor proteins that attach membrane proteins to

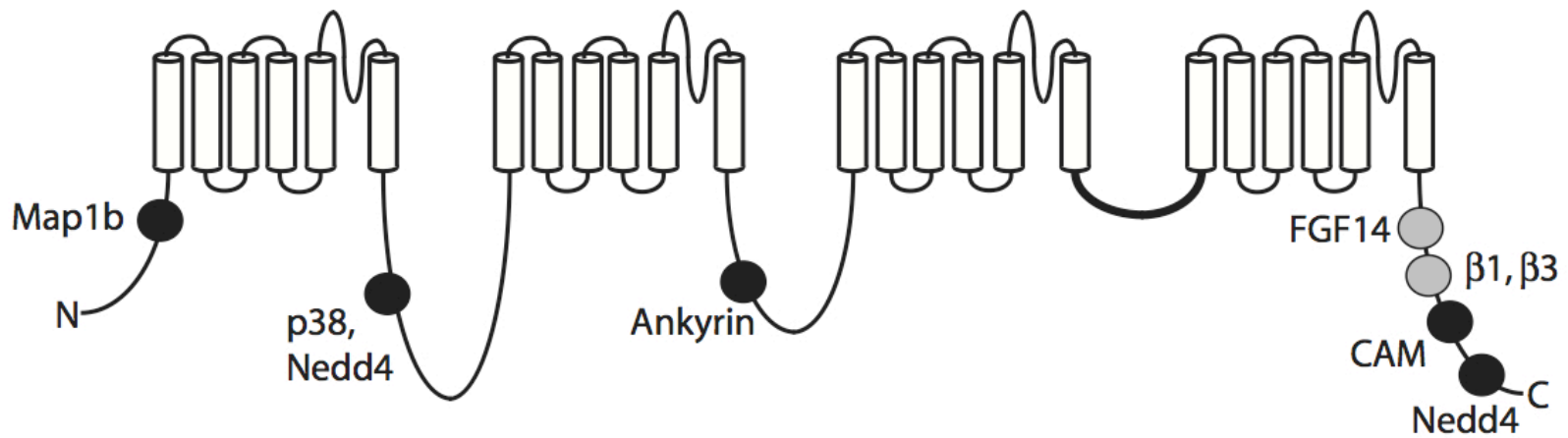


Figure 1.6. Locations of protein interactions with Na_v1.6. Filled circles represent binding sites that have been localized to specific residues of Na_v1.6: Map1b (77-80), p38 (553), ankyrin (1089-1122), calmodulin (1902-1912), and Nedd4 (551-554 and 1943-1945). Grey circles represent binding sites that have not been mapped to specific residues.

spectrin components of the cytoskeleton. Direct interaction between ankyrins and voltage-gated sodium channels is well documented (Srinivasan et al., 1988; Davis et al., 1996; Hill et al., 2008). All vertebrate voltage-gated sodium channels share a conserved ankyrin-binding motif in the second cytoplasmic loop (Na_v1.6 residues 1089-1122) (Lemaitte et al., 2003; Gasser et al., 2012). This motif evolved independently in the voltage-gated potassium and sodium channels (Zakon, 2012), suggesting that interaction with ankyrin is critical for localization the AIS and nodes of Ranvier. Although the specific sequence of the ankyrin-binding motif varies across voltage-gated sodium channels, the proximal half of this motif is consistently rich in valine and proline and the distal half is enriched in glutamic acid and serine residues (Garrido et al., 2003; Lemaitte et al., 2003; Gasser et al., 2012). The ankyrin-binding motif is sufficient to localize a single transmembrane reporter construct to the AIS in cultured hippocampal neurons (Garrido et al., 2003; Lemaitte et al., 2003) and to localize a reporter to the nodes of Ranvier in transfected dorsal root ganglion neurons co-cultured with myelinating Schwann cells (Gasser et al., 2012).

The role of the ankyrin-binding motif in subcellular localization of channels was recently investigated in the context of full length Na_v1.6. Mutation of the invariant glutamic acid E1100 to alanine within the ankyrin-binding motif prevented localization of transfected Na_v1.6 to the AIS and nodes of Ranvier in cultured rat hippocampal neurons (Gasser et al., 2012). Significantly reduced localization of the mutant to AIS and nodes of somatosensory cortex neurons was observed in mice electroporated with the mutant channel *in utero* at E14 (Gasser et al., 2012). These

data confirm that ankyrin binding is necessary for targeting and localization of Na_v1.6 in cell culture and *in vivo*. Interestingly, mutations in conserved residues of the ankyrin-binding motif do not alter the electrophysiological properties of Na_v1.6 (Gasser et al., 2012).

Intracellular FGF. The proteins FGF11-FGF14 are members of the intracellular fibroblast growth factor (iFGF) family. Unlike FGF1-FGF10, iFGF proteins are not secreted and do not bind fibroblast growth factor receptors. iFGFs interact with intracellular targets, including the α subunit of voltage-gated sodium channels (Wittmack et al., 2004; Laezza et al., 2009; Shakkottai et al., 2009). FGF13 interacts with the C-terminus of Na_v1.6 in co-immunoprecipitation and yeast-2-hybrid assays (Wittmack et al., 2004), and colocalizes with Na_v1.6 in neurons from hippocampus, dorsal root ganglia, and dorsal root of the sciatic nerve, as well as cerebellar Purkinje neurons (Wittmack et al., 2004; Rush et al., 2006; Shakkottai et al., 2009). FGF13 has multiple isoforms, including isoforms FGF13-1a and FGF13-1b which are encoded by alternative first exons (Munoz-Sanjuan et al., 2000). Co-transfection of Na_v1.6 and FGF13-1a in ND7/23 cells increases Na_v1.6 current amplitude approximately two-fold, but causes a ~15 mV depolarizing (rightward) shift in channel availability (Rush et al., 2006). Co-expression of Na_v1.6 and FGF13-1b in these cells also increases current amplitude by two-fold, but causes a 4 mV depolarizing shift in voltage-dependent inactivation of the channel (Wittmack et al., 2004). These different effects of FGF13 isoforms on channel properties may allow specific sub-populations of neurons to fine-tune firing properties via alternative splicing of FGF13.

FGF14 also regulates Na_v1.6 activity. *Fgf14* null mice develop ataxia and ~80% of *Fgf14* null cerebellar Purkinje cells do not fire repetitively (Shakkottai et al., 2009). Reduced Na_v1.6 protein at the cell surface was observed in *Fgf14* null cerebellar Purkinje neurons by immunohistochemistry, suggesting that FGF14 is required for Na_v1.6 function (Shakkottai et al., 2009). The two alternate N-termini of FGF14 affect Na_v1.6 properties differently in cultured cells. Co-expression of FGF14-1b and Na_v1.6 reduces current density, while co-expression with the FGF14-1a has no effect (Laezza et al., 2009). FGF14 constructs lacking the N-terminus increased current density when co-expressed with Na_v1.6 (Laezza et al., 2009). The difference between repression of current in cells and enhancement of current in mice highlights the complex nature of the FGF14-Na_v1.6 interaction.

Voltage-gated sodium channel β subunits. The voltage-gated sodium channel β subunits β 1- β 4 are single-transmembrane cell-adhesion molecule proteins with multiple functions including modulating current and surface expression of the α subunit (Patino and Isom, 2010). β 2 and β 4 are covalently linked to the α subunit by disulfide bonds; β 1 and β 3 interact with the C-terminus of the α subunit in a non-covalent manner (Leterrier et al., 2011).

Studies of mice null for the β 1 subunit (*Scn1b*^{-/-}) suggest that interaction between β 1 and Na_v1.6 is required for wild-type expression levels of Na_v1.6 at the distal AIS *in vitro* and *in vivo* (Brackenbury et al., 2010). A higher proportion of Na_v1.1 was observed at the AIS in cultured cerebellar granule neurons and cerebellar Purkinje neuron slices from *Scn1b*^{-/-} mice (Brackenbury et al., 2010). As a consequence of reduced Na_v1.6 at the AIS, slightly reduced levels of resurgent

current were observed in cerebellar granule neuron slices (Brackenbury et al., 2010). Thus, the interaction between $\beta 1$ and $\text{Na}_v1.6$ is important for localization and function of the channel.

Neurite extension during development is mediated by sodium channel activity (Brackenbury et al., 2010). Transfection of $\beta 1$ subunits into a monolayer of Chinese Hamster Lung cells co-cultured with isolated mouse brain neurons positively affects neurite extension in wild type neurons. Transfection of $\beta 1$ had no effect on *Scn8a* null neurons in this co-culture system, demonstrating that some sodium channel current-dependent neurite outgrowth is mediated by $\text{Na}_v1.6$ (Brackenbury et al., 2010).

As described above, $\beta 4$ subunits have been implicated in the generation of resurgent $\text{Na}_v1.6$ current (Aman et al., 2009). Addition of the cytoplasmic tail of the $\beta 4$ subunit is sufficient to restore resurgent current capabilities in cultured neurons treated with proteases to degrade the endogenous channel blocker (Grieco et al., 2005). In cultured cerebellar neurons, the $\beta 4$ subunit is required for generation of resurgent current and contributes to persistent current and repetitive firing (Bant and Raman, 2010). Knockdown of $\beta 4$ by siRNA in cultured cerebellar granule cells reduced resurgent current from ~9% of transient current in control cells to ~3.7% in treated cells. $\beta 4$ knockdown resulted in a 7.7 mV hyperpolarizing shift in the voltage dependence of inactivation and a decrease in repetitive firing, changes that are predicted to reduce neuronal excitability. Most, but not all, subpopulations of neurons that have resurgent current express the $\beta 4$ subunit (Bant and Raman, 2010). However, full-length $\beta 4$ is not sufficient to generate resurgent sodium current

in HEK cells co-transfected with Na_v1.6 (Chen et al., 2008; Aman et al., 2009), suggesting that other molecules are involved in regulating resurgent current in different neuronal populations.

Calmodulin. The IQ motif [I,L,V]QXXXRXXXX[R,K] (Na_v1.6 C-terminal domain residues 1902-1912) binds the calcium responsive protein calmodulin (CAM). The same motif binds apo-CAM, the Ca²⁺ deficient form of calmodulin, and Ca²⁺-bound CAM (Bahler and Rhoads, 2002). All of the voltage-gated sodium channels contain an IQ motif in the C-terminus (Yu and Catterall, 2003; Feldkamp et al., 2011).

In transfected DRG-derived cell lines, mutation of the invariant glutamine in the IQ motif of Na_v1.6 to a glutamic acid resulted in a 62% decrease in current amplitude and increased the time constant of inactivation by approximately 50% (Herzog et al., 2003b). Mutation of the corresponding residue in Na_v1.4 ablated current (Herzog et al., 2003b), demonstrating that the effects of CAM binding are channel-specific.

Addition of Ca²⁺ to the system, converting apo-CAM to CAM, slowed wild-type Na_v1.6 inactivation by ~50% (Herzog et al., 2003b), similar to the effect of mutating the IQ domain of Na_v1.6. The authors suggest that binding of apo-CAM to Na_v1.6 causes channels to inactivate more quickly and that addition of Ca²⁺ increases excitability (Herzog et al., 2003b).

Nedd4. The E3 ubiquitin ligase Nedd4 has a type-I WW domain that binds PXY motifs (residues 1943-1945), and a type-IV WW domain that binds PXP/pTP motifs (residues 551-554) (Abriel et al., 2000; Sudol and Hunter, 2000; Fotia et al.,

2004; Ingham et al., 2004; van Bemmelen et al., 2004; Rougier et al., 2005). Gasser and colleagues showed that S553 in loop 1 of Na_v1.6 is phosphorylated by p38 MAPK to generate a PXpS/pTP motif. *In vitro* studies using chimeric reporter constructs containing either the PXY motif, the PGSP motif, or both motifs fused to eGFP demonstrated that both the PXY motif in the C-terminus and the phosphorylated PGSP motif in loop 1 are necessary for Nedd4 binding and internalization of the reporter construct (Gasser et al., 2010). Reporter constructs containing only one of these domains are not internalized (Gasser et al., 2010). Binding of Nedd4 is predicted to cause ubiquitination of Na_v1.6, targeting it for internalization and degradation. The authors suggest that p38/Nedd4-mediated modulation of Na_v1.6 current density may be part of the neuronal stress response.

Conclusion. The voltage gated sodium channels are a family of large transmembrane proteins that are critical for electrical signaling in neurons, muscles, and heart. Evolutionary expansion has allowed individual channels to diverge in properties and regulation. The electrophysiological properties of Na_v1.6, including persistent and resurgent current, are related to its functions in action potential initiation and repetitive neuronal firing in the cerebellum.

Translational and transcriptional regulation of Na_v1.6 ensures that this channel is expressed in the right cells and at the proper developmental time points. Additional post-transcriptional regulation dictates the subcellular location of the channel and can modify the firing properties. Together, these provide a mechanism for neurons to subtly alter their firing properties to fulfill specific niches *in vivo*.

In vivo mutations in mutant mice and human patients demonstrate that hypoactivity and hyperactivity of Na_v1.6 are both detrimental, but with different effects. Haploinsufficiency appears to cause impaired cognition (Trudeau et al., 2006; McKinney et al., 2008; Rauch et al., 2012), while hyperactivity is associated with epilepsy (Veeramah et al., 2012) (Chapter V). Analysis of mutant and wild type channels *in vivo* and cell culture will continue to provide critical insight into structure-function relationships in Na_v1.6 and the mechanism of pathogenesis for novel mutations in this channel.

Chapter II

Rbfox proteins regulate alternative splicing of neuronal sodium channel *SCN8A*¹

Abstract

The *SCN8A* gene encodes the voltage-gated sodium channel Na_v1.6, a major channel in neurons of the CNS and PNS. *SCN8A* contains two alternative exons, 18N and 18A, that exhibit tissue specific splicing. In brain, the major *SCN8A* transcript contains exon 18A and encodes the full-length sodium channel. In other tissues, the major transcript contains exon 18N and encodes a truncated protein, due to the presence of an in-frame stop codon. Selection of exon 18A is therefore essential for generation of a functional channel protein, but the proteins involved in this selection have not been identified. Using a 2.6 kb *Scn8a* minigene containing exons 18N and 18A, we demonstrate that co-transfection with Fox-1 or Fox-2 initiates inclusion of exon 18A. This effect is dependent on the consensus Fox binding site located 28 bp downstream of exon 18A.

¹This work has been published in: O'Brien, J.E., Drews, V.L., Jones, J.M., Dugas, J.C., Barres, B.A., and Meisler, M.H. (2012). Rbfox proteins regulate alternative splicing of neuronal sodium channel *SCN8A*. *Mol Cell Neurosci* 49, 120-126, with the exception of the discussion of the *cis* elements in splicing of exon 18.

We examined the alternative splicing of human *SCN8A* and found that the postnatal switch to exon 18A is completed later than 10 months of age. In purified cell populations, transcripts containing exon 18A predominate in neurons but are not present in oligodendrocytes or astrocytes. Transcripts containing exon 18N appear to be degraded by nonsense-mediated decay in HEK cells. Our data indicate that RBFOX proteins contribute to the cell-specific expression of Na_v1.6 channels in mature neurons.

Introduction

The gene *SCN8A* encodes sodium channel Na_v1.6, one of the major voltage-gated sodium channels responsible for generation and propagation of action potentials in mammalian neurons. Na_v1.6 is concentrated at the axon initial segment and nodes of Ranvier, and is also present in dendrites and soma of most neurons in the central and peripheral nervous systems (Schaller and Caldwell, 2000; Lorincz and Nusser, 2010). Mutations of Na_v1.6 cause severe movement disorders in the mouse, including tremor, dystonia, ataxic gait, and premature lethality (Meisler et al., 2004). The critical role of Na_v1.6 in the neuronal firing has been demonstrated by the abnormal firing patterns in neurons from mutant mice, including cerebellar Purkinje cells (Raman et al., 1997), dorsal root ganglia C-fibers (Black et al., 2002), spinal sensory neurons (Cummins et al., 2005), trigeminal neurons (Enomoto et al., 2007), subthalamic neurons (Do and Bean, 2004), retinal ganglion cells (Van Wart and Matthews, 2006), prefrontal cortical pyramidal neurons (Maurice et al., 2001), hippocampal CA1 neurons (Royeck et al., 2008), globus pallidus neurons (Mercer et

al., 2007) and cerebellar granule cells (Levin et al., 2006). Reduced repetitive firing and reduced persistent current are common abnormalities. Haploinsufficiency of *SCN8A* has been associated with intellectual disability in a human pedigree (Trudeau et al., 2006).

Neuron-specific alternative splicing is an important component of regulated gene expression in the nervous system (Li et al., 2007). The alternative exons 18A and 18N of *SCN8A* are the product of exon duplication and encode domain 3 transmembrane segments 3 and 4 (Plummer et al, 1997) (**Figure 2.1A**). Transcripts containing exon 18A predominate in brain and encode the active, full-length channel protein (**Figure 2.1B**). Other tissues express two types of *SCN8A* transcripts that do not encode an active channel, transcripts containing exon 18N with an in-frame stop codon, and transcripts that skip exon 18 ($\Delta 18$) (**Figure 2.1B**). An invertebrate homolog of the truncated protein encoded by 18N transcripts was shown to be inactive in functional assays channel activity (Tan et al, 2002). The protein encoded by the $\Delta 18$ transcript has altered topology of transmembrane domains and is unlikely to fold into an active channel. Inclusion of exon 18A is thus essential for production of functional $\text{Na}_v1.6$.

SCN8A exon 18N is conserved in vertebrates from fish to mammals (Plummer et al., 1997; Tan et al., 2002). The related sodium channels *SCN1A*, *SCN2A*, *SCN3A*, and *SCN9A* contain different duplicated alternative exons with in-frame stop codons that also truncate the channel in domain 3 (Oh and Waxman, 1998; Alessandri-Haber et al., 2002; Kerr et al., 2008). Alternative splicing of these stop-codon-containing exons may reinforce the specificity conferred by

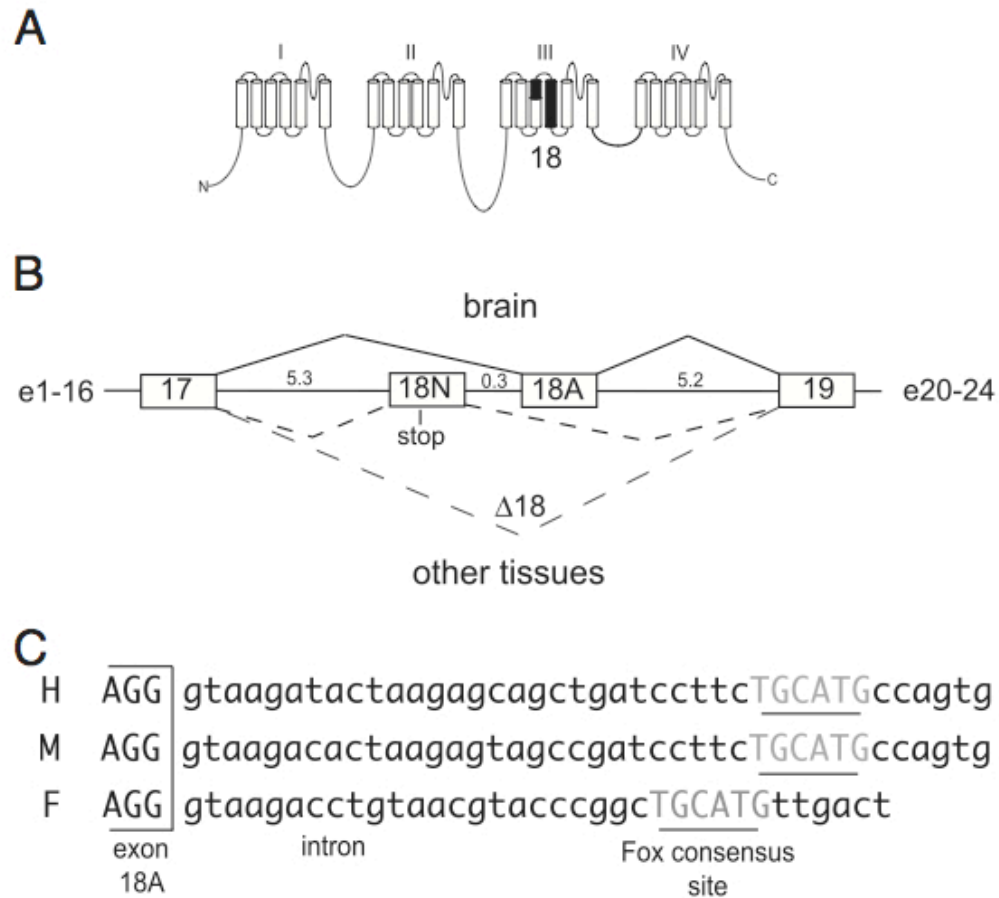


Figure 2.1. Alternative splicing of *SCN8A*. (A) Structure of the full length, four domains, 1980 amino acid residue $\text{Na}_v1.6$ channel protein. The transmembrane segments encoded by exon 18 are shown in black. (B) Genomic structure of exons 18A and 18N. *SCN8A* contains 26 protein coding exons; exons 17 to 19 are expanded. Exon 18N contains an in-frame stop codon. (C) A consensus Fox binding site is located downstream of exon 18A in *SCN8A* genes from human (H), mouse (M) and fugu (F).

transcriptional regulation, by preventing the expression of active channel in non-neuronal cells (Plummer et al., 1997).

The mammalian Fox gene family of RNA binding proteins encodes three related proteins, Rbfox1 (*A2BP1*), Rbfox2 (*RBM9*) and Rbfox3 (*HRNBP3/NeuN*) (Shibata et al., 2000; Lieberman et al., 2001; McKee et al., 2005; Kim et al., 2009). Rbfox1 (Fox-1) and Rbfox2 (Fox-2) are known to regulate neuronal exon splicing (Underwood et al., 2005). In this report, we demonstrate a role for the Fox proteins in the alternative splicing of *SCN8A*.

Materials and Methods

DNA constructs. Fox-1 and Fox-2 cDNAs in the vector pcDNA3.1 were previously described (Underwood et al., 2005) and generously provided by Dr. Douglas Black, UCLA. To generate the *SCN8A* minigene, a 2.6 kb genomic DNA fragment containing exon 18N and exon 18A with 0.9 kb of upstream sequence and 1.2 kb of downstream sequence was amplified from genomic DNA from mouse strain 129X1/SvJ (The Jackson Laboratory, Bar Harbor, ME) and cloned in the vector pDUP4-1 (Modafferi and Black, 1997) (Addgene, Cambridge, MA). pDUP4-1 contains exons 1 and 2 of the beta-globin gene, which provide initiation and termination signals and can be used to distinguish the minigene transcripts from endogenous $Na_v1.6$ transcripts. *Apal* and *BglII* sites were added using primers 1 and 2 (**Table 2.1**). The previously described Fox consensus site mutations TGCgTG and TGacgt (Tang et al., 2009) were introduced into the minigene Fox site 28 bp

downstream of exon 18A by QuikChange Mutagenesis (Agilent) with primer sets 3-4 and 5-6 (**Table 2.1**) using conditions recommended by the supplier.

Cell culture. HEK293T cells were grown in DMEM:F12 media containing 1% Penicillin-Streptomycin supplemented with 10% FBS at 37⁰C in 5% CO₂.

Transfections were performed using Fugene 6 (Roche) and Opti-MEM. HEK293T cells were grown in BD Falcon 6-well plates to 50% confluence and transfected with 2 ug Fox cDNA. Medium was renewed after 24 hours and cells were cultured for an additional 48 hours. For minigene assays, cells were transfected with 1 ug of minigene DNA and 1 ug of Fox cDNA, the medium was changed after 24 hours, and cells were incubated for an additional 24 hours.

RT-PCR. Cells were recovered by scraping into RLT media (Qiagen) with β -mercapthoethanol (0.3 ml/well) and lysed by centrifugation over Qiashedder columns (Qiagen, Valencia, CA). RNA was prepared using the RNEasy kit (Qiagen). Samples were treated with DNase I prior to 1st strand synthesis. cDNA was synthesized from 5 ug RNA using the Superscript 1st strand cDNA kit (Invitrogen, Carlesbad, CA) with an oligo-dT primer for endogenous transcripts and random hexamer probes for minigene transcripts. Primers 11-16 (**Table 2.1**) were used in various combinations for RT-PCR. Amplification was initiated by incubation for 3 min at 94⁰C, followed by 30-40 cycles of 45 seconds at 94⁰C, 45 seconds at 60⁰C, and 45 seconds at 72⁰C, with a final extension for 10 minutes at 72⁰C.

Table 2.1. Primers used in cloning and RT-PCR reactions. Primer concentrations were 5 μ M for RT-PCR and 125 ng/ μ l for Quikchange reactions. F, forward; R, reverse.

Primer	Description	Sequence (5' to 3')
1	Apal exon 18 minigene F	GCGGG CCCCC ATAAT CGGGT ATAAA TAGAA CAGAC TGC
2	BglII exon 18 minigene R	GCGAG ATCTG GTCTC AGAAC TAGCT GATAT GCCGT CACC
3	Fox site 1bp mutant F	GTAGC CGATC CTTCT GCGTG CCAGT GGAAA CTG
4	Fox site 1bp mutant R	CAGTT TCCAC TGGCA CGCAG AAGGA TCGGC TAC
5	Fox site 4bp mutant F	GACAC TAAGA GTAGC CGATC CTTCT GACGT CCAGT GGAAA CTGTT AAAGC ATGCT AG
6	Fox site 4bp mutant R	CTAGC ATGCT TTAAC AGTTT CCACT GGACG TCAGA AGGAT CGGCT ACTCT TAGTG
7	18N 5' splice site mut F	GTGTG TATTT ATCTG TATTC TTTTC CATCT GTTCC ATTAA GTTTG TCTGG
8	18N 5' splice site mut R: 5'	CCAGA CAAAC TTAAT GGAAC AGATG GAAAA GAATA CAGAT AAATA CACAC
9	18N 3' splice site mut F	CAGAC TGTAAGGGC GAGGA CAAGG CTCTT GTCAC CTCTT C
12	18N 3' splice site mut R	GAAGA GGTGA CAAGA GCCTT GTCCT CGCCC TTTAC AGTCT G
11	new exon 17F	AAGTG GACAG CCTAT GGCTT CGTC
12	new exon 19R	AGCCA GAAGA TGAGA CACAC CAGC
13	exon 18A F	CTACT CGGAA CTAGG TGCCA TAAG
14	exon 18A R	CTCTT AAGGG TCTCA AAGCT CTTAG G
15	pDUP4-1 F	CTGAG GAGAA GTCTG CCGTT ACTGC
16	pDUP4-1 R	AACAG CATCA GGAGT GGACA GATCC C

Products were separated on 2% agarose gels, visualized by ethidium bromide staining, and isolated from the gel for sequencing.

Samples of human brain cortex were obtained from the Harvard Brain Tissue Resource Center (#B4925, 9 years; #B3829, 22 years; #B4503, 56 years) and from Stratagene (#540157, fetal 18 weeks). RNA preparation with the Trizol reagent (Invitrogen) and 1st strand cDNA synthesis using Superscript (Invitrogen) were carried out as described (Drews et al., 2005). The quality of RNA preparations was demonstrated by the presence of intact 18S and 28S ribosomal RNA on agarose gels.

Purified neurons, astrocytes and oligodendrocytes. Purified cell populations were isolated at Stanford by the Barres lab and have been characterized in detail (Barres et al., 1988; Barres et al., 1992). Rat retinal ganglion cells (P6-7) and mature oligodendrocytes (P10-12) were purified by immunopanning as described (Goldberg et al., 2002; Dugas et al., 2006). Cells adherent to the final positive selection panning plates after extensive rinsing (T11D7 for RGCs, GC for oligodendrocytes) were scraped off in RLT media. RNA was prepared with the RNEasy kit (Qiagen).

Cortical astroglia (P1-2) were purified by the shake-off method, as described by McCarthy and de Vellis (McCarthy and de Vellis, 1980). Cortical tissue was papain-digested and plated in medium that does not allow neurons to survive. After 4 days, non-adherent cells were removed by shaking and adherent cells were incubated another 2-4 days to allow the monolayer to refill. Medium was then replaced with fresh medium containing AraC (10 mM) to eliminate contaminating

fibroblasts, and incubated for 48 hours. Astrocytes were trypsinized and plated onto 10 cm tissue culture dishes at 2×10^6 cells/plate. After 2 days, cells were removed by scraping for preparation of RNA.

Results

Fox-1 and Fox-2 catalyze splicing of exon 18A from an Scn8a minigene.

We constructed an *Scn8a* minigene containing a 2.6 kb genomic fragment with exon 18N, exon 18A, and adjacent introns, including the Fox binding site located 28 bp downstream of exon 18A (**Figure 2.2A**). In the minigene vector, the *Scn8a* sequences are located between globin exon 1, which provides the initial splice donor site for minigene transcripts, and globin exon 2, which provides the final splice acceptor site. HEK cells transfected with the minigene alone produced transcripts that were spliced from the β -globin donor exon 1 in the construct to exon 18N, and then to globin exon 2, by passing exon 18A completely (**Figure 2.2B**, lane 1). This pattern is typical for non-neural tissues and cells (Plummer et al., 1997). Co-transfection of the minigene with either Fox-1 cDNA or Fox-2 cDNA generated a novel product that contains exon 18A (**Figure 2.2B**). This product results from splicing of the minigene transcript from exon 18N to 18A. This novel transcript is not seen *in vivo*, and may reflect the overexpression of minigene transcript relative to available splice factors, or the absence of a critical factor from HEK cells. However, the production of the 18N plus 18A transcript demonstrates the capability of the Fox proteins to initiate inclusion of exon 18A.

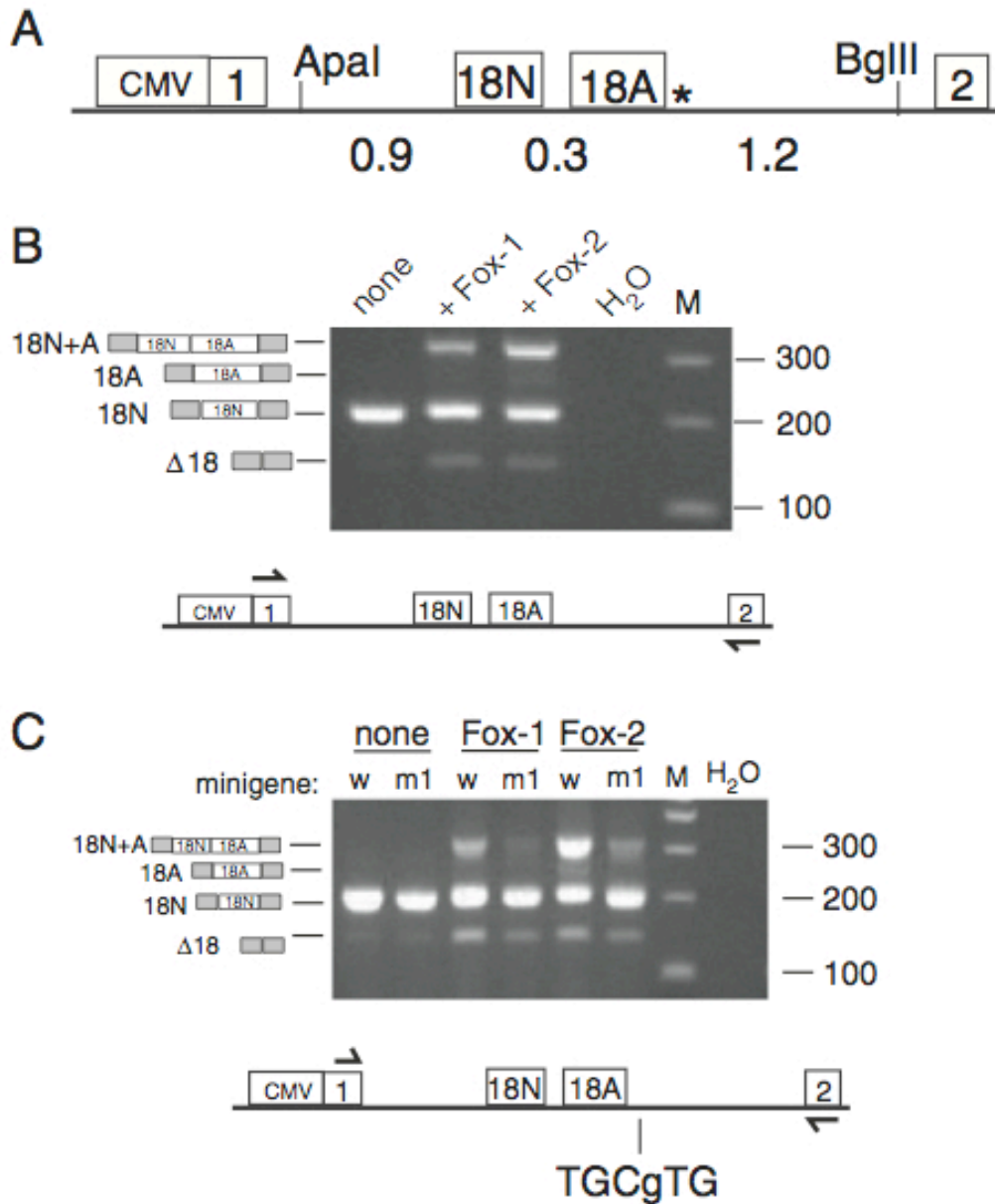


Figure 2.2. Splicing of an *Scn8a* minigene. (A) Structure of the 2.6 kb minigene containing exon 18N, exon 18A, and the Fox binding site TGCATG (asterisk). The CMV promoter and β -globin exons 1 and 2 are indicated; intron sizes in kb; exons not to scale. (B) RT-PCR products amplified from RNA isolated after transfection of HEK cells with the minigene alone (none) or co-transfection with Fox-1 or Fox-2. (C) RT-PCR products from HEK cells transfected with a minigene carrying a 1 bp mutation in the Fox binding site (from TGCATG to TGCgTG). w, wildtype minigene; m1, mutant minigene. RT-PCR primers 15 and 16 in β -globin exons 1 and 2, respectively (Table 2.1). Predicted lengths in bp: 8N + A = 352, 18A = 284, 18N = 229, Δ 18 = 161. The identity of all RT-PCR products in this and other figures was confirmed by sequencing.

Splicing of minigene exon 18A is dependent on the downstream Fox binding site. A perfect copy of the Fox consensus site TGCATG is located 28 bp downstream of exon 18A (**Figure 2.1C**). To determine whether this site is required for splicing of exon 18A by Fox-1 and Fox-2, we introduced a 1 bp mutation that was previously shown to impair Fox protein function (Tang et al., 2009) (**Figure 2.2C**). Co-transfection of the mutated minigene with Fox-1 or Fox-2 resulted in greatly reduced inclusion of exon 18A (**Figure 2.2C**). The data indicate that Fox binding to the consensus site is required for Fox-mediated inclusion of exon 18A.

Fox-1 alters splicing of endogenous SCN8A transcripts in HEK cells. To avoid the high level of minigene transcript expression and to determine whether direct splicing from exon 17 to exon 18A could be generated by the Fox proteins, we examined the splicing of endogenous *Scn8a* transcripts in HEK cells. In non-transfected HEK cells, the 18N and Δ 18 transcripts of *Scn8a* can be detected, but expression of exon 18A is missing, as expected in non-neural tissue (**Figure 2.3A**). Transfection of HEK cells with the Fox-1 cDNA resulted in the appearance of transcripts that are directly spliced from exon 17 to exon 18A, using a reverse primer in exon 18A (**Figure 2.3B**). Fox-1 is thus sufficient to initiate normal inclusion of exon 18A in a non-neuronal cell.

Effect of cycloheximide on transcripts containing exon 18N. The stop codon in exon 18N is located more than 55 bp upstream of the final exon junction, making transcripts containing exon 18N candidates for nonsense-mediated decay (Nicholson et al., 2010). Since cycloheximide inhibits the pioneer round of mRNA

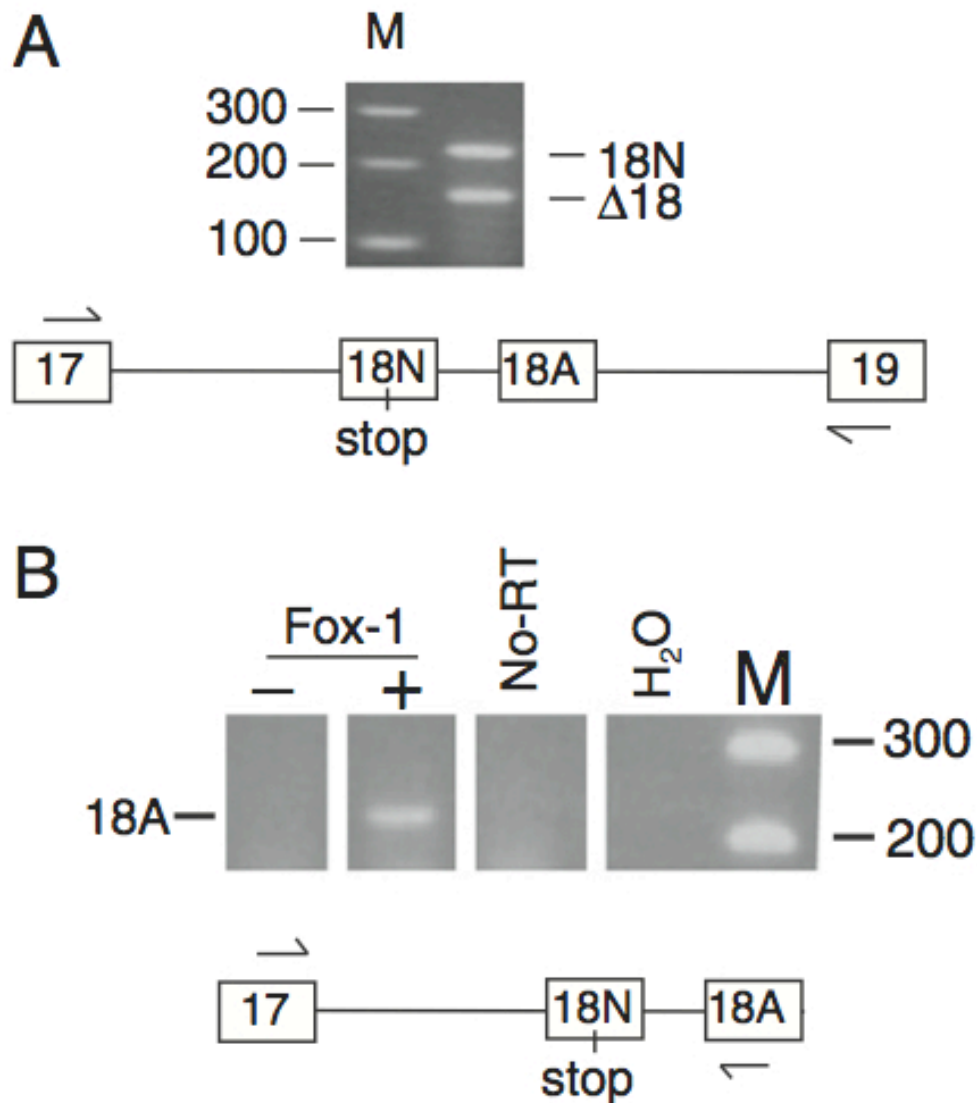


Figure 2.3. Splicing of endogenous *SCN8A* transcripts in HEK cells. (A) RT-PCR products amplified from RNA from untransfected HEK cells with a forward primer in exon 17 and reverse primer in exon 19. PCR product lengths: 18N = 216 bp; Δ18 = 146 bp. The product containing 18A (269 bp) is not present. (B) Transcripts containing exon 18A alone can be amplified only after transfection of the Fox-1 cDNA. Forward primer in exon 17, reverse primer in exon 18A. M, markers: 100-bp ladder.

translation that is required for nonsense-mediated decay, it can be used as an indicator of transcript susceptibility to nonsense-mediated decay. In untreated HEK cells, as shown above, the abundance of transcripts containing exon 18N is low (**Figure 2.4A**). However, treatment with cycloheximide for 5 hours resulted in a substantial increase in the abundance of exon 18N-containing transcripts (**Figure 2.4A**). There was no increase of $\Delta 18$ transcripts amplified by the same primers (**Figure 2.4A**) or of the control transcripts *ATP7A* and *FIG4* that lack internal in-frame stop codons (**Figure 2.4B**). Although cycloheximide does not specifically affect the proteins involved in nonsense mediated decay, the data are consistent with the possibility that transcripts containing exon 18N are degraded *in vivo* by nonsense-mediated decay.

Transcripts containing exon 18A are present in neurons but not in two types of glia. It was previously reported that cultured hippocampal neurons express *Scn8a* transcripts containing exon 18A but epithelial cells from the inner ear do not (Mechaly et al., 2005). To extend this limited data, we examined astrocytes, oligodendrocytes and retinal ganglion neurons purified from whole rat brain between postnatal days P1 and P12. The characteristics of these purified cells have been described in detail (Barres et al., 1988; Barres et al., 1992). During the first two weeks of postnatal life, there is a major switch in the proportion of *Scn8a* transcripts containing exon 18A in rat brain. At P1, there is a comparable abundance of transcripts with and without exon 18A, while at P12 there is a large excess of transcripts containing exon 18A (**Figure 2.5A**). In cells isolated during this time

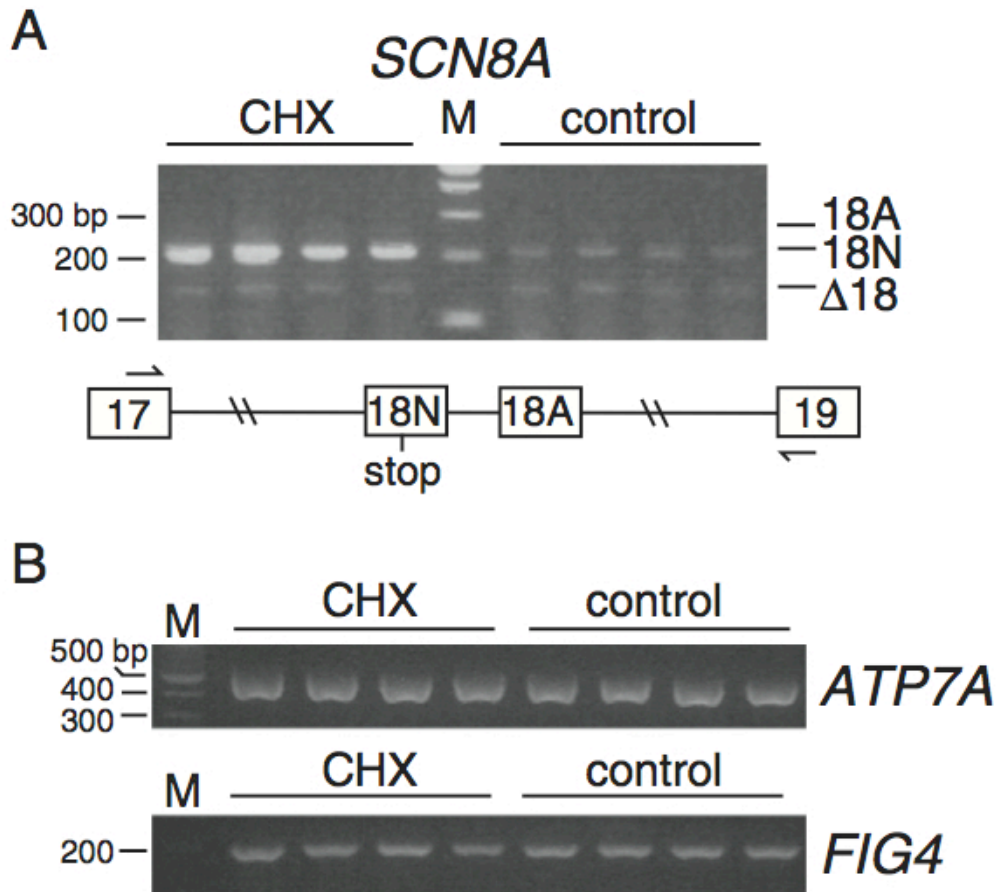


Figure 2.4. Treatment with cycloheximide increases the abundance of *SCN8A* transcripts containing exon 18N. (A) HEK cells were incubated with cycloheximide (CHX, 500 μ g/ml) for 5 h. RT-PCR was carried out with primers 11–12 (**Table 2.1**). Product sizes: 18N = 216 bp, Δ 18 = 146 bp. (B) RT-PCR products from transcripts of *ATP7A* and *FIG4* that do not contain in-frame stop codons. Control, no CHX.

interval, there was robust expression of exon 18A in the purified retinal ganglion neurons (**Figure 2.5A**). In contrast, exon 18A could not be detected in RNA from purified astrocytes or oligodendrocytes (**Figure 2.5A**). This data provides experimental support for the view that transcripts encoding the full length $\text{Na}_v1.6$ channel in brain are concentrated in neuronal cells as a consequence of neuron-specific splicing of exon 18A.

Developmental switch in splicing of human SCN8A. The expression of alternatively spliced transcripts of *SCN8A* in human brain has not previously been characterized. In human fibroblasts, transcripts containing exon 18N and the $\Delta 18$ transcript can be amplified, similar to human HEK cells (**Figure 2.5B**). In fetal brain at 18 weeks of gestation, transcripts containing exon 18A are present, at comparable levels to the other two transcripts (**Figure 2.5B**). By 10 months postnatal, there is only small increase in the proportion of *SCN8A* transcripts containing exon 18A, relative to the two non-neuronal transcripts. The pattern in human brain at 10 months is similar to rodent brain in the early postnatal period up to weaning (**Figure 2.5A** and (Plummer et al., 1997)). By 9 years of age, transcripts containing exon 18A predominate, and the other transcripts were not detected. This pattern persists in at 22 years and 56 years of age (**Figure 2.5B**). The developmental switch to predominance of exon 18A is conserved in human brain, and appears to be delayed until later than 10 mos of age.

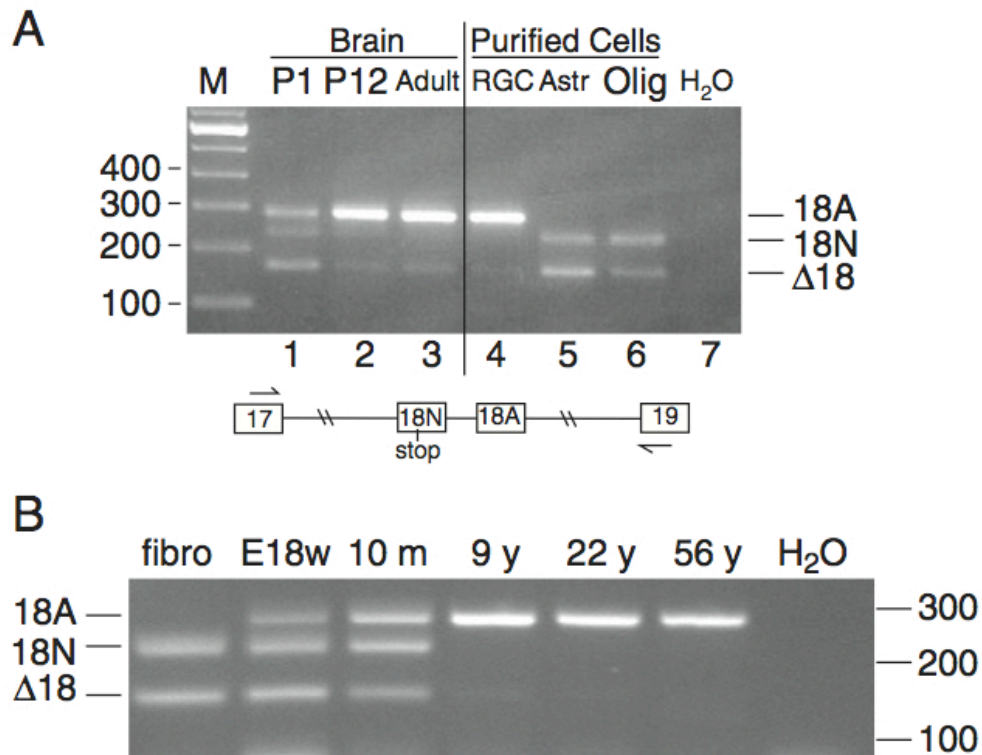


Figure 2.5. *SCN8A* expression in purified neurons and human brain. (A) RT-PCR of RNA from rat brain at ages P1, P12 and adult demonstrates the postnatal switch to transcripts containing exon 18A. Purified retinal ganglia neurons (RGC) (P6–7) express predominantly exon 18A. Purified astrocytes (P1) and oligodendrocytes (P12) do not contain transcripts with exon 18A. M, molecular weight markers in bp. (B) Time course of developmental switch to exon 18A in human brain. The pattern is delayed in comparison with rodent brain; the human pattern at 10 months postnatal resembles rodent brain at postnatal day 1 (P1). fibr, human fibroblast control; E18w, 18 weeks of gestation. Forward primer in exon 17, reverse primer in exon 19; predicted product sizes, 18A = 286, 18N = 231, Δ18 = 163; identity of RT-PCR products was confirmed by sequencing. M, molecular weight markers in bp.

Discussion

Fox proteins and splicing of SCN8A exon 18A. The experiments described here provide evidence for a direct role of the neuronal splice factors Fox-1 and Fox-2 in generation of *SCN8A* transcripts that contain exon 18A and encode the active channel protein. These observations provide a satisfying answer to the mechanism of tissue specificity raised when this pair of duplicated, alternatively spliced exons was described 14 years ago (Plummer et al., 1997). The negative effect of mutating the Fox consensus binding site in the minigene construct strongly supports the role of the Fox proteins in splicing of exon 18A.

Recent studies using knock-out mice provide supporting evidence that the Fox proteins are involved in splicing of exon 18A *in vivo*. Mice with inactivation of *Rbfox1* were recently described, but splicing of exons 18A and 18N was not included in that study (Gehman et al., 2011). However, in mice that are homozygous for inactivation of Fox-2 and heterozygous for inactivation of Fox-1, the proportion of cerebellar *Scn8a* transcripts containing exon 18A is reduced from 80% to 40% (Gehman et al., 2012). The analysis of transfected cells described here, together with the observations in the knock-out mice, provide strong evidence that Fox-1 and Fox-2 contribute to the neuronal expression of full-length $\text{Na}_v1.6$ in mammalian brain.

This conclusion is consistent with previous evidence that the Fox proteins are expressed in neurons (Underwood et al., 2005; Cahoy et al., 2008; Tang et al., 2009). During development of mouse brain, both Fox proteins and *SCN8A* are first detected at embryonic day 12 (Plummer et al., 1997; Underwood et al., 2005; Tang

et al., 2009), and in cultured P19 cells, differentiation towards a neuronal cell fate results in up-regulation of Fox-1 as well as initiation of splicing of *Scn8a* exon 18A (Plummer et al., 1997; Hakim et al., 2010). Fox proteins were previously shown to regulate splicing of another neuronal voltage-gated ion channel gene, $Ca_v1.2$ (Tang et al., 2009), and 5 statistically significant changes in ion channel splicing were recently observed in Fox-1^{-/-} mouse brain (Gehman et al., 2011).

Other cis elements contributing to alternative splicing of exon 18.

Zubovic and colleagues identified an exonic splice enhancer (ESE) in exon 18N and an exonic splice silencer (ESS) in exon 18A (Zubovic et al., 2012). Inclusion of exon 18N and exclusion of exon 18A is greatly supported by the binding of the splice factors SRSF1/2 to the ESE in exon 18N together with binding of hnRNPs and PTB to the ESS in exon 18A. The binding of *trans* splice factors to these *cis* elements along with the binding of Rbfox proteins creates a combinatorial control that results in the *in vivo* splicing pattern of exon 18 (Zubovic et al., 2012).

Fox proteins and Scn8a in non-neural tissues. In addition to neuronal expression, Fox proteins are expressed in ovary and heart (Underwood et al, 2005). We recently reported the presence of transcripts containing exon 18A in isolated cardiac ventricular myocytes (Noujaim et al, 2011), and $Na_v1.6$ protein has been detected by immunostaining in transverse tubules of ventricular myocytes (Maier et al., 2004; Du et al., 2007; Lopez-Santiago et al., 2007). Fox proteins have also been detected in oligodendrocyte precursors, but not in mature oligodendrocytes (Underwood et al., 2005; Cahoy et al., 2008). Similarly, sodium currents have been observed in oligodendrocyte precursors but not in mature oligodendrocytes (Barres

et al., 1990; De Biase et al., 2010). Sodium currents have also been detected in other types of glia (Karadottir et al, 2008; Steinhauser et al, 2002). These observations suggest that Fox proteins may play a role in expression of full length $Na_v1.6$ in non-neuronal cells.

Biological function of alternative exon 18N with the in-frame stop codon.

Exons containing an in-frame stop codon have been referred to as “poison cassettes” (Lareau et al., 2007) that induce nonsense-mediated decay and down-regulate gene expression (Nicholson et al., 2010). Based on DNA sequence alone, inclusion of exon 18N appears to be favored over exon 18A by higher G-C content of adjacent introns and the more favorable nucleotide at the -6 position of the splice acceptor site . Although the level of *SCN8A* transcripts in non-neuronal cells is low, even a small amount of sodium channel protein in these cells could be deleterious to the maintenance of cellular membrane potential (Williams, 1970). Thus the requirement for a neuronal splice factor to generate active channel protein provides added protection against negative effects of low-level expression of channel protein in non-neuronal cells (**Figure 2.6**).

The cockroach sodium channel *para* contains three alternatively spliced copies of the exon that corresponds to $Na_v1.6$ exon 18. The copy designated G3 contains an in-frame stop-codon and incorporation of this exon results in a truncated protein that is nearly identical to the 18N protein (Tan et al., 2002). The available genomic sequence for sodium channels from other invertebrates and vertebrates is not of sufficient quality to determine whether *para* exon G3 and vertebrate exon 18N are derived from a common ancestor or are of independent origin. The truncated

cockroach sodium channel protein failed to generate sodium currents in the *Xenopus* oocyte system (Tan et al., 2002). This is consistent with biophysical studies of site-directed channel mutations in domain 3 that inactivate channel activity (Stuhmer et al., 1989). Truncating mutations of *SCN1A* in patients with Dravet Syndrome that are in domain 3 are clinically as severe as stop codons near the N-terminus of the protein, supporting the view that truncation in domain 3 inactivates the channel (Meisler and Kearney, 2005b). These observations indicate that the truncated Na_v1.6 protein encoded by exon 18N is unlikely to retain channel activity. Consistent with our evidence for nonsense-mediated decay of transcripts containing exon 18N, we have been unable to detect the truncated protein on Western blots of brain homogenates or purified membrane fractions (unpublished observations).

Relationship to alternative exons 5A and 5N. *SCN8A* contains another pair of duplicated, developmentally regulated alternative exons, 5N and 5A, that share a common evolutionary origin with exon 18N and exon 18A (Plummer et al., 1997; Plummer and Meisler, 1999). The structural relationship between the two pairs of exons predicts that the exon duplication event occurred in a two-domain channel prior to generation of the modern four-domain channel. There is a consensus Fox binding site located 359 bp downstream of exon 5A which could enhance inclusion of this exon (Kuroyanagi, 2009), and splicing of exon 5A is reduced in Fox-1^{-/-} mice (Gehman et al., 2011). Exons 5A and 5N confer different biophysical properties in the paralogous channel *SCN5A*, and the splicing switch from exon 5N to exon 5A may be important during neuronal development (Onkal et al., 2008). Additional

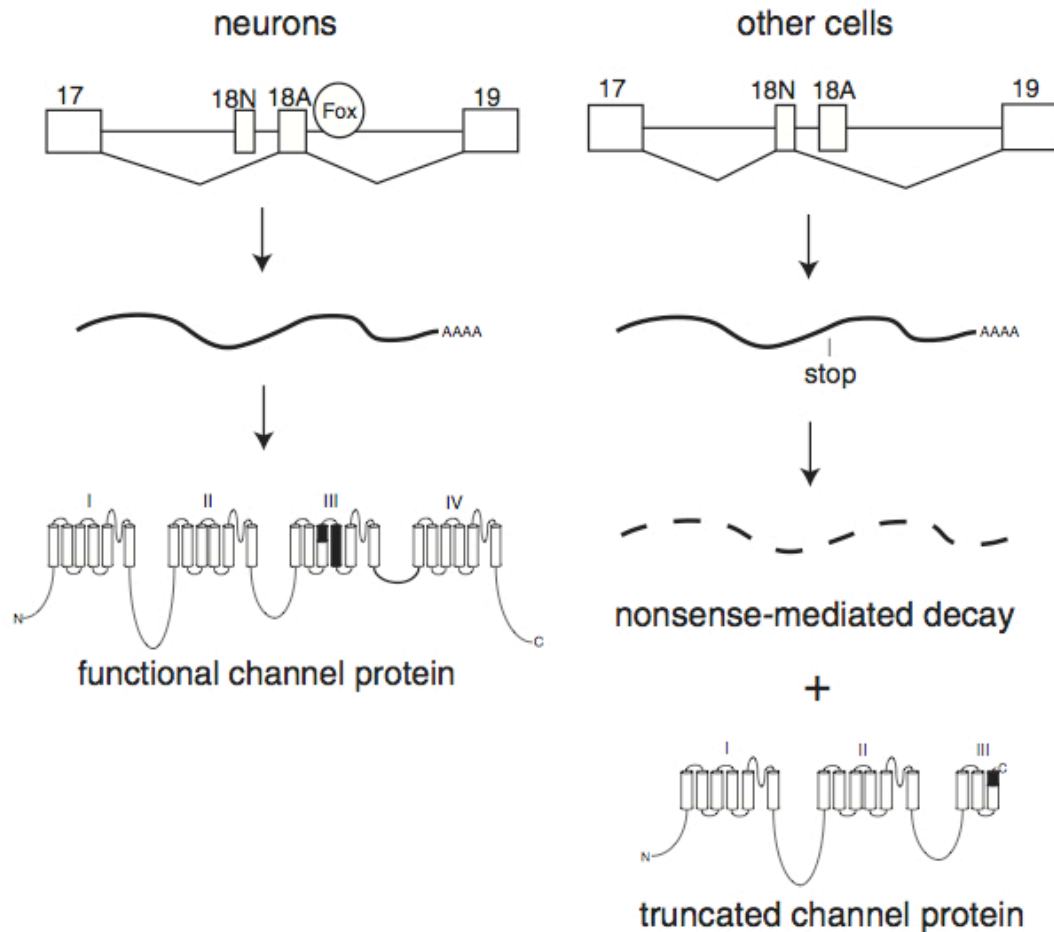


Figure 2.6. Model for restriction of active $\text{Na}_v1.6$ channels to neurons. Splice factors Fox-1 and Fox-2 in neurons generate transcripts containing exon 18A that encode the active sodium channel. In the absence of Fox-1 and Fox-2 in non-neuronal cells, transcripts containing exon 18N are produced and degraded by nonsense-mediated decay. Translation of remaining 18N transcripts generates a truncated protein lacking channel activity (Plummer et al., 1997). The much greater total abundance of $\text{Na}_v1.6$ transcripts in neurons compared with other cells is also a consequence of regulation at the level of transcription.

heterogeneity of *SCN8A* brain transcripts results from use of four alternative 5-noncoding exons and two alternative polyadenylation sites (Drews et al., 2005).

Non-coding regulatory elements and disease. Trans-acting genetic variation in the splice factor *SCNM1* and cis-acting variation in its binding site in exon 3 of *Scn8a* both modify disease severity in *Scn8a^{medJ}* mice (Buchner et al., 2003; Howell et al., 2007). Similarly, mutations in the Fox protein coding sequence or in its binding sites in *SCN8A* could influence the level of expression of full-length $\text{Na}_v1.6$. Haploinsufficiency of $\text{Na}_v1.6$ results in anxiety-related behavior and impaired sleep in the mouse (McKinney et al., 2008; Papale et al., 2010), and cognitive impairment in human patients (Trudeau et al., 2006). Cognitive impairment is also seen in patients with Fox-1 mutations (Bhalla et al., 2004; Martin et al., 2007a), and copy number variants of Fox-1 have been associated with autism (Sebat et al., 2007). The overlap in phenotypes suggests that impaired splicing of *SCN8A* could contribute to the neuropsychiatric effects of Fox-1 mutations. The functional relationship between *SCN8A* and Fox proteins described here will contribute to understanding genetic interactions between these loci and their role in human disease.

Acknowledgements

We are grateful to Dr. Douglas Black for providing the Fox-1 and Fox-2 cDNA constructs and for sharing unpublished data. We thank Dr. Raymond Chan for helpful discussion and critical reading of the manuscript. HEK293T cells were provided by Dr. Lori Isom. This work was supported by USPHS research grant RO1

NS34509 from the NIH to MHM. JCD and BAB were supported by grant RG4059A8 from the National Multiple Sclerosis Society. JEO acknowledges support from the NIH Predoctoral Training Program in Genetics (T32 GM 007544) and the Rackham School of Graduate Studies at the University of Michigan.

Chapter III

Interaction of voltage-gated sodium channel Na_v1.6 (SCN8A) with microtubule-associated protein Map1b²

Abstract

The mechanism by which voltage-gated sodium channels are trafficked to the surface of neurons is not well understood. Our previous work implicated the cytoplasmic N-terminus of the sodium channel Na_v1.6 in this process. We report that the N terminus plus the first transmembrane segment (residues 1-153) is sufficient to direct a reporter to the cell surface. To identify proteins that interact with the 117 residue N-terminal domain, we carried out a yeast-two-hybrid screen of a mouse brain cDNA library. Three clones containing overlapping portions of the light chain of microtubule associated protein Map1b (*Mtap1b*) were recovered from the screen. Interaction between endogenous Na_v1.6 channels and Map1b in mouse

²This work has been published in: O'Brien, J.E., Sharkey, L.M., Vallianatos, C.N., Han, C., Blossom, J.C., Yu, T., Waxman, S.G., Dib-Hajj, S.D., and Meisler, M.H. (2012). Interaction of voltage-gated sodium channel Nav1.6 (SCN8A) with microtubule-associated protein Map1b. *J Biol Chem* 287, 18459-18466, with the exception of the text of the results describing Figure 3.4A.

brain was confirmed by co-immunoprecipitation. Map1b interacts with the N-termini of the related channels Na_v1.1 and Na_v1.2 with reduced affinity. Alanine-scanning mutagenesis of the Na_v1.6 N-terminus demonstrated that residues 77 to 80 (VAVP) contribute to interaction with Map1b. Co-expression of Na_v1.6 with Map1b in neuronal cell line ND7/23 resulted in a 50% increase in current density, demonstrating a functional role for this interaction. Mutation of the Map1b binding site of Na_v1.6 prevented generation of sodium current in transfected cells. The data indicate that Map1b facilitates trafficking of Na_v1.6 to the neuronal cell surface.

Introduction

The voltage-gated sodium channel Na_v1.6 is widely expressed in neurons of the central and peripheral nervous system, and is highly concentrated at the axon initial segment and nodes of Ranvier (Schaller and Caldwell, 2000; Lorincz and Nusser, 2010). Na_v1.6 is required for repetitive firing and generation of resurgent currents in cerebellar Purkinje cells (Raman et al., 1997; Khaliq et al., 2003; Levin et al., 2006) and sensory neurons in dorsal root ganglia (Cummins et al., 2005), and contributes to firing patterns in other types of neurons [reviewed in (O'Brien et al., 2012)]. Spontaneous mutations of Na_v1.6 in the mouse result in neurological disorders including tremor, dystonia, ataxic gait, paralysis and juvenile lethality (Meisler et al., 2004). Two mutations of human *SCN8A* have been described, an inherited protein truncation allele in a family with ataxia and cognitive impairment (Trudeau et al., 2006), and a *de novo* gain-of-function mutation in a child with epileptic encephalopathy (Veeramah et al., 2012).

Voltage-gated sodium channels interact with multiple binding partners that regulate gating properties and subcellular localization (Dib-Hajj and Waxman, 2010). Several protein interaction sites have been mapped to the intracellular loops and C-terminus of the channels. Sequence analysis has identified putative protein-protein interacting motifs and sites for post-translational modification. The only previously described interaction of the N-terminus with cytoplasmic proteins is the specific interaction of Na_v1.8 with the annexin II light chain, which increases channel trafficking to the plasma membrane (Okuse et al., 2002; Poon et al., 2004).

We recently characterized the ENU-induced mouse mutant *Scn8a*^{ataxia3}, in which the amino acid substitution S21P results in trapping of the Na_v1.6 channel protein in the Golgi (Sharkey et al., 2009a). The location of this mutation in the N-terminus suggested that this region might be involved in protein-protein interactions required for trafficking of the channel protein to the cell surface. To test this prediction, we carried out a yeast-two-hybrid screen of a mouse brain cDNA library to identify proteins that interact with the 117 residue N-terminus of the channel. We now report the interaction of Na_v1.6 with the light chain of Map1b, a cytoskeletal protein that binds microtubules and actin (Riederer, 2007). The major sites of expression of Map1b are brain and spinal cord. Among other known cargoes, the light chain of Map1b binds and transports two neuronal membrane-bound proteins, the 5-HT_{3a} receptor (Sun et al., 2008) and the NMDA receptor subunit N3A (Eriksson et al., 2010). The work reported here provides evidence that Na_v1.6 is subject to microtubular transport to the plasma membrane mediated by interaction with the light chain of Map1b.

Materials and Methods

Yeast-two-hybrid assay. The cytoplasmic N-terminus of Na_v1.6 (residues 1-117) was amplified from mouse brain cDNA (strain C57BL/6J) and cloned into the vector pGBKT7 for use as 'bait' in the yeast two hybrid screen. The prey consisted of the mouse brain cDNA library in the vector pGADT7 (Clontech #630489). The yeast-two hybrid screen and directed tests were performed according to recommendations except that yeast were prepared for transformation by placing a 2-3 mm colony into 50 mL YPDA broth. The culture was incubated at 30 °C for 16-20 hours until OD₆₀₀ >1.5. The culture was diluted in YPDA to an OD of 0.2-0.3 and incubated, with shaking, at 30 °C, until an OD=0.4-0.6 was reached. Transformation of yeast with 0.5 ug of each plasmid was performed using the Clontech Yeastmaker Yeast Transformation System 2 protocol (Clontech #630439). All transformed yeast grew on –Leu/-Trp media, which selects for presence of the bait and prey constructs. Interactants were identified by growth on selective –Leu/-Trp/-His/-Ade media which requires interaction between the transformed proteins. The cDNA fragment encoding Map1b (residues 1924-2464) was amplified from mouse brain cDNA and cloned into pGADT7. This fragment encodes the 541 C-terminal residues of Map1b, including the approximately 374 residues of the light chain (Riederer, 2007). The stability of the encoded protein fragment in transfected cells was demonstrated by Western blot. Hybrid N-terminal constructs were cloned by PCR fusion of cDNA residues 1-54 of Na_v1.1 and 55-117 of Na_v1.6 (1A/8A), or residue 1-54 of Na_v1.6 and 55-117 of Na_v1.1 (8A/1A). The fusion products were

cloned into pGBKT7. Deletion constructs based on *NdeI* and *EcoRI* restriction sites were generated in vector pGBKT7 by Dr. W. Clay Brown at the High Throughput Protein Lab, Life Sciences Institute, University of Michigan. Alanine residues were introduced into the N-terminal domain of Nav1.6 by Quikchange XL mutagenesis (Agilent) using the primers listed in **Table 3.1**.

Cloning of the Nav1.6-CD74 fusion protein. A cDNA fragment encoding the N-terminus plus first transmembrane segment of *Scn8a* (residues 1-153) was amplified from the Nav1.6 cDNA clone pcDNA3mod-Nav1.6_R (Herzog et al., 2003a). The pcDNA3-CD74 clone encoding full length human CD74 (residues 1-232), was provided by Dr. Blanch Schwappach, University of Manchester, U.K. (Zuzarte et al., 2009). Residues 1-71 of CD74 were replaced with residues 1-153 of Nav1.6, which removed the cell surface localization signal in the first transmembrane domain of CD74 (Zuzarte et al., 2009). The *ataxia3* mutation p.S21P was introduced into the Nav1.6-CD74 fusion protein by Quikchange XL mutagenesis (Agilent). The coding regions of all constructs were analyzed by Sanger sequencing at the University of Michigan DNA Sequencing core before use in transfection experiments.

Site-directed mutagenesis of the Nav1.6_R cDNA clone. The VAVP(77-80)AAAA mutation was introduced into the tetrodotoxin-resistant Nav1.6 cDNA clone Nav1.6_R (Herzog et al., 2003a) by Quikchange XL mutagenesis (Agilent) using the primers listed in Table 3.1. The entire 6-kb open reading frame was sequenced to confirm the absence of additional mutations prior to functional testing.

Table 3.1. Alanine scanning Quikchange forward primer sequences. Reverse primers are the reverse complement of the forward primer.

	Forward Primer Sequence 5' to 3'
Residue 73-76 AAAA	GAAGA GTTTG CCTTT CATCT ACGGG GACAT CGCGG CAGCC GCGGT TCGG TTCCC CTGGA GGACT TTGAC
Residue 75-78 AAAA	GAAGA GTTTG CCTTT CATCT ACGGG GACAT CCCGC AAGCC GCGGC TCGG TTCCC CTGGA GGACT TTG
Residue 77-80 AAAA	CTTTC ATCTA CGGGG ACATC CCGCA AGGCC TGGCT GCGGC TGCCC TGGAG GACTT TGACC CGTAC TATTT G
Residue 79-82 AAAA	CTTTC ATCTA CGGGG ACATC CCGCA AGGCC TGGTT GCGGC TGCCG CGGCG GACTT TGACC CGTAC TATTT G
Residue 81-84 AAAA	GACAT CCCGC AAGGC CTGGT TCGG TTCCC GCGGC GGCCG CTGAC CCGTA CTATT TGACG CAGAA AACTT TTGTA GTATT AAAC
Residue 83-86 AAAA	CAAGG CCTGG TTGCG GTTCC CCTGG AGGCC GCTGC CGCGT ACTAT TTGAC GCAGA AAAC TTTG
Residue 85-88 AAAA	CAAGG CCTGG TTGCG GTTCC CCTGG AGGAC TTTGC CGCGG CCGCT TTGAC GCAGA AAAC TTTGT AGTAT TAAAC
Residue 87-90 AAAA	CTGGT TCGG TTCCC CTGGA GGACT TTGAC CGGC CGCTG CGGCG CAGAA AACTT TTGTA GTATT AAACA GAGGG AAAC

Immunocytochemistry. HEK293 cells were transfected with 6 ug of DNA using Fugene 6 (Roche). Glass coverslips (Fisherbrand Microscope Coverglass, 12-545-81, 12CIR.-1.5) were prepared for cell culture by coating with poly-L-lysine (Sigma, 0.01% solution, P4832) and sterilized under UV light. After 24 hours, transfected cells were washed with sterile PBS and fixed with 4 % paraformaldehyde-PBS solution (16% PFA, Thermo Scientific, product # 28908). Cells were blocked in 10% donkey serum in PBS (Sigma D9663) and incubated at 4 °C overnight with a 1:750 dilution of anti-CD74 (Santa Cruz Biotechnology CD74 (C-16) goat polyclonal IgG, sc-5438) in 20% donkey serum-PBS. Incubation with DAPI and the secondary antibody, donkey anti-goat (Alexa Fluor-488, Invitrogen, A11055, 1:1000 in 1% donkey serum/PBS) was carried out at room temperature for 1 hour. Coverslips were mounted on glass slides (Fisherbrand Superforst Microscope Slides, precleaned, cat# 12-550-143) with Invitrogen ProLong Gold antifade reagent (P36930). Imaging was performed at the University of Michigan Microscopy and Image Analysis Laboratory using an Olympus FluoView 500 Laser Scanning Confocal Microscope mounted on Olympus IX-71 inverted microscope.

Immunoprecipitation and western blotting. HEK-293 cells were co-transfected with Na_v1.6-CD74 and myc-Map1b as described above. Cell extracts were prepared and immunoprecipitated as described (McEwen et al., 2004). 10 cm plates of confluent cells were lysed in 1 ml of buffer containing 60 mM Tris HCl, pH 7.5, 180 mM NaCl, 1% TritonX-100, and 6 mM EDTA. Lysates were pre-incubated for 1 hr at 4 °C with 5 ul IgG and washed Protein G Sepharose beads. After centrifugation, the supernate was incubated for 1 h at 4 °C with primary antibody, 25

ul anti-CD74 (Santa Cruz Biotechnology, Inc., sc-5438) or 5 ul monoclonal anti-c-myc (Clonotech, 3631206). Protein G Sepharose beads were added and incubated for 1 hr at 4 °C. Beads were centrifuged and washed 3x; the final wash buffer included 0.1% TritonX-100 and 0.02% SDS. Proteins were eluted into 80 ul of electrophoresis sample buffer (0.125 M Tris HCl pH 6.8, 2.5% SDS, 0.025% bromophenol blue, 1 mM β -mercaptoethanol, and 22.5% glycerol in 0.5X PBS). Western blotting was carried out with antibody to CD74 (1:200) and c-myc (1:500) as previously described (Sharkey et al., 2009a).

Brain membrane fractions were prepared from wild type and *Scn8a*^{medTg} null homozygous mice by homogenation in 50 mM Tris HCL, pH 7.5, containing 10 mM EGTA and 5 tablets of Roche Complete Mini Protease Inhibitor Cocktail per 50 ml of buffer. After centrifugation at 3,500 rpm, membrane proteins were pelleted from the supernate by centrifugation at 100,000 x g for 30 min. The membrane pellet was suspended in 0.2 ml of homogenation buffer by titration and 25 ul aliquots were stored at -80°C. For immunoprecipitation, one aliquot of stored membrane protein was diluted to 1 ml in 60 mM Tris HCl buffer containing 1% Triton X-100 (see above) and incubated with 5 ug monoclonal pan-neuronal sodium channel antibody (Sigma, S8809-1MG) for 8 hr at 4 °C. Western blotting was carried out with polyclonal antibody to Na_v1.6 (Alomone, ASC-009, 1:100) or polyclonal antibody to the light chain of Map1b (Santa Cruz Biotechnology, Inc., sc-8971, 1:100).

Electrophysiology. The DRG-derived cell line ND7/23 (Wood et al., 1990) was cultured on 12-mm glass coverslips coated with poly-D-lysine/laminin (BD Biosciences) and transfected using Lipofectamine 2000 (Invitrogen) with 1 ug

DNA/well (0.6 ug of Nav1.6 cDNA, 0.2 ug of pEGFP-C1 (Clontech), and 0.2 ug of either vector pcDNA3 (Clontech) or the Map1b cDNA construct. After 48 hours, cells with robust green fluorescence were selected for recording. Whole-cell voltage-clamp recording was done essentially as described previously (Sharkey et al., 2009b) with a few modifications: 1) EPC-9 amplifier (HEKA Electronics, Lambrecht/Pfalz, Germany) was used in this study; 2) data were filtered at 2.9 kHz, and sampled at a rate of 20 kHz; 3) current-voltage relationship was determined by recording from cells held at -120 mV and stepped to a range of potentials (-80 to 40 mV in 5 mV increments) for 100 ms each; 4) Steady-state fast-inactivation was achieved with a series of 500 ms prepulses (-150 to 0 mV in 10 mV increments), and the fraction of non-inactivated channels were measured by a 40 ms test pulse to 0 mV; 5) dextrose instead of sucrose was used to adjust the osmolarity of pipette solution (315 mosmol/lit) and external solution (323 mosmol/lit); 6) data were analyzed using Pulsefit 8.74 software (HEKA Electronics) and OriginPro 8.1 software (Microcal Software, Northampton, MA), and statistical significance was tested using unpaired Student's t test because data followed a normal distribution.

Results

Cell membrane localization of the CD74 reporter. To determine whether the N-terminus of Nav_v1.6 is sufficient to direct protein localization to the cell membrane, we used the extracellular domain of CD74 (residues 72-232) as a cell surface reporter (Zuzarte et al., 2009). Transfection of HEK293 cells with the CD74 extracellular fragment alone yields diffuse cytoplasmic staining (**Figure 3.1A**). We

cloned a hybrid construct containing the N-terminus and 1st transmembrane segment of Na_v1.6 (residues 1-153) upstream of the extracellular domain of CD74. This protein is localized to the cell surface (**Figure 3.1B**). Introduction of the ataxia3 mutation p.S21P into the hybrid construct did not prevent surface localization (**Figure 3.1C**). The S21P mutation does prevent surface localization of full length Na_v1.6 in primary cultured neurons; the reason for the lack of effect on the CD74 construct in HEK cells is not clear. The experiments indicate that additional residues in the N-terminus are involved in transport of Na_v1.6 to the cell surface.

Yeast-two-hybrid screen. To identify proteins involved in surface localization of Na_v1.6, we screened a mouse brain cDNA library using the N-terminal fragment of Na_v1.6 (residues 1-117) as bait (**Figure 3.2A**). Growth on selective medium identified three independent overlapping clones containing portions of the light chain of the microtubule-associated protein Map1b (**Figure 3.2B**). The interaction was confirmed by a directed yeast-two-hybrid assay using a 541-residue Map1b fragment (residues 1924-2464) including the light chain (**Figure 3.2C**).

Interaction between the Na_v1.6-CD74 fusion protein and Map1b. To determine whether the N-terminus of Na_v1.6 interacts with Map1b in mammalian cells, we cloned the Map1b fragment into the myc-tagged mammalian expression vector pCMV-myc. myc-Map1b and the fusion protein Na_v1.6-CD74 were co-transfected into HEK293 cells. Lysates from co-transfected cells were immunoprecipitated with antibody against CD74 and Western blots were probed with anti-myc antibody. A band corresponding to the myc-tagged Map1b was detected in

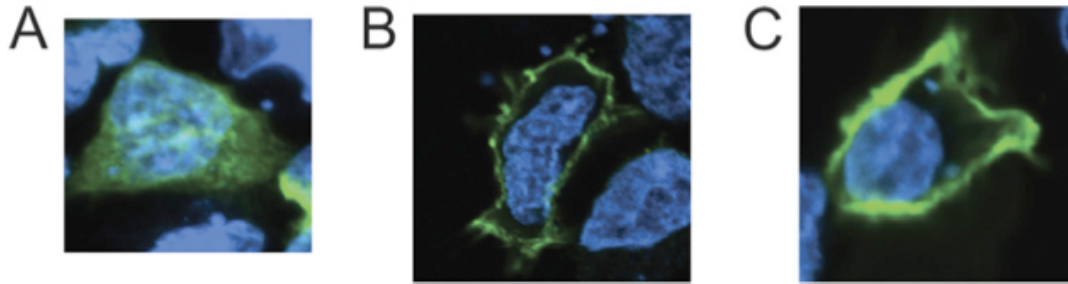


Figure 3.1. The N-terminus and first transmembrane segment of Na_v1.6 are sufficient to direct a reporter protein to the cell surface. Confocal images of HEK293 cells transfected with the reporter constructs and probed with anti-CD4 antibodies are shown. Green, anti-CD74; blue, DAPI. (A) extracellular domain of CD74 lacking membrane-targeting N-terminus. (B) N-terminus and first transmembrane segment of Na_v1.6 fused to the extracellular domain of CD74. (C) *ataxia3* mutation S21P not disrupting surface localization.

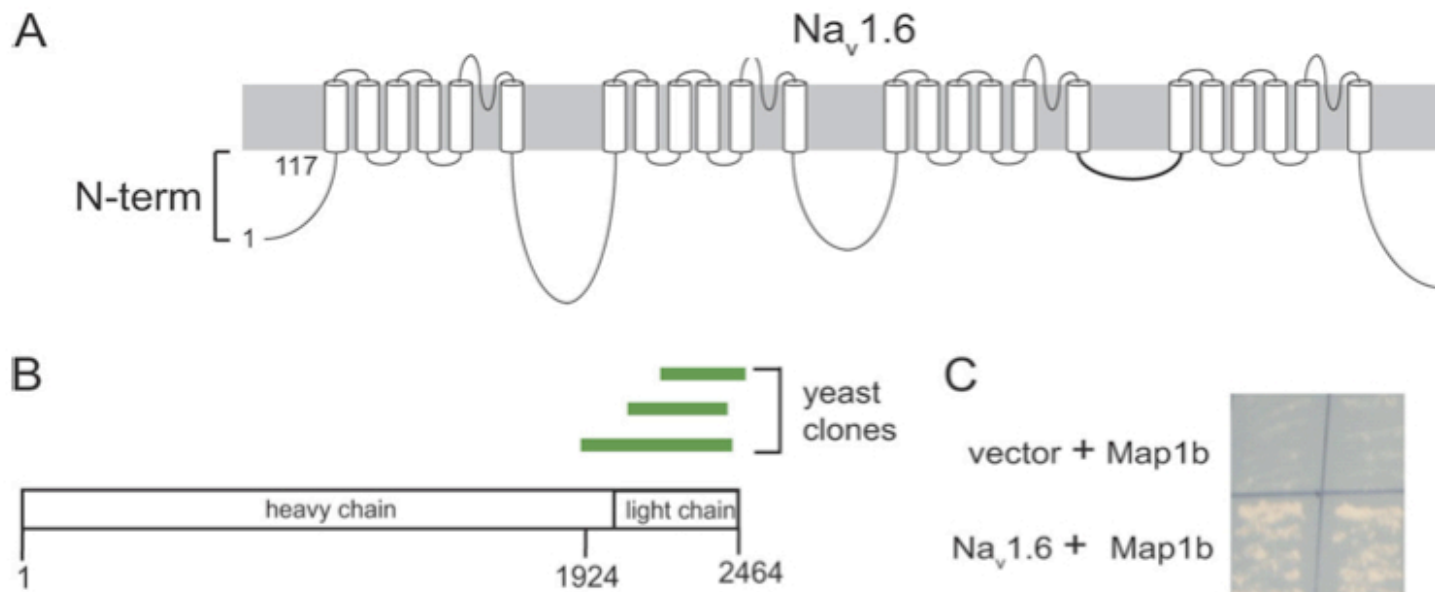


Figure 3.2. Yeast two-hybrid screen using the N-terminus of Nav1.6 as bait identified Map1b as an interactant. (A) schematic of Nav1.6 channel. Residues 1–117 were used as the bait for the yeast two-hybrid screen. (B) location of the three independent clones of Map1b identified in the screen. Residues 1924 –2426 were cloned into the prey vector for the directed yeast two-hybrid and into pCMV-myc for mammalian cell culture experiments. (C) yeast two-hybrid experiments confirming interaction between N-terminus of Nav_v1.6 and Map1b.

the immunoprecipitate, demonstrating interaction (**Figure 3.3A**). The S21P mutation did not prevent co-immunoprecipitation (data not shown).

Interaction of endogenous full length Na_v1.6 with the light chain of Map1b. To assess *in vivo* interaction, we carried out immunoprecipitation of mouse brain membrane protein using a pan-sodium channel antibody, followed by Western blotting with an antibody to the light chain of Map1b. Na_v1.6 was co-immunoprecipitated with the light chain of Map1b from wildtype brain (**Figure 3.3B**). These results demonstrate that the interaction detected in the yeast-two-hybrid system also occurs *in vivo* with full-length endogenous proteins. Map1b was not co-immunoprecipitated from *Scn8a* null brain that lacks Na_v1.6 (**Figure 3.3B**). Since the null brain extracts contain normal levels of the other major sodium channels Na_v1.1 and Na_v1.2 [(Levin and Meisler, 2004) and unpublished observations], the lack of immunoprecipitation of Map1b from null brain suggested that interaction with Map1b might be specific to Na_v1.6.

Map1b binds the N-termini of Na_v1.1 and Na_v1.2 with lower affinity. To directly evaluate the channel specificity of the interaction, we tested the binding of Map1b to the N-terminal domains of Na_v1.1 and Na_v1.2. In a yeast two-hybrid growth experiment, the interaction between the Na_v1.6 N-terminus and Map1b resulted in colony growth on 13/15 plates, while the control interaction with empty vector gave growth on 0/7 plates. In the same experiment, the N-terminus of Na_v1.1 gave growth on 10/15 plates and Na_v1.2 gave growth on 8/15. This data suggests that Na_v1.1 and Na_v1.2 may bind Map1b with lower affinity than Na_v1.6. It will be

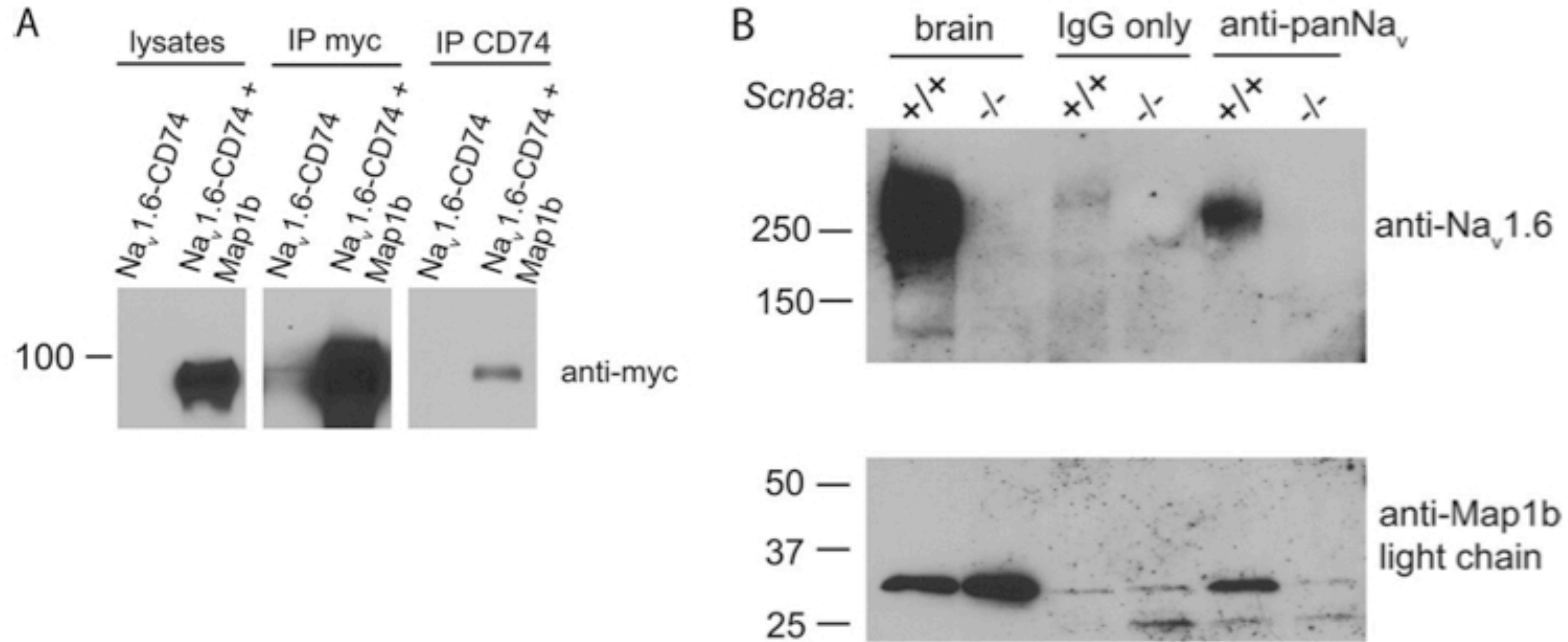


Figure 3.3. Interaction of Na_v1.6 with Map1b. (A) HEK293 cells co-transfected with Na_v1.6-CD74 and myc-Map1b. Map1b light chain co-immunoprecipitates with Na_v1.6-CD74 fusion protein from co-transfected cells. (B) voltage-gated sodium channels and Map1b light chain co-immunoprecipitated from brain membrane fractions from wild-type (+/+) but not Na_v1.6 null (-/-) mice. Lanes contain 50 ug of protein (brain) or 100 ug of protein (immunoprecipitate).

necessary to carry out Western blots to confirm that the protein expression levels of the three N-termini in transformed yeast are comparable.

To localize the Map1b binding site of Na_v1.6, we constructed hybrid clones consisting of residues 1-54 from one channel and residues 55-117 from the other. The construct containing residues 55-117 of Na_v1.6 (1A/8A) interacted with Map1b in the yeast-two-hybrid assay, but the reciprocal construct containing (8A/1A) did not interact (**Figure 3.4B**). This result localized the binding site to residues 55-117 of the N-terminus of Na_v1.6, which differ at 16/62 positions from Na_v1.1 (**Figure 3.4C**).

Localization of the Map1b binding site in Na_v1.6. To further define the Map1b binding site in the distal half of the Na_v1.6 N-terminus, we generated two sets of C-terminal deletion constructs, beginning either at residue 7 or at residue 13 relative to the first methionine in the N-terminus (**Figure 3.5A**). In both sets of constructs, deletion of residues 90-117 did not prevent binding of Map1b, but deletion to residue 80 did prevent binding (**Figure 3.5A**, asterisks). The internal fragment containing residues 38-90 was sufficient for interaction with Map1b (**Figure 3.5A**).

To identify the critical amino acids, we generated seven overlapping 4-residue alanine-substitution mutations of the Na_v1.6 N-terminus between residues 73 to 90 of Na_v1.6. Six of the 7 alanine-substitution constructs retained interaction with Map1b (**Figure 3.5B**). The only non-interacting construct resulted from substitution of AAAA for VAVP (residues 77-80) (**Figure 3.5B**). The corresponding sequence of Na_v1.1 (VSEP) differs from Na_v1.6 at two residues. These experiments localized the Map1b binding site near the center of the cytoplasmic N-terminus of Na_v1.6.

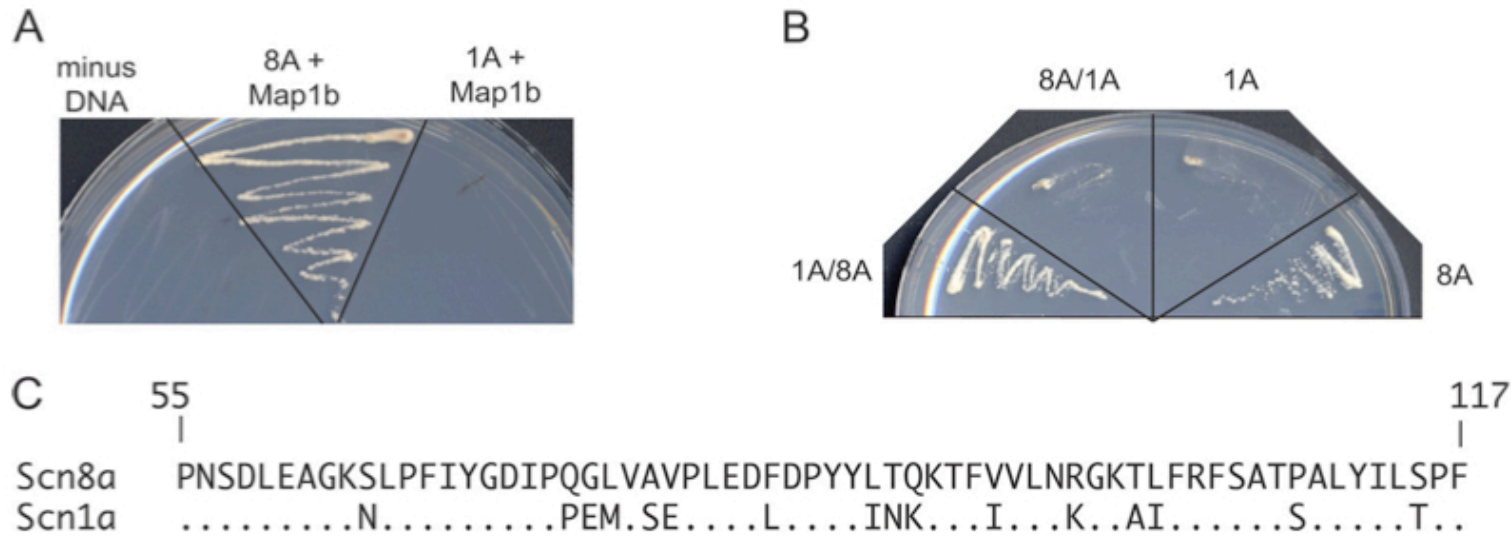


Figure 3.4. Map1b does not bind the N-terminus of Na_v1.1 with high affinity. Co-transformed yeast were plated on selective Leu/ Trp/ His/ Ade medium. All transformed yeast grew on Leu/ Trp medium, which selects for presence of the constructs (data not shown). (A) yeast two-hybrid interaction of Map1b with the N-terminus of Na_v1.6 (8A) and Na_v1.1 (1A). (B) yeast two-hybrid interaction of Map1b with the hybrid constructs 1A(1–54)/8A(55–117) and 8A(1–54)/1A(55–117). (C) residues 55–117 of *Scn8a* and *Scn1a* differ at 16 of 64 residues.

The effect of three pathogenic missense mutations was examined: p.S21P (Sharkey et al., 2009b), p.E82D (Kanai et al., 2004), and p.S107G (Kanai et al., 2004). None of these mutations altered interaction with Map1b, consistent with the mapping data above.

Functional effect of Map1b on Na_v1.6 current in ND7/23 cells.

Measurement of sodium current provides a sensitive assay for the presence of functional sodium channels at the cell surface. To test the effect of Map1b on transport of full length Na_v1.6 to the cell surface, we measured sodium current density in neuron-derived cells transfected with Na_v1.6 alone or co-transfected with Map1b. The transfected ND7/23 cells were analyzed using whole-cell voltage-clamp electrophysiology.

Endogenous ND7/23 currents were blocked by addition of 300nM TTX to the culture medium (Wittmack et al., 2004). ND7/23 cells were transiently transfected with the TTX-resistant construct Na_v1.6_R alone or together with Map1b. Robust sodium currents were detected in both transfections (**Figure 3.6A, B**). However, co-transfection with Map1b resulted in an increase in current density by 50% (p=0.008) (**Figure 3.6C** and **Table 3.2**). Map1b did not affect the voltage-dependence of channel activation and fast-inactivation (**Table 3.2** and **Figure 3.6D**) or cell capacitance (control: 22.5±1.7 pF, n=23; Map1b: 20.2±1.0 pF, n=20; p>0.05).

The data indicate that interaction with Map1b light chain mediates transport of Na_v1.6 to the cell surface. The dependence of Na_v1.6 transport on Map1b may be

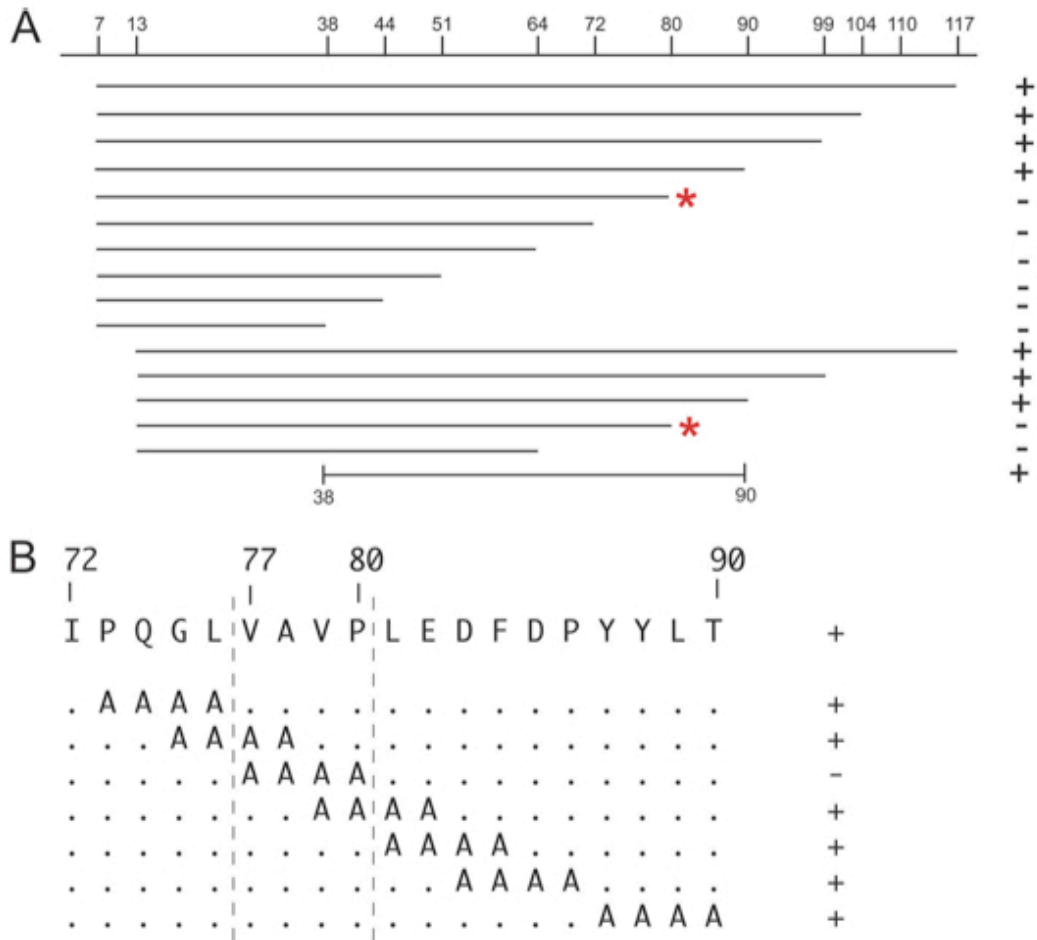


Figure 3.5. Localization of Map1b interaction site within the N-terminus of Na_v1.6. (A) 15 deletion constructs assayed for interaction with Map1b using the yeast-2-hybrid assay. C-terminal deletion to residue 80 or beyond prevented interaction with Map1b (asterisks). The internal residue 38–90 was sufficient for interaction. (B) alanine-scanning constructs spanning the region between residues 73 and 90. Mutation of residues 77–80 prevented interaction with Map1b. +, growth on stringent selection plates; -, no growth.

underestimated in this experiment, since there is robust expression of endogenous Map1b in untransfected ND7/23 cells (**Figure 3.7**), and the Na_v1.6-transfected cells may include cells that did not co-express the Map1b construct.

The VAVP(77-80)AAAA mutation that prevents interaction with Map1b (**Figure 3.5B**) was introduced to the Na_v1.6_R cDNA by site-directed mutagenesis. The mutated and wildtype cDNAs were co-transfected with Map1b into ND7/23 cells. Sodium current was not detected in cells transfected with the AAAA mutant cDNA (**Figure 3.8**). This observation is consistent with an essential role for Map1b in trafficking of Na_v1.6 to the cell surface.

Discussion

A novel Na_v1.6 protein interaction. The functions of the cytoplasmic N-terminus of voltage gated sodium channels are currently not well understood. We demonstrate here that the N-terminus of Na_v1.6 interacts with the adaptor protein Map1b, resulting in an increase in current density without a change in activation or fast-inactivation of the channel. The N-terminus in combination with the first transmembrane segment is also sufficient to direct the CD74 extracellular reporter to the cell surface. Interaction between the mature full-length Na_v1.6 protein and the light chain of Map1b was demonstrated by co-immunoprecipitation from brain extracts. Co-transfection with Map1b resulted in a 50% increase in the sodium current density generated by transfected Na_v1.6, and mutation of the Map1b binding site prevented the generation of sodium currents. The data support a model in which interaction with the light chain of the microtubule-associated protein Map1b

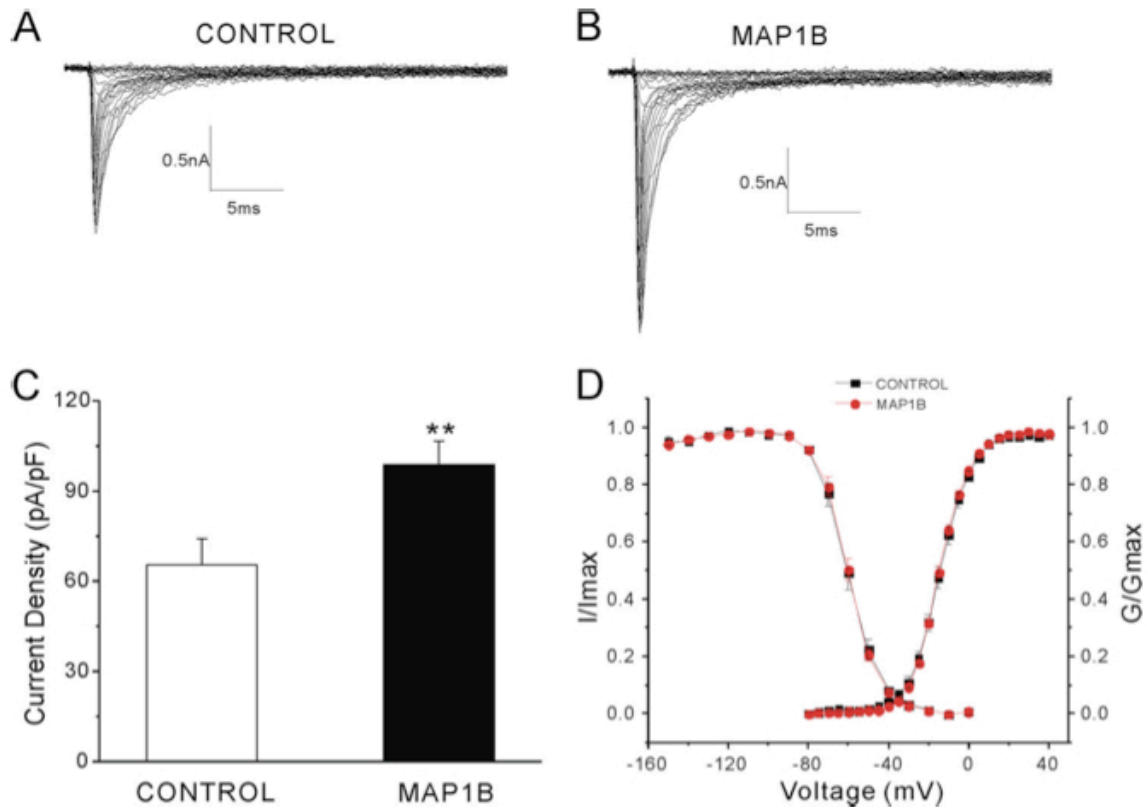


Figure 3.6. Co-expression of Map1b increases Na_v1.6 peak current density in ND7/23 cells transfected with Na_v1.6_R. A and B, representative sodium currents were recorded from ND7/23 cells transiently co-transfected with Na_v1.6_R, EGFP, and vector (n=23) (A) or Map1b (n=20) (B). Cells were held at -120 mV, and sodium currents were elicited by a series of step depolarizations from -80 to -40 mV in 5-mV increments. C, co-expression of Map1b significantly increases current density of Na_v1.6 in ND7/23 cells (**, p<0.01). D, Map1b does not alter activation or steady-state fast inactivation of Na_v1.6.

Table 3.2. Map1b increases the amplitude of Na_v1.6 current in ND7/23 Cells.

	Current Density	Activation		Fast-inactivation	
	pA/pF	V _{1/2} (mV)	k	V _{1/2} (mV)	k
Na _v 1.6	65.5±8.7 (n=23)	-14.2±1.1 (n=14)	7.4±0.4 (n=14)	-59.9±1.6 (n=9)	7.0±0.2 (n=9)
Na _v 1.6 and Map1b	98.7±8.0 (n=20)**	-14.5±0.6 (n=19)	7.1±0.2 (n=19)	-59.7±1.2 (n=15)	6.5±0.2 (n=15)

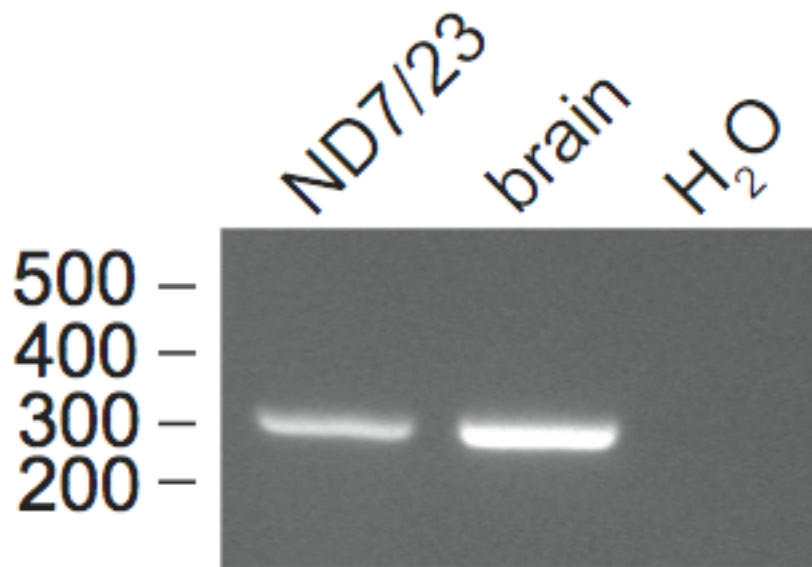


Figure 3.7. The light chain of Map1b is expressed endogenously in ND7/23 cells. 1st strand cDNA was amplified using the forward primer 5' CCTCC CTGTG TATTT GGACC TGTG and the reverse primer 5' CACTG TGCTG CTGCT TGCTA AAACC. Brain, human brain positive control. M, 100 bp ladder.

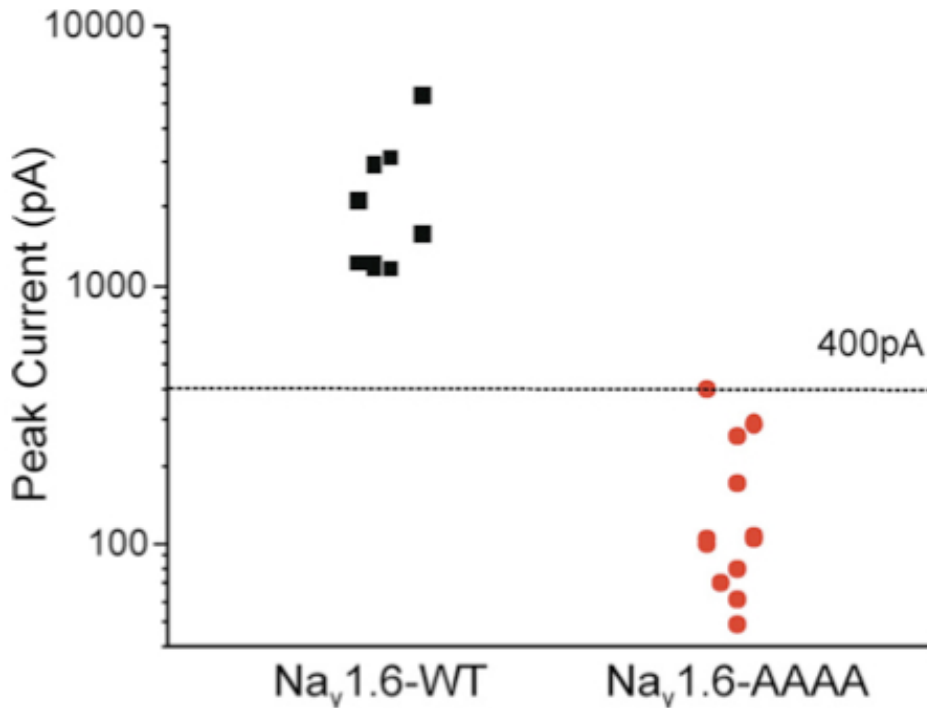


Figure 3.8. Mutation of the Map1b binding site of Na_v1.6_R prevents generation of sodium current in transfected ND7/23 cells. Cells were transfected with Map1b and wild-type Na_v1.6_R or the mutant VAVP(77-80)AAAA-Na_v1.6_R and analyzed by whole cell voltage clamp electrophysiology as described in Figure 3.6. The threshold of 400 pA for peak current represents the minimum required to construct an unambiguous I-V curve. Peak current amplitude for wild-type channels was 1000 pA (n=9), whereas cells transfected with the Na_v1.6_R mutant channel (n=14) did not produce current above threshold.

mediates transport of Na_v1.6 to the cell surface.

Biological role of Map1b. The microtubule-associated protein Map1b contributes to trafficking of several channel and receptor proteins. It directly interacts with the ligand-gated serotonin channel 5-HT_{3a} to mediate channel desensitization (Sun et al., 2008), and binds NMDA receptor subunit 3A (NR3A), which indirectly affects the conductance of the receptor (Eriksson et al., 2010). GABARAP, a molecule with homology to the light chain of Map1b, interacts with the GABA_A receptor and acts as an anchor protein (Everitt et al., 2004). Our work suggests that Na_v1.6 is another neuronal protein that is trafficked along the microtubule network to the cell surface.

The nine paralogous mammalian sodium channel genes share a highly conserved tertiary structure and extensive sequence conservation within the transmembrane segments, but their cytoplasmic domains are more divergent (Catterall et al., 2005; Meisler et al., 2010). Interestingly, the VAVP motif of Na_v1.6 required for interaction with Map1b is not conserved in the other channels. The yeast-two hybrid results suggest that other neuronal voltage-gated sodium channels are capable of interacting with Map1b, but whether they do so *in vivo* has not yet been determined. We hypothesize that Na_v1.1 and Na_v1.2 bind Map1b at a reduced affinity compared to Na_v1.6 due to the difference in residues in the binding site. In vertebrate orthologs of *Scn8a*, the VAVP motif is conserved in reptiles, birds, and marsupials, but not in fish. Further work will be necessary to define a consensus binding motif for the light chain of Map1b.

Consequences of Map1b deficiency in the mouse. Inactivation of Map1b in targeted knockout mice results in juvenile lethality of 55% of homozygotes prior to 4 weeks of age (Meixner et al., 2000). The surviving homozygotes have unexplained weakness and loss of body weight that resemble the effects of muscle atrophy in Na_v1.6 knockout mice (Meixner et al., 2000). Mice carrying a dominant negative allele of Map1b display a more severe phenotype, with embryonic lethality of homozygotes and a movement disorder in heterozygotes that resembles *Scn8a* mutants, including ataxia, hind limb tremor, paralysis (Edelmann et al., 1996). Impaired trafficking of Na_v1.6 could contribute to the phenotype of these mice as well. Unfortunately, the mice are not available for further testing.

Trafficking and subcellular localization of voltage-gated ion channels.

The subcellular trafficking of voltage-gated potassium channels in neurons has been studied extensively (Jensen et al., 2011). These channels appear to be selectively transported to their final locations, rather than randomly transported to the cell surface with subsequent selective removal. Vesicles containing dendritically localized potassium channels are trafficked by myosinV and/or dynein, which are unable to enter the axon due to steric or directional constraints. Neuronal activity appears to regulate the trafficking of voltage-gated potassium channels to specific subcellular locations (Jensen et al., 2011).

Less is known about the clustering and trafficking of voltage-gated sodium channels. Two alternative models for clustering of sodium channels at the axon initial segment (AIS) have been considered: transport to the AIS followed by direct insertion, or nonspecific transport to the cell surface followed by lateral diffusion to

tether points including the AIS (Leterrier et al., 2011). Sodium channels are stabilized at the AIS and at nodes of Ranvier by ankyrin-G, which interacts with a binding site in cytoplasmic loop II-III (Bennett and Lambert, 1999; Dzhashvili et al., 2007; Hill et al., 2008). Adhesion proteins derived from glial cells are also thought to contribute to localization of sodium channels at nodes of Ranvier in myelinated axons. It has been suggested that voltage-gated ion channels are inserted directly into mature nodes, with diffusion limited by myelin and other proteins at the paranode (Leterrier et al., 2011). Analysis of axonal transport in transected sciatic nerve suggests that sodium channels reach the nodes by vesicular trafficking, possibly from the cell body (Zhang et al., 2012). However, the molecular mechanism of transport along the axon to the nodes remains unclear. Since microtubules extend along the full length of the axon, Map1b could play a role in localization of Na_v1.6 to both the AIS and the nodes of Ranvier. Overall, our data support a model in which microtubular trafficking of Na_v1.6 to the cell surface is mediated by interaction with the adaptor protein Map1b (**Figure 3.9**).

Acknowledgements

We thank Drs. Luis Lopez-Santiago and Lori Isom for advice and helpful discussions, and Dr. W. Clay Brown for cloning the N-terminal deletion constructs. We thank Garrett Pepich for his work on the Na_v1.1 and Na_v1.2 yeast-two-hybrid experiments. This work was supported in part by USPHS research grant RO1 NS34509 (MHM). SGW and SDH are funded by grants from the Veterans Administration Medical Research Service and Rehabilitation Research Service. JEO

acknowledges support from the NIH Predoctoral Training Program in Genetics (T32 GM 007544) and the Rackham School of Graduate Studies at the University of Michigan.

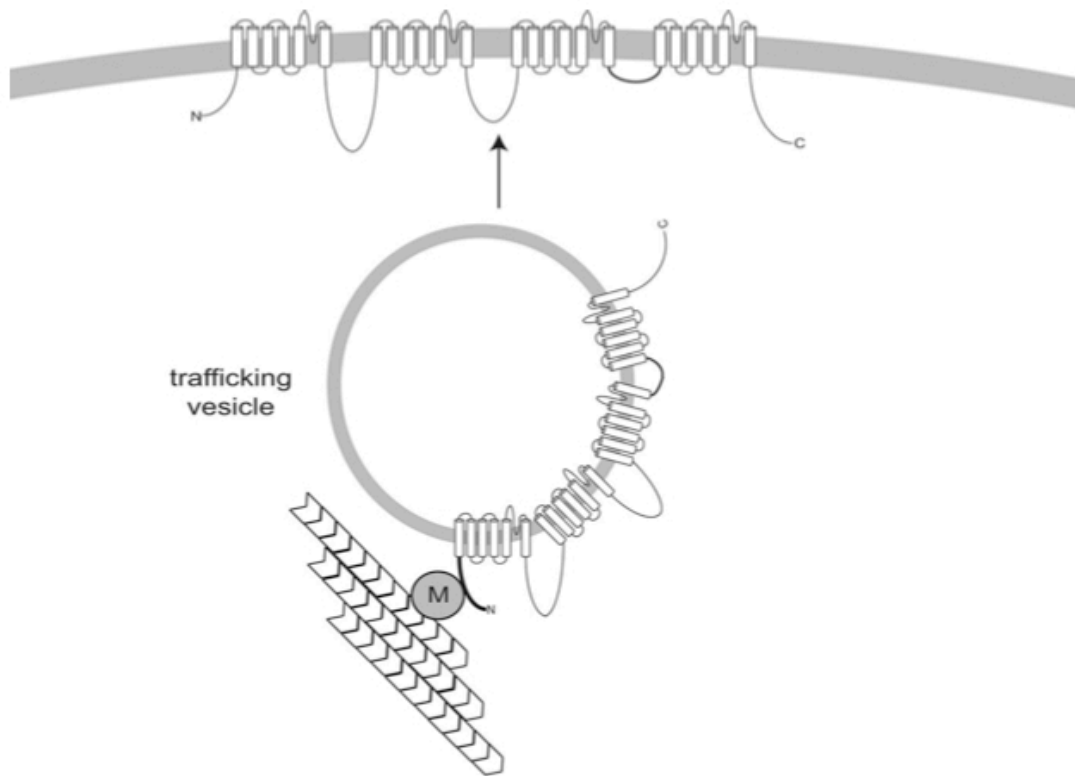


Figure 3.9. Potential role of interaction between Na_v1.6 and Map1b in trafficking of Na_v1.6 to the cell membrane. According to this model, interaction with Map1b facilitates trafficking of Na_v1.6 along axonal microtubules to the AIS or node of Ranvier. At these sites, the channel is stabilized by ankyrin G and other molecules. M, Map1b light chain.

Chapter IV

***De novo* pathogenic mutation of *SCN8A* identified by whole genome sequencing of a family quartet with infantile epileptic encephalopathy and SUDEP³**

Abstract

Individuals with severe, sporadic disorders of infantile onset represent an important class of disease for which discovery of the underlying genetic architecture is not amenable to traditional genetic analysis. Full genome sequencing of affected individuals and their parents provides a powerful alternative strategy for gene discovery. We performed whole genome sequencing (WGS) of a family quartet containing an affected proband and her unaffected parents and sibling. The 15-year-old female proband had a severe epileptic encephalopathy consisting of early-onset seizures, features of autism, intellectual disability, ataxia, and SUDEP (sudden unexplained death in epilepsy).

³This work has been published in: Veeramah, K.R., O'Brien, J.E., Meisler, M.H., Cheng, X., Dib-Hajj, S.D., Waxman, S.G., Talwar, D., Girirajan, S., Eichler, E.E., Restifo, L.L., Erickson, R.P., and Hammer, M.F. (2012). De Novo Pathogenic *SCN8A* Mutation Identified by Whole-Genome Sequencing of a Family Quartet Affected by Infantile Epileptic Encephalopathy and SUDEP. *Am J Hum Genet* 90, 502-510.

We discovered a *de novo* heterozygous missense mutation (c.5302, p.Asn1768Asp) in the voltage-gated sodium channel gene *SCN8A* in the proband. This mutation alters an evolutionarily conserved residue in Na_v1.6, one of the most abundant sodium channels in the brain. Analysis of the biophysical properties of the mutant channel demonstrated a dramatic increase in persistent sodium current, incomplete channel inactivation, and a depolarizing shift in the voltage dependence of steady-state fast-inactivation. Current-clamp analysis in hippocampal neurons transfected with p.Asn1768Asp channels revealed increased spontaneous firing, paroxysmal depolarizing shift (PDS)-like complexes, and an increased firing frequency, consistent with a dominant gain-of-function phenotype in the heterozygous proband. This work identifies an *SCN8A* mutation in an individual with epilepsy and demonstrates the value of WGS for the identification of pathogenic mutations causing severe, sporadic neurological disorders.

Introduction

Massively parallel sequencing technologies are revolutionizing the discovery process for genetic variants that cause disease (Bamshad et al., 2011). Neurodevelopmental disorders such as epilepsy, autism spectrum disorders (ASDs), intellectual disability (ID), and schizophrenia represent a considerable challenge for molecular genetic analysis because of marked genetic heterogeneity, environmental effects on severity and the frequent co-occurrence of seizure, autism, and cognitive phenotypes. Studies of copy number variation (CNV) demonstrated the contribution of *de novo* variants in these disorders (Morrow, 2010; Mitchell, 2011). However,

CNVs appear to contribute to only between 10-25% of affected cases (Girirajan and Eichler, 2010). It is hypothesized that rare or novel point mutations may contribute to many of the remaining cases, under the common disease-multiple rare variant (CD/MRV) model (Gorlov et al., 2010). When the observed phenotype is particularly severe and there is no prior family history of the disorder, it is reasonable to consider a disease model that involves a dominant *de novo* mutation.

Support for this model comes from studies of epileptic encephalopathies, where *de novo* mutations of the sodium channel *SCN1A* (MIM 182389) are a major cause of Dravet Syndrome (MIM 607208) (Marini et al., 2011) while *de novo* mutations in *STXBP1* (MIM 602926) and *ARX* (MIM 300382) have been found in a number of individuals with Early Infantile Epileptic Encephalopathy (MIM 308350) (Pavone et al., 2011). When such mutations arise they are expected to be quickly removed by strong purifying selection (because affected individuals rarely reproduce), and hence would be extremely rare or unique in the population. While the human mutation rate is on the order of $1-2 \times 10^{-8}$ per site per generation (Roach et al., 2010; Conrad et al., 2011), thousands of genes are potentially involved in neurodevelopment (Sepp et al., 2008), suggesting that the number of *de novo* pathogenic mutations could be substantial. Thus, although each individual is expected to have only 0.5 to 1 *de novo* mutation per exome (Lynch, 2010), a model of rare mutations across many genes may explain why severe neurological disorders are relatively common (Vissers et al., 2010).

Whole exome sequencing of parent-offspring trios offers a cost-effective method for screening coding regions for mutations and has been successful in

identifying candidate *de novo* variants in sporadic cases of ID (Vissers et al., 2010), ASDs (O'Roak et al., 2011), and schizophrenia (Girard et al., 2011). However, the limitations of current exome capture and sequencing methodologies include incomplete or variable coverage of exons and the inability to infer ploidy across the genome or survey regulatory variation. Whole genome sequencing (WGS) studies are not limited by these aspects and when implemented in a quartet framework have many attractive analytical advantages. For example, it is possible to precisely infer haplotype phase and the location of recombination events (Roach et al., 2010; Dewey et al., 2011), which can substantially improve the detection and correction of sequencing errors.

In this study, WGS was applied to a family quartet with a sporadic case of severe epileptic encephalopathy. Informed consent was obtained from the family quartet and approved by the Institutional Review Board. The female proband presented with unexplained refractory epilepsy consisting of early-onset brief (2-10 seconds) generalized seizures, beginning at 6 months of age, and later-onset epileptic spasms, beginning at 4 years of age. She also manifested intellectual disability, developmental delay, hypotonia, and coordination and balance difficulties. The proband was able to walk independently just before age 3 and started to use 5-6 word phrases before the age of 4. With the onset of epileptic spasms speech and language skills began to regress over the course of 1-2 years, resulting in the use of occasional single words only. These language and communication problems, in combination with regression in social interaction and development of obsessive-compulsive and repetitive behaviors, led to the classification of autism at the age of

5 years. She was the first-born child of two phenotypically-unaffected parents. Initial electroencephalograms (EEGs) at 6 months showed bi-frontal spikes and brief bursts of fronto-centrally predominant, generalized spike-wave activity lasting for a few seconds at a time. Some of the bursts were associated with clinical seizures. Initial seizures showed no association with fever or illness and occurred very frequently up to 40-50 times per day. Subsequent EEGs after the age of 5 years showed diffuse slowing, multifocal spikes, bifrontal and frontally-predominant generalized spikes, and runs of frontally-predominant slow spike-wave discharges. Several brain MRI scans between the ages of 5 and 15 were normal and a PET scan failed to show any focal abnormalities. At 15 years of age the proband died from sudden unexplained death in epilepsy (SUDEP). An autopsy showed pulmonary edema, consistent with seizure activity prior to death, and did not reveal any other etiology for the sudden demise. Brain microscopic evaluation showed only mild temporal lobe subpial gliosis, consistent with chronic epilepsy.

Given the severity of the disorder and a negative family history, the involvement of a *de novo* mutation was probable. To detect rare CNVs, array-based comparative genomic hybridization (CGH) experiments were performed. We utilized a custom 2x400K Agilent microarray targeted to genomic hotspot regions flanked by segmental duplications or Alu repeats with median probe spacing of 500 bp and probe spacing of 14 kb in the genomic backbone. After quality control filtering and manual curation, 93 CNV calls were identified (see manuscript supplemental data). To identify rare variants of pathogenic significance the CNV pattern was compared to the global CNV map developed from 8,329 controls (Cooper et al., 2011) and 377

additional controls analyzed on the same microarray platform. Allowing for a frequency of <1% in the general population in regions with sufficient coverage (>10 probes), no novel pathogenic CNVs in our proband or any that were previously associated with known genomic disorders were found (Girirajan and Eichler, 2010).

WGS was carried out to look for candidate point mutations or small insertions or deletions. WGS was performed for the quartet by Complete Genomics Incorporated (CGI). CGI performs a massively parallel short-read sequence-by-ligation methodology (Drmanac et al., 2010). Details of library generation, read-mapping to the NCBI reference genome (Build 37, RefSeq Accessions CM000663-CM000686), local *de novo* assembly, and variant-calling protocols have been previously described (Drmanac et al., 2010; Roach et al., 2010). Mean unique sequence coverage ranged from 57X to 77X and 96-97% of the genome was considered fully called across the quartet. A nucleotide position is determined to be fully called if it meets a minimum required confidence score threshold (20 decibels for homozygotes and 40 decibels for heterozygotes) which is calculated taking into account read depth, base call quality values and mapping probabilities. All variants were annotated using ANNOVAR (Wang et al., 2010) based on the UCSC Known Genes Hg19 database, which covers 84,177,555 bp of coding sequence.

31,931 variants were identified from the reference sequence within exons or at splice-site boundaries on all chromosomes. For variants on autosomes, there were 13,395 potentially function-altering variants within the quartet.

To increase variant call quality using Mendelian inheritance rules and information inherent in the quartet, a Hidden Markov Model (HMM) (Roach et al.,

2010) was applied to infer the position of recombination events that demarcate inheritance state (IS) blocks between the two siblings, which has been shown to identify ~70% of expected CGI-generated sequencing errors. Among the potentially functional variants 205 errors were identified based on IS consistency analysis and to unambiguously recover the complete quartet genotype of 58% (1,229/2,103) of the variants that contained missing data.

For the 11,292 variants fully called within the quartet there were 34 violations of Mendelian inheritance rules that would be consistent with a *de novo* mutation within the proband (i.e. the mutation is present in the proband but not in either parent or sibling). Ten of these variants were discarded because they were found in the 1000 Genome Project May 2011 release or the 69 CGI public genomes, or mapped within (a) error-prone regions (defined as containing at least 5 Mendelian Inheritance Errors, with no more than 1000 bp separating any two errors), (b) known segmental duplications (Database of Genomic Variants), (c) repeat sequence (UCSC-defined tracks), (d) suspicious genomic blocks identified by the HMM IS block analysis, or (e) sites that differed significantly in coverage from the genome-wide average. Sanger sequencing demonstrated that 23 of the remaining 24 candidates were false positives, leaving a single, true *de novo* variant in the proband.

To identify potential cis-acting regulatory variants in the whole genome sequence, we evaluated 44,851 variants within the 5' untranslated (UTR) region or within 1 kb upstream of the transcription start site. Of these, 80 qualified as potential *de novo* variants in the proband. After applying the same filtering approach as above, 23 putative *de novo* variants were identified. None of these were validated

as a true variant after Sanger sequencing. There were no *de novo* candidates (including the 5' UTR or 1 kb upstream) on the proband's X chromosomes.

The single validated *de novo* variant was an A > G transition at nucleotide position c.5302 in the coding sequence of *SCN8A* (MIM 600702), resulting in an asparagine (Asn) to aspartate (Asp) substitution at amino acid 1768 (Asn1768Asp). *SCN8A* is one of nine members of the gene family encoding the voltage-gated sodium channel pore-forming alpha subunits (Meisler et al., 2010). The *SCN8A*-encoded channel, Na_v1.6, is composed of four homologous domains, D1 to D4, each containing six transmembrane segments. The subcellular localization of Na_v1.6 includes concentration at the axon initial segment and nodes of Ranvier, and it is widely expressed in the CNS where it regulates firing patterns of excitatory and inhibitory neurons (O'Brien et al., 2012a). The mutated residue is located in the final transmembrane segment adjacent to the C-terminal cytoplasmic domain of the channel (**Figure 4.1**). Asn1768 is invariant in vertebrate and invertebrate sodium channels (**Figure 4.1**). The substitution Asn1768Asp is predicted to be highly deleterious by Polyphen-2 analysis (Adzhubei et al., 2010) (HumDiv score = 0.992, HumVar score = 0.990). Interestingly, an individual with another form of epileptic encephalopathy (Dravet Syndrome) carries a *de novo* mutation in the corresponding residue of the related sodium channel *SCN1A* (Depienne et al., 2009), though the actual functional consequence of this variant has not yet been assessed.

To evaluate the functional consequences of the *de novo* *SCN8A* mutation, the p.Asn1768Asp amino acid substitution was introduced into the tetrodotoxin (TTX)-

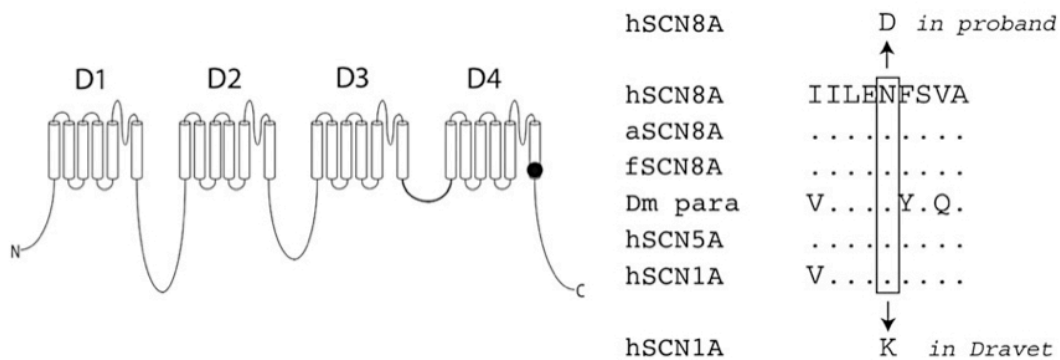


Figure 4.1. The *de novo* proband substitution p.Asn1768Asp in sodium channel *SCN8A*. The altered amino acid residue is located at the cytoplasmic end of transmembrane segment 6 in domain 4 of the channel (for simplicity of display, we use 1-letter amino acid codes). Residue 1768 is evolutionarily conserved in mammalian and invertebrate sodium channels, as indicated by the examples shown on the right. The polar asparagine residue is altered to the charged residue aspartate in our proband. A substitution in the corresponding residue of *SCN1A*, Asn1788Lys, was identified as a *de novo* mutation in an individual with Dravet syndrome, another early-onset epileptic encephalopathy. The following abbreviations are used: h, human; a, anole lizard; f, fish (Fugu); Dm, *Drosophila melanogaster*; para, fly voltage-gated sodium channel (encoded by paralytic); hSCN5A, human cardiac sodium channel; hSCN1A, human neuronal sodium channel; N, Asn; D, Asp; and K, Lys. Dots represent amino acid identity.

resistant derivative of the Na_v1.6 cDNA clone Nav1.6_R (Herzog et al., 2003a; Dib-Hajj et al., 2009). The entire 6-kb open reading frame was sequenced to confirm the absence of additional mutations prior to functional testing by transfection into the dorsal root ganglion (DRG) neuron-derived cell line ND7/23 (Wood et al., 1990) as previously described (Sharkey et al., 2009a). In the presence of 300 nM TTX, endogenous sodium currents are blocked, and currents derived from the transfected Nav1.6_R clones can be studied in isolation. Forty-eight hours after transfection, cells with robust green fluorescence were selected for recording.

Representative families of traces of Na⁺ currents from voltage-clamp recordings are shown in **Figure 4.2A**. The persistent currents at 100 msec after the onset of step-depolarization, normalized to peak transient current, are increased by 7-fold, from an average of 1.8% for wild-type to 13% in the mutant channel (**Figure 4.2A** insets and **Table 4.1**). Despite a 56% reduction in peak current density for cells transfected with the mutant channel, the absolute values of the persistent current [61 +/- 6 pA (n=11) for WT; and 353 +/- 51 pA (n=11) for Asn1768Asp] and persistent current density [2.02 +/- 0.20 pA/pF (n=11) for WT; and 10.51 +/- 1.57 pA/pF (n=11) for Asn1768Asp] were more than five-fold larger for the mutant channels. The voltage-dependence of the persistent current is shown in **Figure 4.2B**, and is greatest at +15 mV. The Asn1768Asp mutation also causes a 13 mV depolarizing shift in the voltage dependence of steady-state fast-inactivation and increases the non-inactivating component of the current (**Figure 4.2C, arrow**). The development of closed-state inactivation is slower for the mutant channels (data for -60 mV shown in **Figure 4.2D**) and, as expected, Asn1768Asp channels produce a substantially

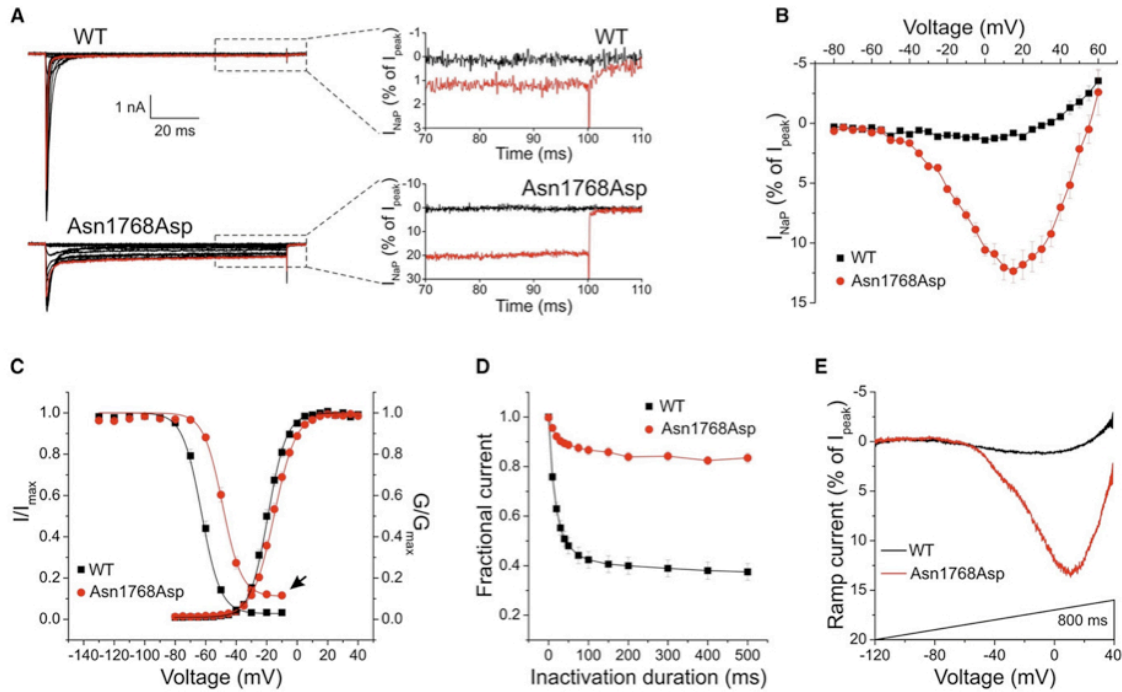


Figure 4.2. Effect of the *de novo* SCN8A substitution p.Asn1768Asp on biophysical properties of the channel. (A) Representative inward currents recorded from ND7/23 cells transiently transfected with Na_v1.6_R WT or mutant channels. Cells were held at -120 mV, and a family of step depolarizations (-80 to -60 mV in 5 mV increments) were applied every 5 s. Insets show persistent inward currents (normalized by maximal transient peak currents) from WT and p.Asn1768Asp channels at the end of a 100 ms step depolarization to -80 mV (black) and -20 mV (red). (B) Voltage dependence of persistent current. The amplitude of persistent current was measured as the mean value of currents 93–98 ms after the onset of depolarization and is presented as a percentage of the maximal transient peak current. (C) Voltage dependence of channel activation and steady-state fast inactivation. Channel activation was analyzed as previously described. Steady-state fast inactivation was assessed with a series of 100 ms step depolarizations (-130 to -10 mV in 10 mV increments) and was followed by a test pulse (-10 mV) so the remaining fraction of noninactivated channels could be measured. The p.Asn1768Asp channels do not completely inactivate, which is consistent with the large persistent current. (D) Development of closed-state inactivation at -60 mV. Cells were held at -120 mV, and closed-state inactivation was assessed with a prepulse set to -60 mV with a duration varying from 0 to 500 ms, and remaining available channels were assessed with a test pulse set to 0 mV (20 ms). (E) Mean ramp currents generated by WT (black) and p.Asn1768Asp (red) channels. The response to a slow ramp stimulus was evaluated with a ramp depolarization from -120 to -40 mV over 800 ms. The p.Asn1768Asp mutation increases the amplitude of the ramp current (normalized by transient peak current; p.Asn1768Asp [13.6 ± 1.9%, n=5, p < 0.05] versus WT [1.2 ± 0.2%, n=7]).

Table 4.1. Biophysical effects of the SCN8A p.Asn1768Asp substitution. Whole-cell voltage-clamp recordings were performed with an Axopatch 200B amplifier (Molecular Devices, Sunnyvale, CA). The pipette solution contained (in mM) 140 CsF, 10 NaCl, 1 EGTA, 10 Dextrose, 10 HEPES (pH 7.3) (with CsOH), and osmolarity was adjusted to 315 mosmol/liter with sucrose. The extracellular bath solution contained (in mM) 140 NaCl, 3 KCl, 20 tetraethylammonium, 1 MgCl₂, 1 CaCl₂, 10 HEPES, 5 CsCl, 0.1 CdCl₂ (pH 7.3) (with NaOH); osmolarity was 325 mosmol/liter. 300 nM tetrodotoxin was added to the extracellular bath solution to block endogenous voltage-gated sodium currents in ND7/23.26 All recordings were conducted at room temperature (~22_ C). Currents were acquired with Clampex 9.2 5 min after establishing whole-cell configuration, sampled at 50 or 100 kHz, and filtered at 5 kHz. The following abbreviations are used: I_{Na}, voltage-gated sodium current; I_{persistent}, sodium current that is resistant to fast inactivation at the end of 100 ms step depolarization; I_{peak}, the maximal transient peak sodium current; V_{1/2,act}, the potential at which activation of sodium channels reaches half maximal; k, the slope factor; A%, the percentage of sodium channels that are resistant to fast inactivation or slow inactivation; n, number of cells. *, p value < 0.05 compared to WT

	I _{Na} Density (pA/pF)	I _{persistent} (% of I _{peak})	Reversal Potential (mV)	Activation			Steady-State Fast Inactivation				Slow Inactivation			
				V _{1/2,act}	k	n	V _{1/2,fast}	k	A%	n	V _{1/2,slow}	k	A%	n
WT	130 ± 21 (20)	1.8 ± 0.3 (11)	69.0 ± 1.6	-19.5 ± 0.8	-6.16 ± 0.27	17	-62.1 ± 1.0	5.61 ± 0.11	2.85 ± 0.51	16	-41.7 ± 1.3	14.2 ± 0.5	3.84 ± 1.01	14
N1768D	57 ± 7 ^a (24)	13.1 ± 0.9 ^a (11)	71.0 ± 1.5	-15.3 ± 0.9 ^a	-6.96 ± 0.25 ^a	14	-48.7 ± 0.9 ^a	5.77 ± 0.17	10.9 ± 0.86 ^a	10	-53.3 ± 1.5 ^a	6.5 ± 0.3 ^a	2.15 ± 0.69	10

enhanced (11-fold larger) response to slow, ramp-like depolarizing stimuli (**Figure 4.2E**). All of these changes are known to increase neuronal excitability; it has been shown that persistent sodium currents contribute to the generation of paroxysmal depolarizing shifts (PDS), a cellular response predictive of recurrent seizures (Chen et al., 2011). The mutation causes a small depolarizing shift of 4 mV in the voltage-dependence of activation (**Figure 4.2C**) and shifts the voltage-dependence of steady-state slow-inactivation by -11.6 mV (not shown), which would reduce the pro-excitatory effects.

The biophysical properties of Asn1768Asp channels are summarized in **Table 4.1**. In heterozygous neurons, mutant and wildtype alpha subunits would be co-expressed and act independently. The direction and magnitude of the pro-excitatory effects of the Asn1768Asp mutation are consistent with a dominantly-expressed phenotype of abnormal neuronal excitability. To test this prediction, we examined the firing patterns of cultured hippocampal neurons expressing transfected mutant and wildtype *Scn8a* cDNAs using current-clamp recordings (**Figure 4.3A-C**).

Spontaneous firing was detected in 3/17 (18%) of neurons transfected with the wildtype *Scn8a* cDNA, and in a significantly higher percentage (10/17; 59%, $p < 0.05$) of neurons transfected with Asn1768Asp (**Figure 4.3B**), which also displayed PDS-like complexes (**Figure 4.3Aii**). In response to current injection, the frequency of action potentials was 2-fold higher in cells expressing the mutant channels (**Figure 4.3C**). These observations demonstrate that expression of the mutant channel results in a phenotype of neuronal hyperexcitability including increased spontaneous firing and PDS-like complexes.

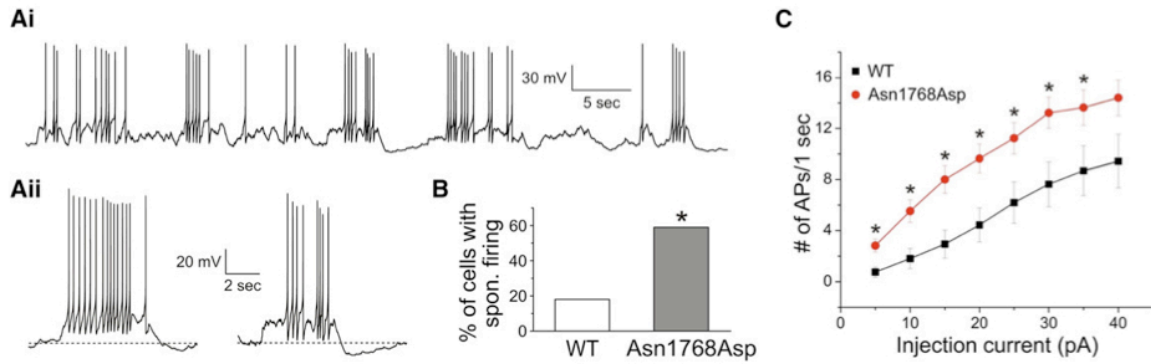


Figure 4.3. Effect of the *de novo* SCN8A Substitution p.Asn1768Asp on hippocampal neuronal excitability. (A) p.Asn1768Asp channels increase excitability of hippocampal neurons. (Ai) An example of spontaneous firing in a neuron transfected with p.Asn1768Asp channels. (Aii) Representative PDS-like complexes recorded from two hippocampal pyramidal neurons transfected with p.Asn1768Asp. The dashed lines indicate -80 mV. (B) Percentage of neurons displaying spontaneous firing. The asterisk indicates $p < 0.05$. (C) Number of action potentials (APs) evoked by a series of 1 s step depolarizing current injections (from 5 to 40 pA with a 5 pA increment). Neurons transfected with p.Asn1768Asp produce more APs than neurons transfected with WT. An asterisk indicates $p < 0.05$.

Discussion

A de novo pathogenic mutation of SCN8A in severe epilepsy. Several factors support a causal role for the *SCN8A* p.Asn1768Asp mutation in the phenotype observed in the proband: (a) *SCN8A* encodes a neuronal sodium channel that is highly abundant in brain (Schaller and Caldwell, 2000; O'Brien et al., 2012a), (b) the mutation produces substantial increase in persistent and ramp currents and results in neuronal hyperexcitability that includes increased spontaneous activity and PDS-like complexes, and (c) heterozygous mutations with similar properties in other closely related neuronal sodium channels are causal for epilepsy (Meisler et al., 2010). This result demonstrates the power of the WGS approach for unbiased discovery of pathogenic mutations in neurological disorders of unknown etiology. Causative variants in severe, early-onset neurological disease are likely to be rare and distributed across many genes, some of which are not on candidate-gene lists (Lu and Wang, 2009). This study presents the fifth member of the voltage-gated sodium channel gene family to be implicated in seizure disorders, in addition to *SCN1A*, *SCN2A* (MIM 182390), *SCN3A* (MIM 182391) and *SCN9A* (MIM 603415) (Meisler et al., 2010). *SCN8A* is the third sodium channel, in addition to *SCN1A* and the cardiac channel *SCN5A* (MIM 600163), to be implicated in SUDEP, which accounts for deaths in up to 38% of people with epilepsies (Devinsky, 2011). In this context, it is interesting that both *Scn1a* and *Scn8a* are expressed at a low level in cardiac myocytes (Maier et al., 2004) and cardiac function is impaired in *Scn8a* null mice (Noujaim et al., 2012).

Na_v1.6 mutations in vivo. The *in vivo* physiological roles of Na_v1.6 have been extensively studied in the mouse. The allele series of recessive *Scn8a* mutations includes missense, hypomorphic, and null alleles (Burgess et al., 1995a; Meisler et al., 2004; Meisler and Kearney, 2005a; Sharkey et al., 2009a). Motor deficits are prevalent due to the important role of Na_v1.6 at nodes of Ranvier in motor neurons. Homozygotes for partial and complete loss-of-function alleles exhibit ataxic gait, tremor, dystonia, muscle atrophy, loss of hind limb function, and juvenile lethality caused by loss of neurotransmitter release at the neuromuscular junction. The single previously reported human *SCN8A* mutation is a premature stop codon identified in a proband with cerebellar ataxia; the mutation co-segregated with cognitive impairment but did not result in seizures (Trudeau, 2006). Likewise, heterozygous *Scn8a*^{+/-} mice exhibit an anxiety-like behavioral disorder but do not have spontaneous seizures (McKinney et al., 2008). Thus haploinsufficiency of *SCN8A* does not cause epilepsy in human or mouse. However, spike-wave discharge patterns are seen in certain *Scn8a* heterozygotes (Papale et al., 2009), and heterozygosity for an *Scn8a* null allele can suppress seizures in a mouse *Scn1a*^{+/-} model of Dravet Syndrome (Martin et al., 2007b), demonstrating physiological interaction between these two sodium channels in determining neuronal excitability.

Gain of function mutations in voltage-gated sodium channels lead to hyperexcitability. The mutation in the proband is a gain-of-function allele of *SCN8A* and causes a large increase in ramp and persistent currents and incomplete channel inactivation. Increased persistent current is a common characteristic of gain-

of-function mutations of *SCN1A* in individuals with generalized epilepsy with febrile seizures plus (GEFS+), and is characteristic of pathogenic mutations of *SCN2A* and *SCN3A* (Spampanato et al., 2001; Vanoye et al., 2006; Holland et al., 2008; Estacion et al., 2010; Liao et al., 2010; Volkers et al., 2011). The Q54 mouse model expresses an *Scn2a* mutant channel with elevated persistent current that causes a dominant seizure disorder (Kearney et al., 2001). Notably, transfection of hippocampal neurons with p.Asn1768Asp channels resulted in hyperexcitability that included increased spontaneous activity and PDS-like complexes. The effect of the proband's *SCN8A* mutation on persistent current is considerably more severe than the other reported examples, which strongly supports a causal role in the severe, dominant epileptic encephalopathy.

Identification of an epileptic encephalopathy distinct from Dravet syndrome. Mutations in human *SCN1A* are the most common genetic cause of inherited and sporadic epilepsy, with >700 proband mutations reported thus far, including >80% of individuals with Dravet Syndrome (Catterall et al., 2008; Marini et al., 2011; Poduri and Lowenstein, 2011). More than 90% of the *SCN1A* mutations in individuals with Dravet Syndrome arose *de novo* and more than 50% are loss-of-function mutations, demonstrating that, unlike with *SCN8A*, haploinsufficiency for *SCN1A* results in seizures (Meisler and Kearney, 2005a; Meisler et al., 2010). Our proband displays many features typically found in individuals with Dravet Syndrome, such as onset in infancy of seizures that ultimately become refractory to therapeutic intervention with concomitant regression of developmental abilities leading to epileptic encephalopathy. However, consistent with a distinct genetic basis, there

are also important differences: (a) our proband did not manifest prolonged generalized or unilateral febrile and afebrile seizures in the first year of life; (b) rather than distinct myoclonic seizures as seen in typical Dravet Syndrome, our proband had late-onset epileptic spasms characterized by repetitive clusters of jerks with the classical EEG pattern of spasms (i.e., high-amplitude delta wave followed by background suppression); and (c) a period of normal development was not seen in our proband. Further characterization of individuals with *SCN8A* mutations will help to delineate the clinical variability within this group and distinguish the phenotypes of carriers of pathogenic mutations at *SCN8A* and *SCN1A*.

Candidate variants from a recessive disease model. We also evaluated the WGS data from our quartet for a model of inherited homozygous recessive disease. Variants with a frequency >1% in the 1000 Genomes Project or present in the CGI public genomes were excluded as potential candidates. Seven genes fit a recessive inheritance pattern in the proband only (**Table 4.2**). Two of these (*NRP2* and *UNC13C*) were cases of compound heterozygosity that appeared functionally relevant based on the Autworks database and biomedical literature. Both parents were heterozygous for non-synonymous variants of *NRP2* (*neuropilin 2*, MIM 602070) and *UNC13C* (*Homolog of C. elegans UNC13C*). The inherited variants were predicted to be deleterious by PolyPhen-2 analysis (HumDiv >0.993) and were extremely rare, with frequencies <1.0% in the NHLBI Exome Sequencing Project (NHLBI Exome Sequencing Project (ESP). Seattle, 2011). The maternally-inherited *NRP2* allele, also transmitted to the brother, is p.Arg334Cys (rs14144673) while the

Table 4.2. Candidate variants under a homozygote recessive disease model.

Recessive Type	Chr.	Position	Ref.	Variant	KG Gene Name	KG_mRNA Transcript	KG Coding Change	KG Protein Change	Father	Mother	Sibling	Proband	dbSNP 132 rs#	Polyphen 2 Score	1000 Genome Freq	Present CGI	Autworks Xref
Simp	1	33960715	C	T	ZSCAN2	uc001bxj.3 uc009vui.2	c.C2771T c.C2768T	p.T924I p.T923I	01	01	01	11	?	0.48	?	N	
Simp	3	111901062	A	T	SLC9A10	uc010hqc.2 uc011bhu.1 uc003dyu.2	c.T2423A c.T356A c.T2567A	p.I808N p.I119N p.I856N	01	01	01	11	146697807	0.18	?	N	
Simp	3	113045485	C	A	WDR52	uc003ead.1	c.G1866T	p.W622C	01	01	01	11	?	?	?	N	
Simp	19	45206933	G	A	CEACAM16	uc010xxd.1 uc002ozq.2	c.G352A c.G529A	p.E118K p.E177K	01	01	00	11	183860695	?	0.002	N	
Simp	1	33236824	C	T	KIAA1522	uc010ohm.1 uc001bvv.2 uc001bv.1	c.C1900T c.C1867T c.C2044T	p.P634S p.P623S p.P682S	01	01	0N	11	?	0.50	?	N	
Comp	2	206592624	C	T	NRP2	uc002vav.2	c.C1000T	p.R334C	00	01	01	01	114144673	1.00	?	N	Ataxia, Autism, Epilepsy, Hypoxia, Stroke,
	2	206605378	C	T	NRP2	uc002vav.2	c.C1282T	p.R428W	01	00	00	01	139711818	1.00	?	N	Ataxia, Autism, Epilepsy, Hypoxia, Stroke,
Comp	15	54306012	C	G	UNC13C	uc002ack.2,	c.C912G	p.D304E	00	01	00	01	149448818	?	0.008	N	
	15	54919253	T	C	UNC13C	uc002acm.2 uc002ack.2,	c.T350C c.T6587C	p.V117A p.V2196A	01	00	00	01	146433220	?	0.004	N	

paternally-inherited allele is p.Arg428Trp (rs139711818). The maternally-inherited *UNC13C* allele is p.Asp304Glu (rs149448818) and the paternally-inherited allele is p.Val2196Ala (rs146433220).

NRP2 is a transmembrane receptor for class 3 semaphorins, secreted proteins that are essential for guiding axon pathfinding and sorting during central and peripheral nervous system development (Pellet-Many et al., 2008). *NRP2* polymorphisms have been associated with autism (Wu et al., 2007) and *NRP2* is a candidate gene for juvenile myoclonic epilepsy (Ratnapriya et al., 2010). *Nrp2*-deficient mice display increased neuronal excitability and susceptibility to chemically induced seizures (Gant et al., 2009). Loss-of-function *Nrp2* mutations in homozygous mice cause defects of axon-tract formation, with fiber bundles misrouted, disorganized, or missing (Pellet-Many et al., 2008). Moreover, loss of *Nrp2* causes increased cortical and hippocampal dendritic spine numbers (Tran et al., 2009) and decreased numbers of hippocampal interneurons and GABAergic synapses (Gant et al., 2009). The *UNC13* gene family encodes highly conserved proteins, most of which are expressed in neurons where they serve a crucial function in synaptic vesicle fusion for neurotransmitter release (Brose et al., 2000; Basu et al., 2007). Disrupting the function of any single *Unc13* gene can impair neuronal function in mouse mutants, including synaptic plasticity (Rosenmund et al., 2002) and motor learning (Augustin et al., 2001), without disrupting neuronal morphology.

It has often been suggested that inheritance of modifier loci contributes to the wide phenotypic variability of individuals with *SCN1A* mutations (Meisler et

al., 2010). With WGS data it is now possible to predict the identity of specific candidate modifier variants in individuals. In the present case, *NRP2* variants could plausibly enhance seizures through neuronal hyperexcitability and loss of inhibitory synapses, while *UNC13C* variants could reduce seizure activity by inhibiting synaptic vesicle release and thereby increasing the threshold for synaptic transmission. Animal models will be required to test the role of genetic interactions in modifying the phenotypic expression of *SCN8A* gain-of-function mutations.

In summary, by performing high-coverage WGS of a family quartet we have identified a *de novo* mutation in *SCN8A* that can account for the epileptic encephalopathy that eventually resulted in SUDEP in the proband. Recent whole genome and whole exome approaches have been remarkably successful in identifying amino-acid altering *de novo* mutations in individuals with severe neurological disorders. However, in most cases to date, direct support for causality has been lacking, and knowledge of the gene or protein function has allowed only predictions about the consequences of a particular mutation. We have confirmed the pathogenicity of our candidate *SCN8A*-Asn1768Asp mutation through biophysical characterization of the channel and electrophysiological analysis in primary neurons. Given the likely importance of rare variants with large effects in disease etiology (Gorlov et al., 2010; Robinson et al., 2011), such follow-up functional analysis will be vital as an increasing number of *de novo* or extremely rare variants are discovered through WGS of probands and their families.

Acknowledgments

Support for this work was provided by the National Institute of Health to KRV (R01 HG005226), MHM (R01 NS34509), and JEO (T32 GM007544). SGW and SDH are funded by grants from the Veterans Administration Medical Research Service and Rehabilitation Research Service. SG and EEE are funded by HHMI. LLR is funded by Autism Speaks and the Arizona Center for Biology of Complex Diseases. We thank Tanya Karafet, Daniel Wolf and Kimiko Della Croce for the *de novo* variant validation by PCR and sequencing. The authors declare they have no financial conflict of interest.

Web Resources

The URLs for data presented herein are as follows:

ANNOVAR: <http://www.openbioinformatics.org/annovar/>

UCSC Known Genes database: <http://genome.ucsc.edu/>

Complete Genomics Incorporated Public Genomes: <ftp2.completegenomics.com>

1000 Genomes May 2011 Data Release:

<http://www.1000genomes.org/node/506/>

Database of Genomic Variants (DGV): <http://projects.tcag.ca/variation/>

PolyPhen2: <http://genetics.bwh.harvard.edu/pph2/>

SCN1A Variant database: <http://www.molgen.ua.ac.be/SCN1AMutations/>

Autworks: <http://autworks.hms.harvard.edu/>

Online Mendelian Inheritance in Man: <http://www.omim.org>

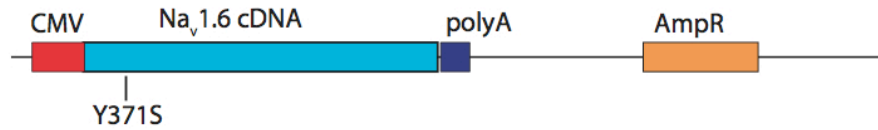
Chapter V

Generation of Na_v1.6 cDNA constructs for electrophysiology and intracellular trafficking experiments.

Introduction. The Na_v1.6 cDNA constructs (**Figure 5.1**) (Herzog et al., 2003a; Gasser et al., 2012) are critical reagents for the characterization of human and mouse mutations of *SCN8A*. Mammalian Na_v1.6 cDNA is notoriously unstable, so the generation of a stable and modifiable cDNA construct by the Waxman lab (2003) was a significant advancement in the voltage-gated sodium channel field. pcDNA3Nav1.6_R (Herzog et al., 2003a) and pcDNA3Nav1.6_R-GFP (Gasser et al., 2012) are low-copy, large (12 and 14 kb, respectively), and prone to rearrangement and introduced mutations during all bacterial growth steps. Both cDNAs contain the p.Tyr371Ser mutation, which eliminates the tetrodotoxin-sensitivity of Na_v1.6. This permits specific recording from cDNA constructs in the presence of endogenous Na_v1.6, which is necessary for electrophysiological characterization of mutant plasmids in transfected neurons.

We first described a *de novo* mutation in *SCN8A*, p.Asn1768Asp, in a patient with epileptic encephalopathy (Chapter IV) (Veeramah et al., 2012). Since then, five additional *SCN8A* mutations have been identified in patients with

A pcDNA3Na_v1.6_R (12 kb)



B pcDNA3Na_v1.6_R-GFP (14 kb)

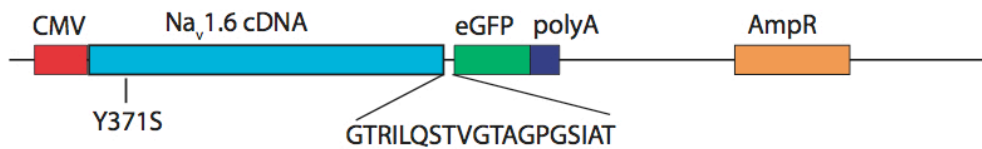


Figure 5.1. Na_v1.6 cDNA constructs (A) pcDNA3Na_v1.6_R (Herzog et al., 2003a) and (B) pcDNA3Na_v1.6_R-GFP (Gasser et al., 2012). These plasmids contain a CMV promoter (nucleotides 251-961), mouse Na_v1.6 cDNA (993-6929), an SV40 polyadenylation site, modifications which render them low copy, and an ampicillin resistance cassette. Both constructs have the Y371S mutation, which renders the channel resistant to tetrodotoxin. This permits specific recording from these cDNAs in the presence of endogenous Na_v1.6. In pcDNA3Nav1.6_R-GFP, a 19-residue linker joins the Na_v1.6 and eGFP open reading frames (see Gasser et al., 2012 for details). Drawn to scale.

infantile onset epileptic encephalopathy (M. Hammer, Univ. Arizona, pers. comm.). Heterozygous null mutations in $Na_v1.6$ have been implicated in intellectual disability (Trudeau et al., 2006). The electrophysiological properties of these human mutations are tested by mutagenesis of the $Na_v1.6$ cDNA, followed by transfection of mutant cDNA into the dorsal root ganglion (DRG) neuron-derived cell line ND7/23 (Wood et al., 1990) and cultured primary hippocampal neurons (Veeramah et al., 2012) by the Waxman lab at Yale University. These functional assays can detect subtle changes in the electrophysiological properties of the mutant channels that may predispose them to hyper- or hypoexcitability.

The ability to introduce mutations into the $Na_v1.6$ cDNA is necessary for evaluation of mutant channels in cell culture. I have generated ten mutant constructs from the wild-type $Na_v1.6$ cDNA clones described above (**Table 5.1**), and developed an efficient protocol for the mutagenesis of these plasmids. In this chapter, I describe the process and provide details that may assist in recognizing false positive clones. I also describe constructs that I generated for further characterization of human mutations and channel trafficking assays.

Methods for cloning $Na_v1.6$ cDNA. The $Na_v1.6$ cDNA constructs are prone to rearrangement and introduction of undesired mutations during bacterial growth. Therefore, bacterial growth on plates and in liquid media is carried out at 27°C for 40 hours. A high concentration of ampicillin [100 ug/mL] is necessary to provide selection for 40 hours. Visible bacterial growth after only 16 hours is indicative of contamination, plasmid rearrangement, or defective selection.

Table 5.1. Mutated Na_v1.6 cDNA clones generated during this thesis research. The mutations were introduced into pcDNA3Na_v1.6_R, except for #10, which is in pcDNA3Na_v1.6_R-GFP.

	Mutation	Project	Source of Mutation, Comments
1	p.Ser21Ala	Phospo-dead S21 (<i>ataxia3</i> follow-up) (Sharkey et al 2009a)	Unpublished, current density ~75% of wild type (L. Lopez-Santiago)
2	p.Ser21Glu	Phospo-mimetic S21 (<i>ataxia3</i> follow-up)	Unpublished, current density ~50% of wild type (L. Lopez-Santiago)
3	p.VAVP(77-80)AAAA	Map1b binding site	Chapter III
4	p.Arg223Gly	Patient mutation, epileptic encephalopathy	M. Hammer, pers. comm. (Utrecht, the Netherlands)
5	p.Thr767Ile	Patient mutation, epileptic encephalopathy	M. Hammer, pers. comm. (Mississippi, Baylor)
6	p.Arg1617Gln	Patient mutation, intellectual disability	Rauch et al., 2012
7	p.Asn1768Asp	Patient mutation, epileptic encephalopathy	Chapter IV
8	p.Arg1907Trp	Patient mutation, ALS	unpublished
9	p.Ile1750del	Mouse mutant, <i>Scn8a</i> ^{9J}	Jones et al., 2013, in preparation
10	p.VAVP(77-80)AAAA	Live-cell trafficking studies, J. Salzer	unpublished

Bacterial colonies that contain intact Na_v1.6 are usually smaller than standard bacterial colonies, but larger than the satellite colonies that develop when antibiotic selection has failed.

I have found QuikChange XL II mutagenesis (Agilent) to be the most efficient way to introduce point mutations or deletions into the Na_v1.6 cDNA. The process is described in **Figures 5.2** and **5.3**. The efficiency of mutagenesis is fairly high (~75%). I use a plasmid-specific positive control for all QuikChange reactions. Agilent recommends using their internal control, but I have found that the conditions for mutagenesis of the Agilent control are too different from those used for mutagenesis of Na_v1.6 cDNA to serve as an effective control. I have used the p.Ser21Ala mutagenesis reaction as a positive control, but any previously successful mutagenesis reaction would suffice. The positive control serves as an indicator for the quality of the reagents and the effectiveness of the cycling protocol. QuikChange reactions are carried out as recommended by the manufacturer, with the modifications noted in **Figure 5.2**.

The probability of rearrangement during the bacterial growth stage after transformation of the QuikChange reaction is ~80%, and therefore 40-50 minipreps must be screened. We use the restriction enzymes *PvuII* and *NcoI* to determine if plasmids are rearranged (**Figure 5.4**). A positive control, preferably the QuikChange reaction template, is necessary for all restriction digests to assess for completeness of digestion. The mutated site in plasmids with wild type diagnostic digest patterns is sequenced using primers surrounding the

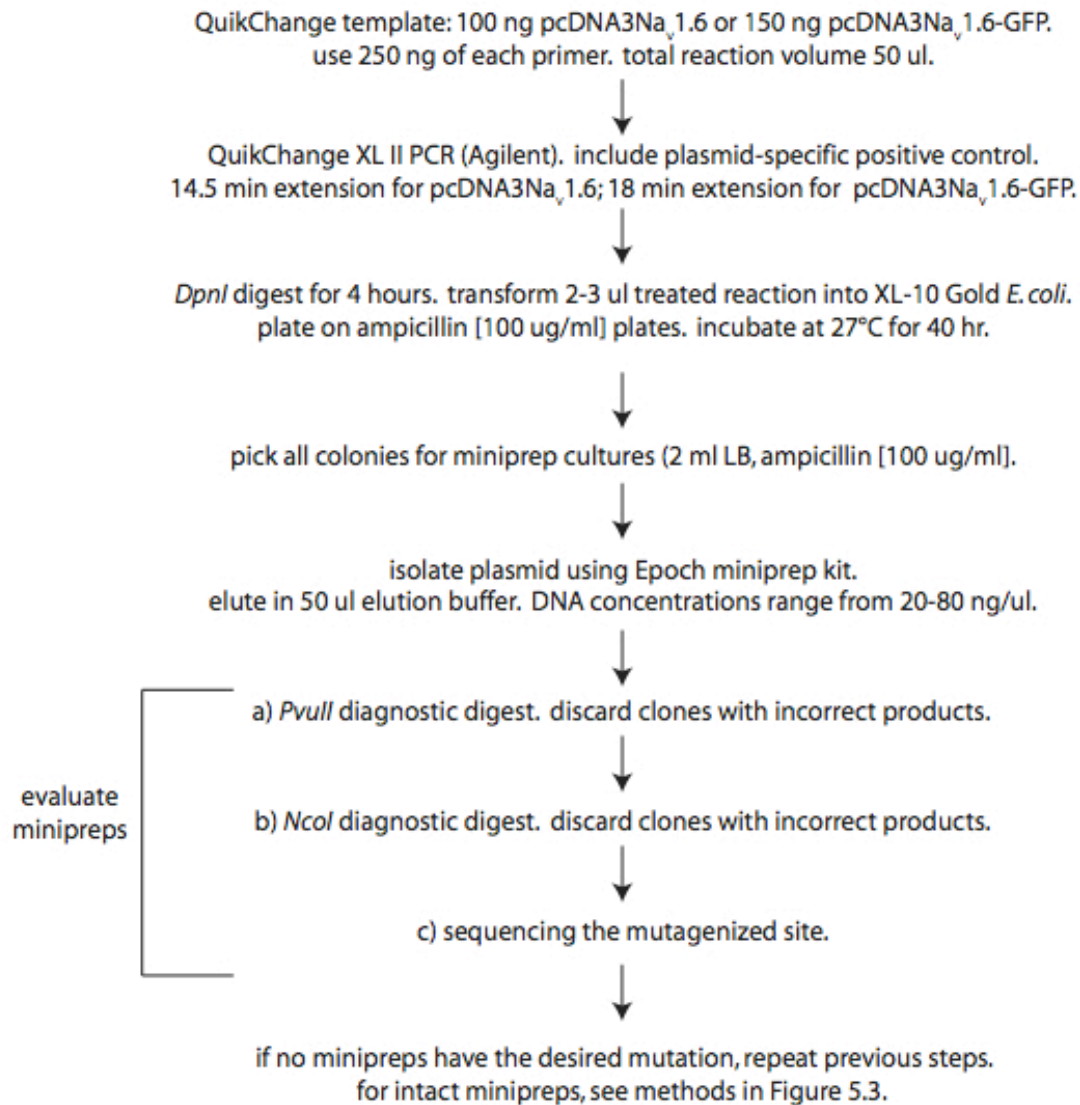


Figure 5.2. QuikChange mutagenesis and miniprep screening protocol for Na_v1.6 cDNA. *NcoI* and *PvuII* restriction patterns are shown in Figure 5.4.

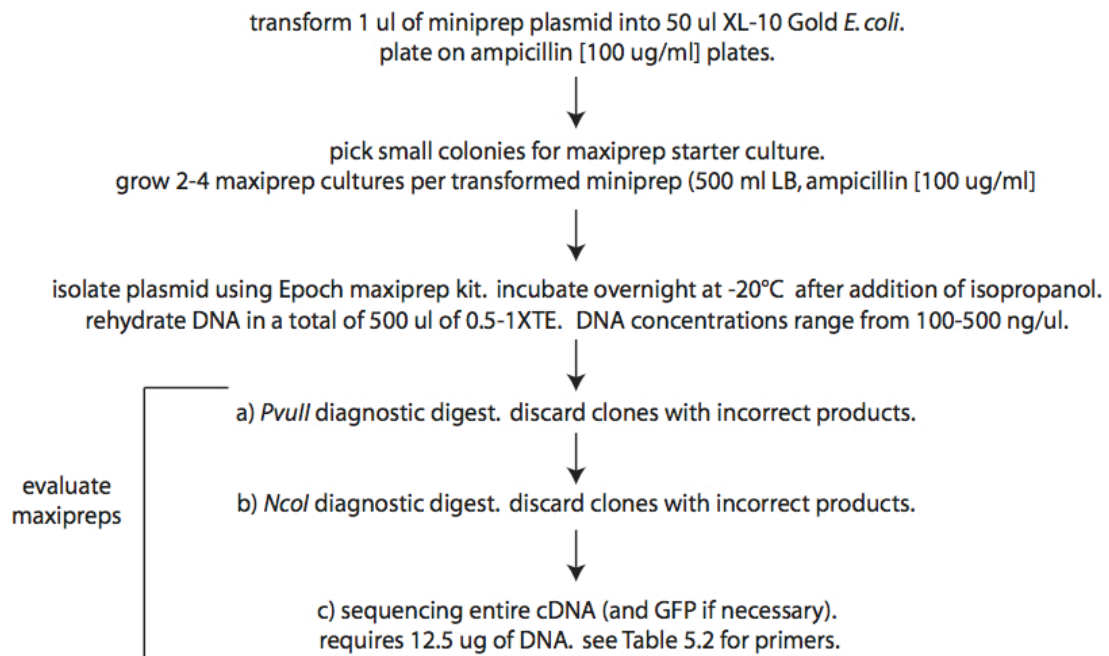


Figure 5.3. Maxiprep preparation and screening protocol for Na_v1.6 cDNA. *NcoI* and *PvuII* restriction patterns are shown in Figure 5.4.

introduced mutation. Miniprep yields are generally 20-80 ng/ul. Higher concentrations are indicative (but not entirely predictive) of rearranged plasmids.

Sequencing the entire 6 kb cDNA is necessary to ensure that no additional mutations have been introduced during bacterial growth. This requires 12.5 ug of DNA and 25 sequencing primers (**Table 5.2**). Therefore, maxipreps are necessary to obtain enough plasmid for sequencing and subsequent experiments (**Figure 5.3**). 2 ml starter cultures are incubated at 27°C for 8 hours and then used to prime the 500 ml maxiprep cultures. Plasmids are isolated from maxiprep cultures using the Epoch kit with one modification: after the addition of isopropanol to precipitate the DNA, the solution is incubated at -20°C overnight; this increases DNA yield approximately 2-fold. Approximately 1 out of 3 maxiprep cultures will yield plasmid without newly introduced point mutations. I set up 2-4 maxiprep cultures per miniprep plasmid in order to obtain enough plasmid for both sequencing and subsequent experiments (>100ug DNA). It is advisable to resuspend maxipreps in 0.5X-1X TE instead of ddH₂O to stabilize the DNA. Typical maxiprep concentrations are usually 0.1-0.5 ug/ul. Higher concentrations are, as above, indicative of rearrangements or other point mutations.

Constructs for characterization of novel human mutations. I have generated three cDNA constructs for electrophysiological characterization of patient mutations. One patient, from Utrecht, is heterozygous for the *de novo* mutation p.Arg223Gly (**Figure 5.5A**) in DIS4 (the voltage sensing transmembrane segment S4 of domain 1) (**Figure 1.1**). The functional effects of

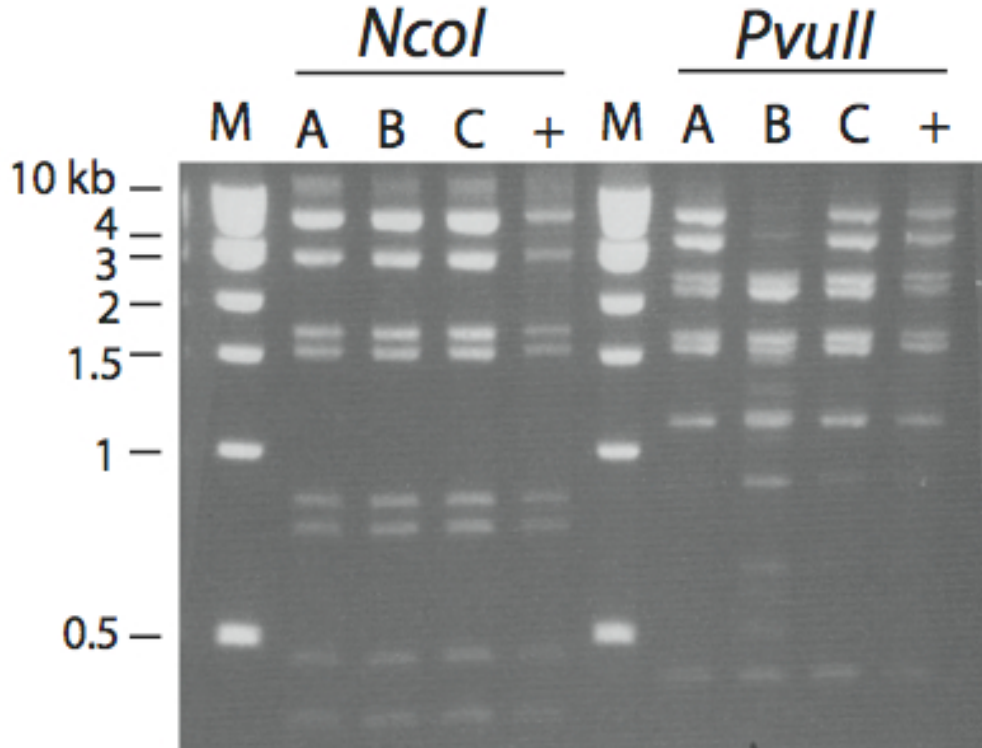


Figure 5.4. Wild-type restriction digest fragment patterns for pcDNA3Na_v1.6_R. Maxipreps A, B, and C were digested with *NcoI* (left) and *PvuII* (right). Plasmid B was rearranged, as demonstrated by the *PvuII* digest. +, positive control (intact Na_v1.6 cDNA previously confirmed by digest and full sequencing). M, 1 kb ladder. Sizes of predicted *NcoI* fragments: 4028 bp, 2613 bp, 1614 bp, 1485 bp, 813 bp, 735 bp, 462 bp, 366 bp, 12 bp. Sizes of predicted *PvuII* fragments: 4285 bp, 3127 bp, 2037 bp, 1521 bp, 1097 bp, 61 bp. *PvuII* does not always digest as predicted, so it is essential to use a positive control.

Table 5.2. Sequencing primers for the coding sequence of pcDNA3Nav1.6_R and pcDNA3Nav1.6_R-GFP. Primer start position: location in the plasmid of the first nucleotide of the primer. The 5' UTR is derived from CMV (nucleotides 251-961). The Na_v1.6 open reading frame initiates at nucleotide 993. The GFP open reading frame initiates at nucleotide 6986. Primers were designed by L. Sharkey.

Primer No.	Primer start position	Sequencing direction	Primer sequence 5' to 3'
1	725	F	TCAAC GGGAC TTTCC A
2	1058	R	CAGCG ACTCG GGGGT G
3	1168	F	TGGAG GCGGG GAAGA G
4	1498	R	TAAAT CCCTG TGAAT G
5	1979	F	CGCCG GGCAA TGCCC A
6	1996	R	TCTGG GCATT GCCCG G
7	2358	F	GGCAC CGTCT CAGAA G
8	2429	R	CTCAG ATGAG CTCCT C
9	2887	F	GCCTG CGGCG CAGCG T
10	2902	R	ACGCT GCGCC GCAGG C
11	3334	R	TGTTT GAATT GTGGC G
12	3916	F	TGAGC TCCTT CAGCG C
13	4309	R	AGGTT CTCGA AATCA G
14	4441	F	GGAAT ACTTG GATCC A
15	4869	R	GGGAC TTTAT GGCAC C
16	4921	F	GGGTG GTGGT GAACG C
17	5339	R	GCCGA AGATG ATGAA G
18	5420	F	CATCT TCATG ACAGA G
19	5831	R	TAGGG TCGGG GAGAC G
20	5924	F	GTCGC TGCCC GCCCT G
21	6317	R	GGCGC TTTCC TCTGT G
22	6407	F	GCTGG CCGAC TTTGC C
23	6771	R	GTGCC TCCAT TCTCC A
24	7113	R	GTGGC ACCTT CCAGG G

mutation of the Arg223 residue in other sodium channels are summarized in **Table 5.3**. Arg223 is invariant in all sequenced vertebrate, invertebrate, and bacterial sodium channels (**Figure 5.5A**). The p.Arg223Gly mutation is predicted to be probably (HumDiv=0.986) or possibly damaging (HumVar=0.715) by PolyPhen-2 (Adzhubei et al., 2010). The corresponding residue of *SCN5A* (Arg222) is mutated to glutamine in patients with reversible ventricular ectopy (Mann et al., 2012). We recently found that the p.Arg223Gly mutant channel is not stable in transfected HEK cells cultured at 37°C (**Figure 5.6**). Recording of this channel at 30°C indicates an increased response to a small slow depolarization (ramp current), consistent with a hyperexcitability phenotype (S. Dib-Hajj and S. Waxman, pers. comm.).

A second epileptic encephalopathy patient from Mississippi is heterozygous for the *de novo* mutation p.Thr767Ile (**Figure 5.5B**). Thr767 is located in DIIS1 (the first transmembrane segment of domain 2). This residue is conserved in vertebrates and invertebrates (**Figure 5.5B**). The patient mutation p.Thr767Ile is predicted to be deleterious (HumDiv=1.000, HumVar=0.999). This channel is stable in transfected HEK cells cultured at 37°C (**Figure 5.6**). Recording of the p.Thr767Ile mutant channel in ND7/23 cells indicates a 10 mV hyperpolarizing (leftward) shift in the voltage dependence of activation, consistent with hyperexcitability (S. Dib-Hajj and S. Waxman, pers. comm.). The Waxman lab is currently testing the properties of the p.Thr767Ile channel in transfected hippocampal neurons.

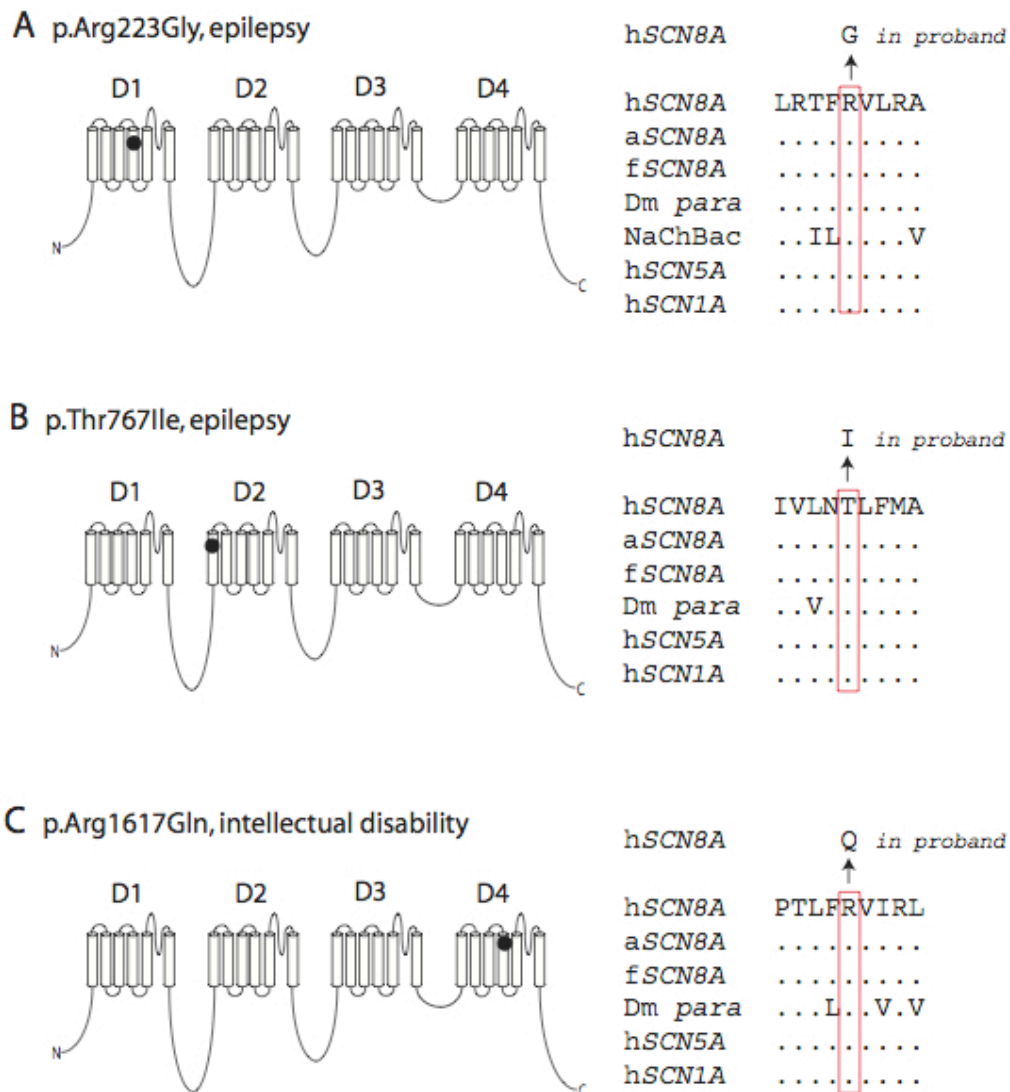


Figure 5.5. De novo patient mutations in SCN8A. The mutated residues are conserved in vertebrate orthologs and paralogs and in invertebrate channels. (A) Arg223 is located in the voltage sensing transmembrane segment of domain 1. (B) Thr767 is located in the first transmembrane segment of domain 2. (C) Arg1617 is located in the voltage sensing transmembrane segment of domain 4. Abbreviations: h, human; a, anole lizard; f, fish (Fugu); Dm, *Drosophila melanogaster*; para, fly voltage-gated sodium channel (encoded by paralytic), NaChBac, bacterial one-domain voltage gated sodium channel; hSCN5A, human cardiac sodium channel; hSCN1A, human neuronal sodium channel. One-letter amino acid codes are used. Dots represent amino acid identity.

Table 5.3. *SCN8A* p.Arg223Gly: Functional effects of corresponding mutations in other sodium channels.

Channel	Organism	Substitution	Functional effect	Reference
NaChBac	Bacteria	R->C	Slight leftward shift in conductance/voltage relationship	(DeCaen et al., 2011)
Na _v 1.2	Rat	R->Q	Leftward shift in voltage of activation	(Stuhmer et al., 1989)
NaChBac	Bacteria	R->C	Destabilization of resting state	(Yarov-Yarovoy et al., 2012)
NaChBac	Bacteria	R->K	More positive voltage dependence of activation; "interaction of E43 with R2 stabilizes closed state"	(Paldi and Gurevitz, 2010)
Na _v 1.5	Human	R->Q	"unique differential leftward voltage-dependent shifts in activation and inactivation properties of human voltage-gated Na(+) channels with the R222Q mutation, consistent with increasing channel excitability at precisely the voltages corresponding to the resting membrane potential of cardiomyocytes."	(Mann et al., 2012; Nair et al., 2012)
Na _v 1.6	Human, Mouse	R->G	Decreased stability, increased ramp current	S. Dib-Hajj and S. Waxman, pers. comm.

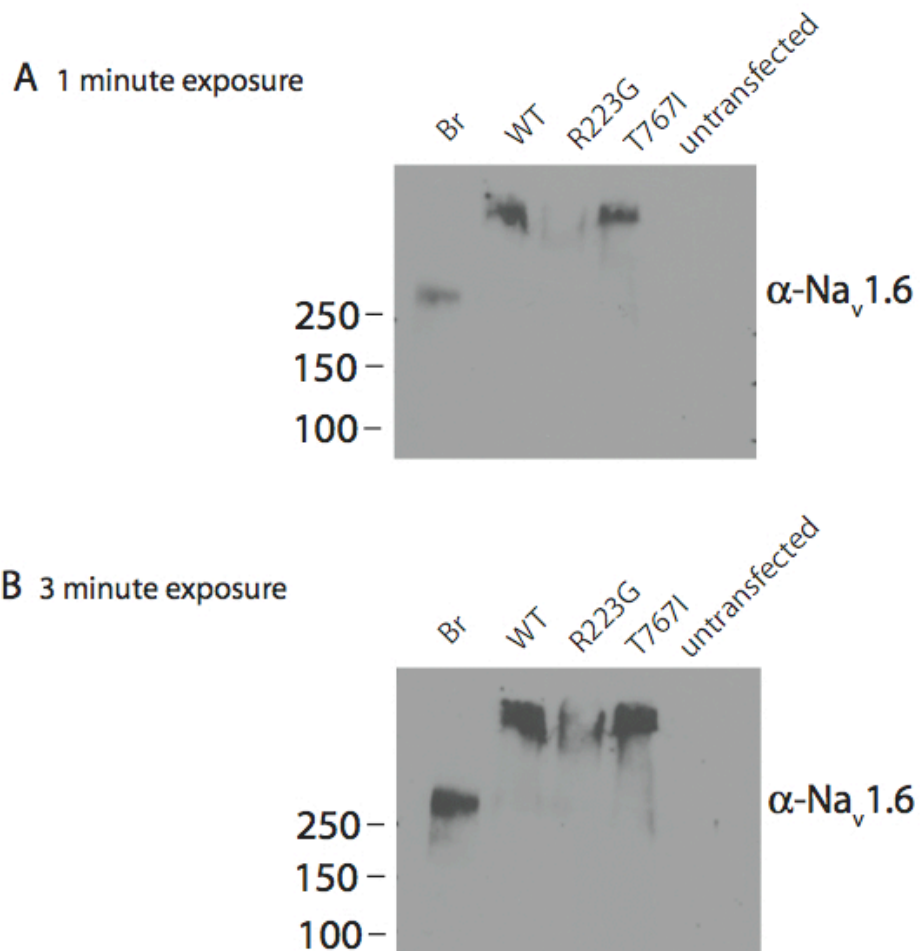


Figure 5.6. p.Arg223Gly is less stable than wild type channel in HEK cells. Western blot of lysates from HEK-293 cells transfected with wild-type or mutant $\text{Na}_v1.6$ cDNA. Lysates were run on a 4-15% gradient BioRad Criterion gel. Br, 75 ug of wild type brain membrane protein. Cells were transfected with 1 ug cDNA and incubated at 37°C for 24 hours before lysis. 1° antibody, polyclonal anti- $\text{Na}_v1.6$ (Alomone ASC-009), 1:100. 2° antibody, anti-rabbit, 1:5000. $\text{Na}_v1.6$ from transfected cells consistently migrates more slowly than $\text{Na}_v1.6$ from brain. The basis for this difference is not known, but may be excess glycosylation of the channel.

The *de novo* mutation p.Arg1617Gln (**Figure 5.5C**) was recently identified in a patient with severe intellectual disability (Rauch et al., 2012). Arg1617 is located in DIVS4 (the voltage sensing transmembrane segment of domain 4) and is invariant in vertebrate and invertebrate sodium channels. p.Arg1617Gln is predicted to be deleterious (HumDiv=1.000, HumVar=0.999). We are collaborating with the Waxman lab to test the functional effects of this mutation in cultured cells.

Na_v1.6 cDNA construct for trafficking studies in cell culture. To follow up the experiments described in Chapter III, we are interested in elucidating the role of Map1b in trafficking and subcellular localization of Na_v1.6. Dr. James Salzer at NYU is examining the trafficking of wild type and Map1b-binding-site-mutant Na_v1.6 in cell culture models of myelinated dorsal root ganglion neurons (Zhang et al., 2012). Co-cultures of neurons and Schwann cells develop an axon initial segment and nodes of Ranvier, which will allow us to determine whether interaction with Map1b is critical for localization of Na_v1.6 to these regions. Using the Na_v1.6-GFP fusion protein will permit examination of channel trafficking in real-time and specific detection of mutant channel in the presence of endogenous Na_v1.6.

To this end, I introduced the Map1b binding site mutation VAVP(77-80)AAAA (Chapter III) into the tetrodotoxin-resistant Na_v1.6-GFP fusion protein (Gasser et al., 2012). The primers used to introduce the AAAA mutation into pcDNA3Nav1.6_R (O'Brien et al., 2012b) (Chapter III) were also used for the generation of this clone. Colonies were grown, prepared, and screened as described in **Figures 5.2** and **5.3**.

Wild type and mutant Na_v1.6 have been nucleofected into co-cultured dorsal root ganglion neurons by the Salzer lab as previously described (Zhang et al., 2012),

and trafficking assays are currently in progress. Preliminary evidence suggests that the mutant channel may be less efficiently localized to nodes.

Conclusion. Working with the Na_v1.6 cDNA plasmids is technically difficult. I have developed protocols to efficiently mutagenize these plasmids. These methods, combined with the previously described growth conditions (Herzog et al., 2003), have made possible the electrophysiological characterization of several human epilepsy mutations. Additional constructs will be functionally tested during the coming months. Electrophysiological analysis of mutant constructs allows us to identify mutants with functional abnormalities, such as increased persistent current, hyperpolarizing (leftward) shifts in activation, or depolarizing (rightward) shifts in inactivation, that may account for the clinical abnormalities in patients. Mutants with unusual properties may warrant further study in the mouse.

Acknowledgements. I thank Christen Frei for assistance in cloning the p.Arg1617Gln mutation into the Na_v1.6 cDNA.

Chapter VI

Conclusions

Dissertation Findings and Significance. The work described in this dissertation has advanced the voltage-gated sodium channel field in three areas. First, I described a splicing mechanism that is partially responsible for restricting expression of full-length $\text{Na}_v1.6$ to neuronal tissues (Chapter II). Mutually exclusive splicing of exon 18A and exon 18N was first described in 1997. I identified the role of RBFOX splice factors in this splicing event. Binding of neuron-specific RBFOX proteins downstream of exon 18A promotes its inclusion in neuronal tissues. In the absence of these factors, there is inclusion of exon 18N and generation of transcripts containing an upstream in-frame stop codon that are targeted for nonsense-mediated decay. Thus, alternative splicing of exon 18 serves as an on/off switch for full-length $\text{Na}_v1.6$.

Second, I identified interaction between the N-terminus of $\text{Na}_v1.6$ and the light chain of microtubule-associated protein Map1b (Chapter III). This is the first known interaction localized to the N-terminus of $\text{Na}_v1.6$. $\text{Na}_v1.6$ and Map1b co-immunoprecipitated from mouse brain membrane fractions, verifying this interaction

in vivo. Co-transfection of Map1b with Na_v1.6 increased current density without altering electrophysiological properties of the channel, suggesting that the interaction increases the number of stable channels at the cell surface.

Third, I contributed to characterization of three *de novo* mutations in Na_v1.6 in patients with severe epileptic encephalopathy. The first of these mutations, p.Asn1768Asp, renders the channel hyperexcitable due to increased persistent current (Chapter IV). This supports a mechanism of pathogenesis in which overactivity of Na_v1.6 causes neurons to fire aberrantly and leads to an epileptic phenotype. This mutation was the first to implicate *SCN8A* as a cause of severe epilepsy. The second mutation, p.Thr767Ile causes a hyperpolarizing shift in the voltage dependence of activation, which also leads to hyperexcitability (Chapter V). The characterization of the third *de novo* mutation, p.Arg223Gly, is in progress (Chapter V). We have initiated a collaboration with the Waxman Lab at Yale University to assess pathogenicity of novel protein-coding variants in Na_v1.6 in which we introduce mutations into the Na_v1.6 cDNA (Chapters IV and V), and the Waxman Lab determines the electrophysiological properties of the mutant channels in transfected neuron-derived ND7/23 cells and cultured hippocampal neurons.

Non-pathogenic variation in SCN8A. Nine predicted deleterious amino acid substitutions have been identified in more than one individual in the Exome Variant Server, a catalog of variants in patients with heart, lung, and blood disorders (<http://evs.gs.washington.edu/EVS/>) (**Table 6.1**). Interestingly, none of these variants are located in the highly conserved transmembrane segments, and no stop

Table 6.1. Recurring missense variants in *SCN8A* identified in patients with heart, lung, and blood disorders (<http://evs.gs.washington.edu/EVS/>).

	Variant	Domain	Heterozygote Frequency	Allele Frequency	Polyphen prediction
1	p.Trp45Arg	N-terminus	2/6,263	0.00016	probably damaging
2	p.Gln475Arg	I-II Loop	3/5,890	0.00025	possibly damaging
3	p.Thr607Ala	I-II Loop	2/6,075	0.00016	benign
4	p.Asn686Asp	I-II Loop	2/5,906	0.00017	possibly damaging
5	p.Ser1050Gly	II-III Loop	2/6,434	0.00016	benign
6	p.Trp1055Arg	II-III Loop	2/6,452	0.00015	probably damaging
7	p.Arg1237Lys	IIIS1-2 linker	2/6,492	0.00015	benign
8	p.Thr1583Ile	IVS2-3 linker	2/6,310	0.00016	benign
9	p.Pro1921Thr	C-terminus	2/6,132	0.00016	benign

codons have been observed. This suggests that the most deleterious and pathogenic types of *SCN8A* mutations are very rare in the general population.

Modeling human mutations of SCN8A. The currently identified mutations in *SCN8A* fall into two distinct groups: those associated with severe epilepsy (Chapters IV and V), and those associated with intellectual disability (Trudeau et al., 2006; Rauch et al., 2012). Analysis of the p.Asn1768Asp mutation suggests that some Na_v1.6 mutations that cause epileptic encephalopathy are gain-of-function changes that result in channel hyperactivity (Veeramah et al., 2012).

We are currently examining functional consequences in cultured cells of the p.Arg1617Gln mutation that was identified in a patient with intellectual disability (Rauch et al., 2012). We predict that this mutant channel will have reduced excitability or function because of the cognitive deficits previously described in haploinsufficient individuals (Trudeau et al., 2006). Loss-of-function mutations in *SCN8A* may be more common than has been reported to date. These alleles may remain unobserved because phenotypes associated with haploinsufficiency are sub-clinical, or whole genome and/or exome sequencing has not yet been undertaken on a sufficiently large scale.

Mutant channels can be tested for pathogenicity by electrophysiology in transfected cells. Although electrophysiological assessment is an essential part of the characterization of a mutant channel, it does not reveal how a mutation affects the complex neuronal firing in the brain. Characterizing mutations in mouse models provides a more complete model of channel pathogenicity. For dominant mutations, transgenic models can be used. Although the effects of overexpressing wild-type

Na_v1.6 in mice have not been tested, overexpression of the closely related neuronal channel Na_v1.2 is not detrimental (Kearney et al., 2001). The normal temporal regulation of Na_v1.6 (Plummer et al., 1997) may be difficult to recapitulate in a transgene driven by a non-endogenous promoter (Kearney et al., 2001). Na_v1.6 can also be targeted by homologous recombination (Levin and Meisler, 2004), but this process is inefficient in *Scn8a* compared to genes that are actively expressed in mouse ES cells (e.g., ~10% targeting in *Fig4*) (Ferguson et al., 2012).

Because of these difficulties, we are investigating the use of TAL effector nuclease (TALEN) targeting technology (Sung et al., 2013) to introduce the p.Asn1768Asp epilepsy mutation into mice. TALEN-targeted alleles have the capability to combine the endogenous gene regulation of a knock-in with the cost and generation time of a transgenic model, making them an attractive option for generation of mouse models. Homologous recombination induced by TALENs was recently accomplished in fertilized mouse eggs using either oligodeoxynucleotides or a targeting vector as a substrate (Wefers et al., 2013).

In unpublished experiments, we designed two TALENs that will bind and induce a double stranded break in exon 24 of *Scn8a* near amino acid residue 1768. TALEN activity was tested by PNA Bio Inc. using an assay that detects TALEN-induced mismatch repair. Briefly, TALEN pairs are transfected into NIH3T3 cells. Genomic DNA is isolated and amplified using primers specific to the targeted region (*Scn8a* exon 24). PCR products are treated with the mismatch-repair-sensitive endonuclease T7E1 and products are visualized on an agarose gel. Since there is no substrate for homologous recombination in this assay, all TALEN-induced breaks

in the genome are repaired using the mismatch repair pathway. Thus, the level of T7E1 digestion serves as an indicator of TALEN activity.

The most active pair of TALEN mRNAs was co-injected into the male pronucleus of (SJLxB6)F2 fertilized eggs with a circular targeting plasmid containing ~4 kb of mouse genomic DNA, including the p.Asn1768Asp mutation and synonymous substitutions in the TALEN binding sites (to ensure that the TALENs would not cut repeatedly). The double stranded break introduced by the TAL effector nucleases permits homologous recombination with the plasmid and incorporation of the engineered DNA sequence into exon 24. Preliminary genotyping by PCR indicates that the engineered sequence was introduced successfully in the homozygous and heterozygous state (J. M. Jones, pers. comm.). Southern blots to confirm these observations are in progress.

One difficulty in generating TALENs for voltage-gated sodium channels is the high level of sequence identity between family members. Off-target binding of the TALENs could lead to integration of the p.Asn1768Asn mutation into *Scn4a* or *Scn5a*, the channels that have the highest nucleotide similarity in the TALEN binding sites (only 2 mismatches, compared to 3+ mismatches in the other sodium channels). We observed 11 on-target mutations in *Scn8a*, two mutations in *Scn5a*, and no mutations in *Scn4a* among the first 20 pups.

We will use the p.Asn1768Asp mouse model to examine the effect of hyperexcitability of Na_v1.6 on specific subpopulations of neurons in the brain. Inhibitory Purkinje neurons and excitatory cortical pyramidal neurons will be of particular interest, since they rely heavily on Na_v1.6 for their firing properties. This

mouse model will also allow us to test the role of p.Asn1768Asp in the sudden unexplained death in epilepsy observed in the patient carrying this mutation (Veeramah et al., 2012). If the mouse model exhibits premature lethality, we could monitor mutants using EEGs to detect potential seizure events associated with death. We also plan to evaluate treatments for this disease using this mouse. Since the p.Asn1768Asp channel does not close completely (as evidenced by the increased persistent current), low doses of open-state channel blocker drugs such as phenytoin might preferentially target the mutant channel and ameliorate a seizure phenotype.

Map1b in trafficking and subcellular localization of Na_v1.6. As described in Chapter III, I investigated the role of microtubule-associated protein Map1b in cell-surface localization of Na_v1.6. Mutation of the Map1b binding site in Na_v1.6 resulted in reduced current density, suggesting that mutant channel has reduced ability to reach the cell surface. Possible mechanisms include retention of the mutant channel in the ER or Golgi, or defective trafficking of the channel after insertion into trafficking vesicles.

To further investigate the role of Map1b in channel trafficking and localization, I mutated the Map1b binding site VAVP to AAAA in the GFP-Na_v1.6 cDNA (Gasser et al., 2012) (Chapter V). We are collaborating with Dr. James Salzer at NYU, who will study the trafficking of the mutant channel in nucleofected dorsal root ganglia co-cultured with Schwann cells (Zhang et al., 2012). These co-cultures develop an AIS and nodes, and will allow us to examine whether Map1b binding is necessary for subcellular localization of Na_v1.6 to these sites. We will also be able to determine

the intracellular location of the mutant Na_v1.6 to identify which step in trafficking is defective.

It may also be possible to assess channel trafficking in brains of mice electroporated with the VAVP(77-80)AAAA-Na_v1.6-GFP channel *in utero* at E14 using the method described by Hedstrom and colleagues (2007). Electroporated mice were sacrificed at P27, and the location of the mutant protein was determined by immunohistochemistry using antibodies against GFP (Hedstrom et al., 2007; Gasser et al., 2012). This would provide a way to assay the trafficking of the mutant channel in the context of the brain *in vivo*.

Recent work from the Waxman lab has shown that the ankyrin-binding motif in intracellular loop 2 is necessary for localization of Na_v1.6 to the AIS and nodes (Gasser et al., 2012). The authors write that the ankyrin-binding motif is “sufficient” for localization of the channel to these domains. However, sufficiency was determined in the context of a single-transmembrane reporter construct (Gasser et al., 2012). Since Na_v1.6 already contains an ankyrin-binding motif, a traditional test of sufficiency may be logically impossible. A more appropriate test would be to add the ankyrin-binding domain to a large, multi-domain transmembrane protein, such as Ca_v3.1, that is not normally located at the AIS or nodes.

In the context of the full-length channel, Map1b and ankyrin may work sequentially during targeting and localization. For example, Map1b may tether vesicles containing Na_v1.6 to microtubules during transport from the Golgi to the axon. On reaching the AIS, sodium channels could bind ankyrin and be targeted to their subcellular locations in the axon. Map1b may alternatively function as a

secondary anchor once the channel is inserted into the extracellular membrane, working in concert with ankyrin. A combination of Map1b and ankyrin might tether Na_v1.6 to both microtubules and spectrin components of the cytoskeleton, providing a more secure anchoring system for the channel at the AIS and nodes. Experiments using the mutated VAVP(77-80)AAAA-Na_v1.6-GFP channel (Chapter V) could help determine the role of Map1b in the extensive targeting and trafficking process.

Potential non-conducting functions of Na_v1.6 suggested by study of the mutant Scn8a^{9J}. We are characterizing a spontaneous mutation of Na_v1.6, *Scn8a^{9J}*, which deletes isoleucine residue 1750 in DIVS6 (Jones et al., 2013). The mutant channel has no detectable current in transfected HEK cells or ND7/23 cells. There was no repetitive firing in Purkinje neurons from mutant brain slices. However, this mutant survives much longer than *Scn8a* null mice, with 40% of homozygotes surviving past 8 months of age and a maximum lifespan of longer than a year. Mutant protein is present in membrane fractions and at nodes in the sciatic nerve (Jones et al., 2013). It is possible that mutant channels are electrophysiologically active in cell types that were not analyzed to date. It will be important to examine the gating current of *Scn8a^{9J}* mutant channels to determine whether they are capable of responding to changes in membrane potential.

Another possibility is that alternative, non-conducting functions of Na_v1.6 are preserved in *Scn8a^{9J}*. For example, the *Scn8a^{9J}* mutant protein is localized to nodes of Ranvier (Jones et al., 2013), where it may contribute to protein-protein interactions that stabilize other proteins such as voltage-gated potassium channels. Mutants of Na_v1.6 lacking channel protein would then result in both sodium channel

and potassium channel deficiencies, either of which could prevent action potentials. It could be of interest to examine potassium currents in neurons cultured from *Scn8a*^{9J} homozygous mutant mice. *Scn8a*^{9J} mice will be useful for investigation of alternative functions of voltage-gated sodium channels *in vivo*.

Future identification of novel binding partners of Na_v1.6. The function and regulation of Na_v1.6 is a complex process that requires the action of many different proteins. The known interactions of Na_v1.6 were summarized in **Figure 1.6**. Na_v1.6 may interact with additional molecules *in vivo*, and these interactions could contribute to trafficking, subcellular localization, non-channel functions, and regulation of the electrophysiological properties of the channel.

We propose to insert an avidin tag into Na_v1.6 for biotin labeling and pulldown followed by mass spectrometry to identify interacting proteins. It will be important to insert this tag at a location that will not interfere with the subcellular localization or function of Na_v1.6. For example, Na_v1.6 cDNA has been tagged at the C-terminus with GFP and RFP without affecting electrophysiological properties or localization of the channel (Gasser et al., 2012), suggesting that the C-terminus would be a good location for adding an intracellular avidin tag. Alternatively, intracellular regions with low evolutionary conservation could provide locations to insert the tag.

There are multiple ways to introduce the avidin tag, including TALEN-based homologous recombination or recombineering in a rat BAC that contains the Na_v1.6 genomic DNA sequence and endogenous promoter. It may be useful to use homozygous tagged channel alleles in order to eliminate competition with the wild type channel.

Interactions identified using mass spectroscopy could be verified by co-immunoprecipitation with Na_v1.6 from brain membrane fractions, co-localization in mouse neurons or sciatic nerves, or co-transfection with Na_v1.6 in cells to detect the functional effect on the electrophysiology of the channel. Identification of novel interacting proteins would provide potential targets for therapies for patients with neurological disorders.

Haploinsufficiency of neuronal voltage-gated sodium channels.

Mutations in the major neuronal voltage-gated sodium channels are associated with seizure disorders (e.g., epileptic encephalopathies, Dravet syndrome, GEFS+), and intellectual disability and autism (Weiss et al., 2003; Trudeau et al., 2006; Catarino et al., 2011; Rauch et al., 2012). Loss-of-function mutations in *SCN1A* (Na_v1.1) are a major cause of Dravet Syndrome, a severe form of epilepsy with neuronal hyperexcitability (Catarino et al., 2011). It is surprising that loss-of-function mutations in a voltage-gated sodium channel cause a phenotype associated with overactivity of neurons. Catterall and others have proposed that reduced levels of Na_v1.1 in inhibitory GABAergic neurons causes reduced firing of these neurons, leading to global hyperexcitability and seizures in a *Scn1a*^{+/-} mouse model of Dravet Syndrome (Yu et al., 2006; Cheah et al., 2012). However, both inhibitory bipolar neurons and excitatory pyramidal neurons derived from Dravet patient iPSCs have approximately 3-fold increased sodium currents and spontaneous bursting (Liu et al., 2013), with no change in the voltage dependences of activation and inactivation of the channels. Additionally, not all Na_v1.1 epilepsy mutations are loss-of-function. p.Arg1648His is a gain-of-function mutation in Na_v1.1 identified in a GEFS+ patient.

This mutation causes increased recovery from inactivation and leads to hyperexcitability (Spampanato et al., 2001). The data support a model in which global hyperexcitability, originating by multiple mechanisms, leads to epilepsy.

Loss-of-function mutations in Na_v1.6 have been associated with intellectual disability in humans (Trudeau et al., 2006; Rauch et al., 2012) and anxiety-like phenotypes in mice (McKinney et al., 2008). Mutations that cause gross hyperexcitability may cause epilepsy, while mutations that result in hypoexcitability may be more likely to cause intellectual disability.

A proposed mechanism for haploinsufficiency of neuronal voltage-gated sodium channels. Haploinsufficiency of Na_v1.1 or Na_v1.6 may result in some subcellular locations normally filled by these channels to be occupied by other voltage-gated sodium channels (**Figure 6.1**). Channel mislocalization would alter the firing properties of the neuron and cause the channel-specific haploinsufficiency phenotypes described above.

Potential increased localization of Na_v1.6 to replace Na_v1.1 at the AIS in Dravet (*SCN1A*^{+/-}) neurons is predicted to increase the probability of axon potential initiation, because Na_v1.6 has a more hyperpolarized voltage dependence of activation than Na_v1.1 in heterologous systems and cultured neurons (Chen et al., 2008; Kole et al., 2008; Royeck et al., 2008; Hu et al., 2009). Thus, increased Na_v1.6 at the AIS would lower the action potential threshold, leading to overall neuronal hyperexcitability in mutant neurons. Increased accumulation of Na_v1.6 at the AIS (approximately twice wild type levels) has been associated with seizures in *Celf4*^{-/-} mice (Sun et al., 2013).




Channel	Genotype	Predicted Channel Distribution in AIS	Predicted Neuronal Excitability	Known Patient Phenotype
all	normal	 Na _v 1.1 Na _v 1.6 Na _v 1.2	normal	none
<i>SCN8A</i> Na _v 1.6	+/-	 Na _v 1.1 Na _v 1.6 Na _v 1.2	decreased	intellectual disability
<i>SCN1A</i> Na _v 1.1	+/-	 Na _v 1.1 Na _v 1.6 Na _v 1.2	increased	seizures (Dravet syndrome)

Figure 6.1. Proposed model of haploinsufficiency. The channel composition of the AIS may change in response to deficiency of specific channels, leading to hyperexcitability and epilepsy or to hypoexcitability and intellectual disability.

In the *Scn8a^{med}* null mouse, Na_v1.2 is localized to the distal AIS (Van Wart and Matthews, 2006), demonstrating that a channel with different electrophysiological properties can replace the missing channel *in vivo*. Replacement of Na_v1.6 with Na_v1.2 may decrease action potential firing (Van Wart and Matthews, 2006; Chen et al., 2008). Likewise, reduced Na_v1.6 at the AIS in patients with intellectual disability could reduce neuronal activity.

Specific populations of neurons, including the cortical and cerebellar interneurons (Lorincz and Nusser, 2008), retinal ganglion cells, and a subset of CA3 hippocampal neurons (Van Wart et al., 2007), exhibit distinct localizations of Na_v1.1 to the proximal AIS and Na_v1.6 to the distal AIS. In *Scn1a^{+/-}* mice and Dravet patient derived neurons, there may be encroachment of Na_v1.6 into the proximal AIS. Conversely, neurons from *Scn8a^{+/-}* mice and patients with intellectual disability could contain increased Na_v1.1 or Na_v1.2 localization at the distal AIS (**Figure 6.1**). To test this model, one could co-stain wild type, *Scn1a^{+/-}*, and *Scn8a^{+/-}* neurons for ankyrin (to mark the total AIS), Na_v1.1, and Na_v1.6, to determine the proportion of AIS containing Na_v1.6 as described previously (Van Wart et al., 2007; Lorincz and Nusser, 2008).

Biomedical Implications. The work described in this dissertation has provided insight into the basic biology and mechanism of disease of Na_v1.6. The Meisler lab has carried out candidate gene screening of *SCN8A* in ataxia, essential tremor (Sharkey et al., 2009b), autism, and amyotrophic lateral sclerosis (unpublished), but few mutations were identified. When I started my work, in 2007, a single inherited variant in Na_v1.6 had been identified in a family with intellectual

disability (Trudeau et al., 2006). Since then, the introduction of next-generation sequencing has identified several *de novo* mutations of Na_v1.6 in patients with epileptic encephalopathy and intellectual disability (Chapters IV and V). We collaborated with electrophysiologists to characterize the first gain-of-function pathogenic human mutation in Na_v1.6 (Veeramah et al., 2012). In doing so, we established an effective ongoing collaboration for future characterization of additional newly identified human variants of Na_v1.6 in cultured cells. Several more mutations are in the pipeline. The development of mouse models for some of these human mutations will provide insight into the role of Na_v1.6 in epilepsy and intellectual disability *in vivo*. Mouse models may also permit testing potential treatments for these disorders, such as sodium channel blockers or newly identified compounds, as well as screening for genetic modifiers defining novel therapeutic targets.

References

ASSP splice predictor, <http://www.es.embnet.org/~mwang/assp.html>.

Abriel, H., Kamynina, E., Horisberger, J.D., and Staub, O. (2000). Regulation of the cardiac voltage-gated Na⁺ channel (H1) by the ubiquitin-protein ligase Nedd4. *FEBS letters* 466, 377-380.

Adzhubei, I.A., Schmidt, S., Peshkin, L., Ramensky, V.E., Gerasimova, A., Bork, P., Kondrashov, A.S., and Sunyaev, S.R. (2010). A method and server for predicting damaging missense mutations. *Nat Methods* 7, 248-249.

Alessandri-Haber, N., Alcaraz, G., Deleuze, C., Jullien, F., Manrique, C., Couraud, F., Crest, M., and Giraud, P. (2002). Molecular determinants of emerging excitability in rat embryonic motoneurons. *J Physiol* 541, 25-39.

Aman, T.K., and Raman, I.M. (2007). Subunit dependence of Na channel slow inactivation and open channel block in cerebellar neurons. *Biophys J* 92, 1938-1951.

Aman, T.K., Grieco-Calub, T.M., Chen, C., Rusconi, R., Slat, E.A., Isom, L.L., and Raman, I.M. (2009). Regulation of persistent Na current by interactions between beta subunits of voltage-gated Na channels. *J Neurosci* 29, 2027-2042.

Aman, T.K., and Raman, I.M. (2010). Inwardly permeating Na ions generate the voltage dependence of resurgent Na current in cerebellar Purkinje neurons. *J Neurosci* 30, 5629-5634.

Augustin, I., Korte, S., Rickmann, M., Kretschmar, H.A., Sudhof, T.C., Herms, J.W., and Brose, N. (2001). The cerebellum-specific Munc13 isoform Munc13-3 regulates cerebellar synaptic transmission and motor learning in mice. *J Neurosci* 21, 10-17.

Bahler, M., and Rhoads, A. (2002). Calmodulin signaling via the IQ motif. *FEBS letters* 513, 107-113.

Bamshad, M.J., Ng, S.B., Bigham, A.W., Tabor, H.K., Emond, M.J., Nickerson, D.A., and Shendure, J. (2011). Exome sequencing as a tool for Mendelian disease gene discovery. *Nat Rev Genet* 12, 745-755.

Bant, J.S., and Raman, I.M. (2010). Control of transient, resurgent, and persistent current by open-channel block by Na channel beta4 in cultured cerebellar granule neurons. *Proc Natl Acad Sci U S A* 107, 12357-12362.

Barres, B.A., Silverstein, B.E., Corey, D.P., and Chun, L.L. (1988). Immunological, morphological, and electrophysiological variation among retinal ganglion cells purified by panning. *Neuron* 1, 791-803.

Barres, B.A., Koroshetz, W.J., Chun, L.L., and Corey, D.P. (1990). Ion channel expression by white matter glia: the type-1 astrocyte. *Neuron* 5, 527-544.

Barres, B.A., Hart, I.K., Coles, H.S., Burne, J.F., Voyvodic, J.T., Richardson, W.D., and Raff, M.C. (1992). Cell death and control of cell survival in the oligodendrocyte lineage. *Cell* 70, 31-46.

Basu, J., Betz, A., Brose, N., and Rosenmund, C. (2007). Munc13-1 C1 domain activation lowers the energy barrier for synaptic vesicle fusion. *J Neurosci* 27, 1200-1210.

Bennett, V., and Lambert, S. (1999). Physiological roles of axonal ankyrins in survival of premyelinated axons and localization of voltage-gated sodium channels. *J Neurocytol* 28, 303-318.

Bhalla, K., Phillips, H.A., Crawford, J., McKenzie, O.L., Mulley, J.C., Eyre, H., Gardner, A.E., Kremmidiotis, G., and Callen, D.F. (2004). The de novo chromosome 16 translocations of two patients with abnormal phenotypes (mental retardation and epilepsy) disrupt the A2BP1 gene. *J Hum Genet* 49, 308-311.

Black, J.A., Renganathan, M., and Waxman, S.G. (2002). Sodium channel Na(v)1.6 is expressed along nonmyelinated axons and it contributes to conduction. *Brain Res Mol Brain Res* 105, 19-28.

Boiko, T., Rasband, M.N., Levinson, S.R., Caldwell, J.H., Mandel, G., Trimmer, J.S., and Matthews, G. (2001). Compact myelin dictates the differential targeting of two sodium channel isoforms in the same axon. *Neuron* 30, 91-104.

Boiko, T., Van Wart, A., Caldwell, J.H., Levinson, S.R., Trimmer, J.S., and Matthews, G. (2003). Functional specialization of the axon initial segment by isoform-specific sodium channel targeting. *J Neurosci* 23, 2306-2313.

Brackenbury, W.J., Djamgoz, M.B., and Isom, L.L. (2008). An emerging role for voltage-gated Na⁺ channels in cellular migration: regulation of central nervous system development and potentiation of invasive cancers. *Neuroscientist* 14, 571-583.

Brackenbury, W.J., Calhoun, J.D., Chen, C., Miyazaki, H., Nukina, N., Oyama, F., Ranscht, B., and Isom, L.L. (2010). Functional reciprocity between Na⁺ channel Nav1.6 and beta1 subunits in the coordinated regulation of excitability and neurite outgrowth. *Proc Natl Acad Sci U S A* 107, 2283-2288.

Brose, N., Rosenmund, C., and Rettig, J. (2000). Regulation of transmitter release by Unc-13 and its homologues. *Curr Opin Neurobiol* 10, 303-311.

- Buchner, D.A., Trudeau, M., and Meisler, M.H. (2003). SCNM1, a putative RNA splicing factor that modifies disease severity in mice. *Science* *301*, 967-969.
- Buchner, D.A., Seburn, K.L., Frankel, W.N., and Meisler, M.H. (2004). Three ENU-induced neurological mutations in the pore loop of sodium channel Scn8a (Na(v)1.6) and a genetically linked retinal mutation, rd13. *Mamm Genome* *15*, 344-351.
- Burgess, D.L., Kohrman, D.C., Galt, J., Plummer, N.W., Jones, J.M., Spear, B., and Meisler, M.H. (1995a). Mutation of a new sodium channel gene, Scn8a, in the mouse mutant 'motor endplate disease'. *Nat Genet* *10*, 461-465.
- Burgess, D.L., Kohrman, D.C., Galt, J., Plummer, N.W., Jones, J.M., Spear, B., and Meisler, M.H. (1995b). Mutation of a new sodium channel gene, Scn8a, in the mouse mutant 'motor endplate disease'. *Nat Genet* *10*, 461-465.
- Cahoy, J.D., Emery, B., Kaushal, A., Foo, L.C., Zamanian, J.L., Christopherson, K.S., Xing, Y., Lubischer, J.L., Krieg, P.A., Krupenko, S.A., Thompson, W.J., and Barres, B.A. (2008). A transcriptome database for astrocytes, neurons, and oligodendrocytes: a new resource for understanding brain development and function. *J Neurosci* *28*, 264-278.
- Carrithers, M.D., Chatterjee, G., Carrithers, L.M., Offoha, R., Iheagwara, U., Rahner, C., Graham, M., and Waxman, S.G. (2009). Regulation of podosome formation in macrophages by a novel splice variant of the sodium channel SCN8A. *J Biol Chem*.
- Catarino, C.B., Liu, J.Y., Liagkouras, I., Gibbons, V.S., Labrum, R.W., Ellis, R., Woodward, C., Davis, M.B., Smith, S.J., Cross, J.H., Appleton, R.E., Yendle, S.C., McMahon, J.M., Bellows, S.T., Jacques, T.S., Zuberi, S.M., Koepp, M.J., Martinian, L., Scheffer, I.E., Thom, M., and Sisodiya, S.M. (2011). Dravet syndrome as epileptic encephalopathy: evidence from long-term course and neuropathology. *Brain* *134*, 2982-3010.
- Catterall, W.A., Goldin, A.L., and Waxman, S.G. (2005). International Union of Pharmacology. XLVII. Nomenclature and structure-function relationships of voltage-gated sodium channels. *Pharmacol Rev* *57*, 397-409.
- Catterall, W.A., Dib-Hajj, S., Meisler, M.H., and Pietrobon, D. (2008). Inherited neuronal ion channelopathies: new windows on complex neurological diseases. *J Neurosci* *28*, 11768-11777.
- Cheah, C.S., Yu, F.H., Westenbroek, R.E., Kalume, F.K., Oakley, J.C., Potter, G.B., Rubenstein, J.L., and Catterall, W.A. (2012). Specific deletion of NaV1.1 sodium channels in inhibitory interneurons causes seizures and premature death in a mouse model of Dravet syndrome. *Proc Natl Acad Sci U S A* *109*, 14646-14651.
- Chen, S., Su, H., Yue, C., Remy, S., Royeck, M., Sochivko, D., Opitz, T., Beck, H., and Yaari, Y. (2011). An increase in persistent sodium current contributes to intrinsic neuronal bursting after status epilepticus. *J Neurophysiol* *105*, 117-129.

Chen, Y., Yu, F.H., Sharp, E.M., Beacham, D., Scheuer, T., and Catterall, W.A. (2008). Functional properties and differential neuromodulation of Na(v)1.6 channels. *Mol Cell Neurosci* 38, 607-615.

Chioni, A.M., Brackenbury, W.J., Calhoun, J.D., Isom, L.L., and Djamgoz, M.B. (2009). A novel adhesion molecule in human breast cancer cells: voltage-gated Na⁺ channel beta1 subunit. *Int J Biochem Cell Biol* 41, 1216-1227.

Conrad, D.F., Keebler, J.E.M., Depristo, M.A., Lindsay, S.J., Zhang, Y., Casals, F., Idaghdour, Y., Hartl, C.L., Torroja, C., Garimella, K.V., Zilversmit, M., Cartwright, R., Rouleau, G.A., Daly, M., Stone, E.A., Hurler, M.E., Awadalla, P., and Project, G. (2011). Variation in genome-wide mutation rates within and between human families. *Nat Genet* 43, 712-714.

Cooper, G.M., Coe, B.P., Girirajan, S., Rosenfeld, J.A., Vu, T.H., Baker, C., Williams, C., Stalker, H., Hamid, R., Hannig, V., Abdel-Hamid, H., Bader, P., Mccracken, E., Niyazov, D., Leppig, K., Thiese, H., Hummel, M., Alexander, N., Gorski, J., Kussmann, J., Shashi, V., Johnson, K., Rehder, C., Ballif, B.C., Shaffer, L.G., and Eichler, E.E. (2011). A copy number variation morbidity map of developmental delay. *Nat Genet*, 1-11.

Crill, W.E. (1996). Persistent sodium current in mammalian central neurons. *Annu Rev Physiol* 58, 349-362.

Cummins, T.R., Dib-Hajj, S.D., Herzog, R.I., and Waxman, S.G. (2005). Nav1.6 channels generate resurgent sodium currents in spinal sensory neurons. *FEBS letters* 579, 2166-2170.

Davis, J.Q., Lambert, S., and Bennett, V. (1996). Molecular composition of the node of Ranvier: identification of ankyrin-binding cell adhesion molecules neurofascin (mucin⁺/third FNIII domain⁻) and NrCAM at nodal axon segments. *J Cell Biol* 135, 1355-1367.

De Biase, L.M., Nishiyama, A., and Bergles, D.E. (2010). Excitability and synaptic communication within the oligodendrocyte lineage. *J Neurosci* 30, 3600-3611.

De Repentigny, Y., Cote, P.D., Pool, M., Bernier, G., Girard, S., Vidal, S.M., and Kothary, R. (2001). Pathological and genetic analysis of the degenerating muscle (dmu) mouse: a new allele of Scn8a. *Hum Mol Genet* 10, 1819-1827.

Depienne, C., Trouillard, O., Saint-Martin, C., Gourfinkel-An, I., Bouteiller, D., Carpentier, W., Keren, B., Abert, B., Gautier, A., Baulac, S., Arzimanoglou, A., Cazeneuve, C., Nabbout, R., and LeGuern, E. (2009). Spectrum of SCN1A gene mutations associated with Dravet syndrome: analysis of 333 patients. *J Med Genet* 46, 183-191.

Devinsky, O. (2011). Sudden, unexpected death in epilepsy. *N Engl J Med* 365, 1801-1811.

Dewey, F.E., Chen, R., Cordero, S.P., Ormond, K.E., Caleshu, C., Karczewski, K.J., Whirl-Carrillo, M., Wheeler, M.T., Dudley, J.T., Byrnes, J.K., Cornejo, O.E., Knowles, J.W., Woon, M., Sangkuhl, K., Gong, L., Thorn, C.F., Hebert, J.M., Capriotti, E., David, S.P., Pavlovic, A., West, A., Thakuria, J.V., Ball, M.P., Zaranek, A.W., Rehm, H.L., Church, G.M., West, J.S., Bustamante, C.D., Snyder, M., Altman, R.B., Klein, T.E., Butte, A.J., and Ashley, E.A. (2011). Phased whole-genome genetic risk in a family quartet using a major allele reference sequence. *PLoS Genet* 7, e1002280.

Dib-Hajj, S.D., Choi, J.S., Macala, L.J., Tyrrell, L., Black, J.A., Cummins, T.R., and Waxman, S.G. (2009). Transfection of rat or mouse neurons by biolistics or electroporation. *Nature protocols* 4, 1118-1126.

Dib-Hajj, S.D., and Waxman, S.G. (2010). Isoform-specific and pan-channel partners regulate trafficking and plasma membrane stability; and alter sodium channel gating properties. *Neurosci Lett* 486, 84-91.

Do, M.T., and Bean, B.P. (2004). Sodium currents in subthalamic nucleus neurons from Nav1.6-null mice. *J Neurophysiol* 92, 726-733.

Drews, V.L., Lieberman, A.P., and Meisler, M.H. (2005). Multiple transcripts of sodium channel SCN8A (Na(V)1.6) with alternative 5'- and 3'-untranslated regions and initial characterization of the SCN8A promoter. *Genomics* 85, 245-257.

Drews, V.L., Shi, K., de Haan, G., and Meisler, M.H. (2007). Identification of evolutionarily conserved, functional noncoding elements in the promoter region of the sodium channel gene SCN8A. *Mamm Genome* 18, 723-731.

Drmanac, R., Sparks, A.B., Callow, M.J., Halpern, A.L., Burns, N.L., Kermani, B.G., Carnevali, P., Nazarenko, I., Nilsen, G.B., Yeung, G., Dahl, F., Fernandez, A., Staker, B., Pant, K.P., Baccash, J., Borcharding, A.P., Brownley, A., Cedeno, R., Chen, L., Chernikoff, D., Cheung, A., Chirita, R., Curson, B., Ebert, J.C., Hacker, C.R., Hartlage, R., Hauser, B., Huang, S., Jiang, Y., Karpinchyk, V., Koenig, M., Kong, C., Landers, T., Le, C., Liu, J., McBride, C.E., Morenzoni, M., Morey, R.E., Mutch, K., Perazich, H., Perry, K., Peters, B.A., Peterson, J., Pethiyagoda, C.L., Pothuraju, K., Richter, C., Rosenbaum, A.M., Roy, S., Shafiq, J., Sharanovich, U., Shannon, K.W., Sheppy, C.G., Sun, M., Thakuria, J.V., Tran, A., Vu, D., Zaranek, A.W., Wu, X., Drmanac, S., Oliphant, A.R., Banyai, W.C., Martin, B., Ballinger, D.G., Church, G.M., and Reid, C.A. (2010). Human genome sequencing using unchained base reads on self-assembling DNA nanoarrays. *Science* 327, 78-81.

Du, Y., Huang, X., Wang, T., Han, K., Zhang, J., Xi, Y., Wu, G., and Ma, A. (2007). Downregulation of neuronal sodium channel subunits Nav1.1 and Nav1.6 in the sinoatrial node from volume-overloaded heart failure rat. *Pflugers Arch* 454, 451-459.

Dugas, J.C., Tai, Y.C., Speed, T.P., Ngai, J., and Barres, B.A. (2006). Functional genomic analysis of oligodendrocyte differentiation. *J Neurosci* 26, 10967-10983.

- Dzhashiashvili, Y., Zhang, Y., Galinska, J., Lam, I., Grumet, M., and Salzer, J.L. (2007). Nodes of Ranvier and axon initial segments are ankyrin G-dependent domains that assemble by distinct mechanisms. *J Cell Biol* 177, 857-870.
- Edelmann, W., Zervas, M., Costello, P., Roback, L., Fischer, I., Hammarback, J.A., Cowan, N., Davies, P., Wainer, B., and Kucherlapati, R. (1996). Neuronal abnormalities in microtubule-associated protein 1B mutant mice. *Proc Natl Acad Sci U S A* 93, 1270-1275.
- Enomoto, A., Han, J.M., Hsiao, C.F., and Chandler, S.H. (2007). Sodium currents in mesencephalic trigeminal neurons from Nav1.6 null mice. *J Neurophysiol* 98, 710-719.
- Eriksson, M., Samuelsson, H., Bjorklund, S., Tortosa, E., Avila, J., Samuelsson, E.B., Benedikz, E., and Sundstrom, E. (2010). MAP1B binds to the NMDA receptor subunit NR3A and affects NR3A protein concentrations. *Neurosci Lett* 475, 33-37.
- Estacion, M., Gasser, A., Dib-Hajj, S.D., and Waxman, S.G. (2010). A sodium channel mutation linked to epilepsy increases ramp and persistent current of Nav1.3 and induces hyperexcitability in hippocampal neurons. *Exp Neurol* 224, 362-368.
- Everitt, A.B., Luu, T., Cromer, B., Tierney, M.L., Birnir, B., Olsen, R.W., and Gage, P.W. (2004). Conductance of recombinant GABA (A) channels is increased in cells co-expressing GABA(A) receptor-associated protein. *J Biol Chem* 279, 21701-21706.
- Feldkamp, M.D., Yu, L., and Shea, M.A. (2011). Structural and Energetic Determinants of Apo Calmodulin Binding to the IQ Motif of the Na(V)1.2 Voltage-Dependent Sodium Channel. *Structure* 19, 733-747.
- Ferguson, C.J., Lenk, G.M., Jones, J.M., Grant, A.E., Winters, J.J., Dowling, J.J., Giger, R.J., and Meisler, M.H. (2012). Neuronal expression of Fig4 is both necessary and sufficient to prevent spongiform neurodegeneration. *Hum Mol Genet* 21, 3525-3534.
- Fotia, A.B., Ekberg, J., Adams, D.J., Cook, D.I., Poronnik, P., and Kumar, S. (2004). Regulation of neuronal voltage-gated sodium channels by the ubiquitin-protein ligases Nedd4 and Nedd4-2. *J Biol Chem* 279, 28930-28935.
- Gant, J.C., Thibault, O., Blalock, E.M., Yang, J., Bachstetter, A., Kotick, J., Schauwecker, P.E., Hauser, K.F., Smith, G.M., Mervis, R., Li, Y., and Barnes, G.N. (2009). Decreased number of interneurons and increased seizures in neuropilin 2 deficient mice: implications for autism and epilepsy. *Epilepsia* 50, 629-645.
- Garrido, J.J., Fernandes, F., Moussif, A., Fache, M.P., Giraud, P., and Dargent, B. (2003). Dynamic compartmentalization of the voltage-gated sodium channels in axons. *Biol Cell* 95, 437-445.

Gasser, A., Cheng, X., Gilmore, E.S., Tyrrell, L., Waxman, S.G., and Dib-Hajj, S.D. (2010). Two Nedd4-binding motifs underlie modulation of sodium channel Nav1.6 by p38 MAPK. *J Biol Chem* 285, 26149-26161.

Gasser, A., Ho, T.S., Cheng, X., Chang, K.J., Waxman, S.G., Rasband, M.N., and Dib-Hajj, S.D. (2012). An ankyrinG-binding motif is necessary and sufficient for targeting Nav1.6 sodium channels to axon initial segments and nodes of Ranvier. *J Neurosci* 32, 7232-7243.

Gehman, L.T., Stoilov, P., Maguire, J., Damianov, A., Lin, C.H., Shiue, L., Ares, M., Jr., Mody, I., and Black, D.L. (2011). The splicing regulator Rbfox1 (A2BP1) controls neuronal excitation in the mammalian brain. *Nat Genet.* 43, 706-711.

Gehman, L.T., Meera, P., Stoilov, P., Shiue, L., O'Brien, J.E., Meisler, M.H., Ares, M., Jr., Otis, T.S., and Black, D.L. (2012). The splicing regulator Rbfox2 is required for both cerebellar development and mature motor function. *Genes Dev* 26, 445-460.

Girard, S.L., Gauthier, J., Noreau, A., Xiong, L., Zhou, S., Jouan, L., Dionne-Laporte, A., Spiegelman, D., Henrion, E., Diallo, O., Thibodeau, P., Bachand, I., Bao, J.Y.J., Tong, A.H.Y., Lin, C.-H., Millet, B., Jaafari, N., Joobar, R., Dion, P.A., Lok, S., Krebs, M.-O., and Rouleau, G.A. (2011). Increased exonic de novo mutation rate in individuals with schizophrenia. *Nat Genet*, 1-5.

Girirajan, S., and Eichler, E.E. (2010). Phenotypic variability and genetic susceptibility to genomic disorders. *Hum Mol Genet* 19, R176-187.

Goldberg, J.L., Espinosa, J.S., Xu, Y., Davidson, N., Kovacs, G.T., and Barres, B.A. (2002). Retinal ganglion cells do not extend axons by default: promotion by neurotrophic signaling and electrical activity. *Neuron* 33, 689-702.

Gorlov, I., Gorlova, O., Frazier, M., Spitz, M., and Amos, C. (2010). Evolutionary evidence of the effect of rare variants on disease etiology. *Clin Genet* 79, 199-206.

Grieco, T.M., Malhotra, J.D., Chen, C., Isom, L.L., and Raman, I.M. (2005). Open-channel block by the cytoplasmic tail of sodium channel beta4 as a mechanism for resurgent sodium current. *Neuron* 45, 233-244.

Hakim, N.H., Kounishi, T., Alam, A.H., Tsukahara, T., and Suzuki, H. (2010). Alternative splicing of Mef2c promoted by Fox-1 during neural differentiation in P19 cells. *Genes Cells*.

Hartshorne, R.P., and Catterall, W.A. (1981). Purification of the saxitoxin receptor of the sodium channel from rat brain. *Proc Natl Acad Sci U S A* 78, 4620-4624.

Hedstrom, K.L., Xu, X., Ogawa, Y., Frischknecht, R., Seidenbecher, C.I., Shrager, P., and Rasband, M.N. (2007). Neurofascin assembles a specialized extracellular matrix at the axon initial segment. *J Cell Biol* 178, 875-886.

- Hernandez-Plata, E., Ortiz, C.S., Marquina-Castillo, B., Medina-Martinez, I., Alfaro, A., Berumen, J., Rivera, M., and Gomora, J.C. (2012). Overexpression of NaV 1.6 channels is associated with the invasion capacity of human cervical cancer. *Int J Cancer* 130, 2013-2023.
- Herzog, R.I., Cummins, T.R., Ghassemi, F., Dib-Hajj, S.D., and Waxman, S.G. (2003a). Distinct repriming and closed-state inactivation kinetics of Nav1.6 and Nav1.7 sodium channels in mouse spinal sensory neurons. *The Journal of physiology* 551, 741-750.
- Herzog, R.I., Liu, C., Waxman, S.G., and Cummins, T.R. (2003b). Calmodulin binds to the C terminus of sodium channels Nav1.4 and Nav1.6 and differentially modulates their functional properties. *J Neurosci* 23, 8261-8270.
- Hill, A.S., Nishino, A., Nakajo, K., Zhang, G., Fineman, J.R., Selzer, M.E., Okamura, Y., and Cooper, E.C. (2008). Ion channel clustering at the axon initial segment and node of Ranvier evolved sequentially in early chordates. *PLoS Genet* 4, e1000317.
- Hille, B. (1992). *Ionic channels of excitable membranes*, 2nd edn (Sunderland, Mass.: Sinauer Associates).
- Hille, B. (2001). *Ionic channels of excitable membranes*, 3rd edn (Sunderland, Mass.: Sinauer).
- Holland, K.D., Kearney, J.A., Glauser, T.A., Buck, G., Keddache, M., Blankston, J.R., Glauser, I.W., Kass, R.S., and Meisler, M.H. (2008). Mutation of sodium channel SCN3A in a patient with cryptogenic pediatric partial epilepsy. *Neurosci Lett* 433, 65-70.
- Howell, V.M., Jones, J.M., Bergren, S.K., Li, L., Billi, A.C., Avenarius, M.R., and Meisler, M.H. (2007). Evidence for a direct role of the disease modifier SCNM1 in splicing. *Hum Mol Genet* 16, 2506-2516.
- Hu, W., Tian, C., Li, T., Yang, M., Hou, H., and Shu, Y. (2009). Distinct contributions of Na(v)1.6 and Na(v)1.2 in action potential initiation and backpropagation. *Nature neuroscience* 12, 996-1002.
- Ingham, R.J., Gish, G., and Pawson, T. (2004). The Nedd4 family of E3 ubiquitin ligases: functional diversity within a common modular architecture. *Oncogene* 23, 1972-1984.
- Isom, L.L., De Jongh, K.S., and Catterall, W.A. (1994). Auxiliary subunits of voltage-gated ion channels. *Neuron* 12, 1183-1194.
- Isom, L.L. (2001). Sodium channel beta subunits: anything but auxiliary. *Neuroscientist* 7, 42-54.

Jensen, C.S., Rasmussen, H.B., and Misonou, H. (2011). Neuronal trafficking of voltage-gated potassium channels. *Mol Cell Neurosci* 48, 288-297.

Jones, J.M., O'Brien, J.E., Dionne, L., Dell'Orco, J., Althaus, A.L., Pal, D., Lopez-Santiago, L.F., Dib-Hajj, S.D., Isom, L.L., Waxman, S.G., Dowling, J.J., Parent, J.M., Shakkottai, V.G., Shrager, P., Murphy, G.G., and Meisler, M.H. (2013). Spontaneous mutation of the anesthetic binding site of sodium channel Nav1.6. in preparation.

Kanai, K., Hirose, S., Oguni, H., Fukuma, G., Shirasaka, Y., Miyajima, T., Wada, K., Iwasa, H., Yasumoto, S., Matsuo, M., Ito, M., Mitsudome, A., and Kaneko, S. (2004). Effect of localization of missense mutations in SCN1A on epilepsy phenotype severity. *Neurology* 63, 329-334.

Kearney, J.A., Plummer, N.W., Smith, M.R., Kapur, J., Cummins, T.R., Waxman, S.G., Goldin, A.L., and Meisler, M.H. (2001). A gain-of-function mutation in the sodium channel gene *Scn2a* results in seizures and behavioral abnormalities. *Neuroscience* 102, 307-317.

Kearney, J.A., Buchner, D.A., De Haan, G., Adamska, M., Levin, S.I., Furay, A.R., Albin, R.L., Jones, J.M., Montal, M., Stevens, M.J., Sprunger, L.K., and Meisler, M.H. (2002). Molecular and pathological effects of a modifier gene on deficiency of the sodium channel *Scn8a* (Na(v)1.6). *Hum Mol Genet* 11, 2765-2775.

Kerr, N.C., Holmes, F.E., and Wynick, D. (2008). Novel mRNA isoforms of the sodium channels Na(v)1.2, Na(v)1.3 and Na(v)1.7 encode predicted two-domain, truncated proteins. *Neuroscience* 155, 797-808.

Khaliq, Z.M., Gouwens, N.W., and Raman, I.M. (2003). The contribution of resurgent sodium current to high-frequency firing in Purkinje neurons: an experimental and modeling study. *J Neurosci* 23, 4899-4912.

Kim, K.K., Adelstein, R.S., and Kawamoto, S. (2009). Identification of neuronal nuclei (NeuN) as Fox-3, a new member of the Fox-1 gene family of splicing factors. *J Biol Chem* 284, 31052-31061.

Kohrman, D.C., Plummer, N.W., Schuster, T., Jones, J.M., Jang, W., Burgess, D.L., Galt, J., Spear, B.T., and Meisler, M.H. (1995). Insertional mutation of the motor endplate disease (med) locus on mouse chromosome 15. *Genomics* 26, 171-177.

Kohrman, D.C., Harris, J.B., and Meisler, M.H. (1996). Mutation detection in the med and medJ alleles of the sodium channel *Scn8a*. Unusual splicing due to a minor class AT-AC intron. *J Biol Chem* 271, 17576-17581.

Kole, M.H., Ilschner, S.U., Kampa, B.M., Williams, S.R., Ruben, P.C., and Stuart, G.J. (2008). Action potential generation requires a high sodium channel density in the axon initial segment. *Nature neuroscience* 11, 178-186.

Kole, M.H., and Stuart, G.J. (2008). Is action potential threshold lowest in the axon? *Nature neuroscience* 11, 1253-1255.

Krzemien, D.M., Schaller, K.L., Levinson, S.R., and Caldwell, J.H. (2000). Immunolocalization of sodium channel isoform NaCh6 in the nervous system. *J Comp Neurol* 420, 70-83.

Kuroyanagi, H. (2009). Fox-1 family of RNA-binding proteins. *Cell Mol Life Sci* 66, 3895-3907.

Laezza, F., Lampert, A., Kozel, M.A., Gerber, B.R., Rush, A.M., Nerbonne, J.M., Waxman, S.G., Dib-Hajj, S.D., and Ornitz, D.M. (2009). FGF14 N-terminal splice variants differentially modulate Nav1.2 and Nav1.6-encoded sodium channels. *Mol Cell Neurosci* 42, 90-101.

Lareau, L.F., Inada, M., Green, R.E., Wengrod, J.C., and Brenner, S.E. (2007). Unproductive splicing of SR genes associated with highly conserved and ultraconserved DNA elements. *Nature* 446, 926-929.

Lemaitte, G., Walker, B., and Lambert, S. (2003). Identification of a conserved ankyrin-binding motif in the family of sodium channel alpha subunits. *J Biol Chem* 278, 27333-27339.

Leterrier, C., Brachet, A., Dargent, B., and Vacher, H. (2011). Determinants of voltage-gated sodium channel clustering in neurons. *Semin Cell Dev Biol* 22, 171-177.

Levin, S.I., and Meisler, M.H. (2004). Floxed allele for conditional inactivation of the voltage-gated sodium channel *Scn8a* (Nav1.6). *Genesis* 39, 234-239.

Levin, S.I., Khaliq, Z.M., Aman, T.K., Grieco, T.M., Kearney, J.A., Raman, I.M., and Meisler, M.H. (2006). Impaired motor function in mice with cell-specific knockout of sodium channel *Scn8a* (Nav1.6) in cerebellar purkinje neurons and granule cells. *Journal of Neurophysiology* 96, 785-793.

Li, Q., Lee, J.A., and Black, D.L. (2007). Neuronal regulation of alternative pre-mRNA splicing. *Nat Rev Neurosci* 8, 819-831.

Liao, Y., Anttonen, A.K., Liukkonen, E., Gaily, E., Maljevic, S., Schubert, S., Bellan-Koch, A., Petrou, S., Ahonen, V.E., Lerche, H., and Lehesjoki, A.E. (2010). SCN2A mutation associated with neonatal epilepsy, late-onset episodic ataxia, myoclonus, and pain. *Neurology* 75, 1454-1458.

Lieberman, A.P., Friedlich, D.L., Harmison, G., Howell, B.W., Jordan, C.L., Breedlove, S.M., and Fischbeck, K.H. (2001). Androgens regulate the mammalian homologues of invertebrate sex determination genes *tra-2* and *fox-1*. *Biochem Biophys Res Commun* 282, 499-506.

Liu, Y., Lopez-Santiago, L.F., Yuan, Y., Jones, J.M., Zhang, H., O'Malley, H.A., Patino, G.A., O'Brien, J.E., Rusconi, R., Gupta, A., Thompson, R.C., Natowicz, M.R., Meisler, M.H., Isom, L.L., and Parent, J.M. (2013). Dravet Syndrome patient-derived neurons suggest a novel epilepsy mechanism. *Annals of Neurology in press*.

Lopez-Santiago, L.F., Meadows, L.S., Ernst, S.J., Chen, C., Malhotra, J.D., McEwen, D.P., Speelman, A., Noebels, J.L., Maier, S.K., Lopatin, A.N., and Isom, L.L. (2007). Sodium channel *Scn1b* null mice exhibit prolonged QT and RR intervals. *J Mol Cell Cardiol* 43, 636-647.

Lorincz, A., and Nusser, Z. (2008). Cell-type-dependent molecular composition of the axon initial segment. *J Neurosci* 28, 14329-14340.

Lorincz, A., and Nusser, Z. (2010). Molecular identity of dendritic voltage-gated sodium channels. *Science* 328, 906-909.

Lu, Y., and Wang, X. (2009). Genes associated with idiopathic epilepsies: a current overview. *Neurol Res* 31, 135-143.

Lundin, L.G. (1993). Evolution of the vertebrate genome as reflected in paralogous chromosomal regions in man and the house mouse. *Genomics* 16, 1-19.

Lynch, M. (2010). Rate, molecular spectrum, and consequences of human mutation. *Proc Nat Acad Sci USA* 107, 961-968.

Mackenzie, F.E., Parker, A., Parkinson, N.J., Oliver, P.L., Brooker, D., Underhill, P., Lukashkina, V.A., Lukashkin, A.N., Holmes, C., and Brown, S.D. (2009). Analysis of the mouse mutant *Cloth-ears* shows a role for the voltage-gated sodium channel *Scn8a* in peripheral neural hearing loss. *Genes Brain Behav* 8, 699-713.

Maier, S.K., Westenbroek, R.E., Yamanushi, T.T., Dobrzynski, H., Boyett, M.R., Catterall, W.A., and Scheuer, T. (2003). An unexpected requirement for brain-type sodium channels for control of heart rate in the mouse sinoatrial node. *Proc Natl Acad Sci U S A* 100, 3507-3512.

Maier, S.K., Westenbroek, R.E., McCormick, K.A., Curtis, R., Scheuer, T., and Catterall, W.A. (2004). Distinct subcellular localization of different sodium channel alpha and beta subunits in single ventricular myocytes from mouse heart. *Circulation* 109, 1421-1427.

Marini, C., Scheffer, I.E., Nabbout, R., Suls, A., De Jonghe, P., Zara, F., and Guerrini, R. (2011). The genetics of Dravet syndrome. *Epilepsia* 52 *Suppl* 2, 24-29.

Martin, C.L., Duvall, J.A., Ilkin, Y., Simon, J.S., Arreaza, M.G., Wilkes, K., Alvarez-Retuerto, A., Whichello, A., Powell, C.M., Rao, K., Cook, E., and Geschwind, D.H. (2007a). Cytogenetic and molecular characterization of *A2BP1/FOX1* as a candidate gene for autism. *Am J Med Genet B Neuropsychiatr Genet* 144B, 869-876.

- Martin, M.S., Tang, B., Papale, L.A., Yu, F.H., Catterall, W.A., and Escayg, A. (2007b). The voltage-gated sodium channel *Scn8a* is a genetic modifier of severe myoclonic epilepsy of infancy. *Hum Mol Genet* *16*, 2892-2899.
- Martin, M.S., Dutt, K., Papale, L.A., Dube, C.M., Dutton, S.B., de Haan, G., Shankar, A., Tufik, S., Meisler, M.H., Baram, T.Z., Goldin, A.L., and Escayg, A. (2010). Altered function of the *SCN1A* voltage-gated sodium channel leads to gamma-aminobutyric acid-ergic (GABAergic) interneuron abnormalities. *J Biol Chem* *285*, 9823-9834.
- Maurice, N., Tkatch, T., Meisler, M., Sprunger, L.K., and Surmeier, D.J. (2001). D1/D5 dopamine receptor activation differentially modulates rapidly inactivating and persistent sodium currents in prefrontal cortex pyramidal neurons. *J Neurosci* *21*, 2268-2277.
- McCarthy, K.D., and de Vellis, J. (1980). Preparation of separate astroglial and oligodendroglial cell cultures from rat cerebral tissue. *J Cell Biol* *85*, 890-902.
- McEwen, D.P., Meadows, L.S., Chen, C., Thyagarajan, V., and Isom, L.L. (2004). Sodium channel beta1 subunit-mediated modulation of Nav1.2 currents and cell surface density is dependent on interactions with contactin and ankyrin. *J Biol Chem* *279*, 16044-16049.
- McKee, A.E., Minet, E., Stern, C., Riahi, S., Stiles, C.D., and Silver, P.A. (2005). A genome-wide in situ hybridization map of RNA-binding proteins reveals anatomically restricted expression in the developing mouse brain. *BMC Dev Biol* *5*, 14.
- McKinney, B.C., Chow, C.Y., Meisler, M.H., and Murphy, G.G. (2008). Exaggerated emotional behavior in mice heterozygous null for the sodium channel *Scn8a* (*Nav1.6*). *Genes Brain Behav* *7*, 629-638.
- Mechaly, I., Scamps, F., Chabbert, C., Sans, A., and Valmier, J. (2005). Molecular diversity of voltage-gated sodium channel alpha subunits expressed in neuronal and non-neuronal excitable cells. *Neuroscience* *130*, 389-396.
- Meisler, M.H., Plummer, N.W., Burgess, D.L., Buchner, D.A., and Sprunger, L.K. (2004). Allelic mutations of the sodium channel *SCN8A* reveal multiple cellular and physiological functions. *Genetica* *122*, 37-45.
- Meisler, M.H., and Kearney, J.A. (2005a). Sodium channel mutations in epilepsy and other neurological disorders. *J Clin Invest* *115*, 2010-2017.
- Meisler, M.H., and Kearney, J.A. (2005b). Sodium channel mutations in epilepsy and other neurological disorders. *J Clin Invest* *115*, 2010-2017.
- Meisler, M.H., O'Brien, J.E., and Sharkey, L.M. (2010). Sodium channel gene family: epilepsy mutations, gene interactions and modifier effects. *The Journal of physiology* *588*, 1841-1848.

Meixner, A., Haverkamp, S., Wassle, H., Fuhrer, S., Thalhammer, J., Kropf, N., Bittner, R.E., Lassmann, H., Wiche, G., and Propst, F. (2000). MAP1B is required for axon guidance and is involved in the development of the central and peripheral nervous system. *J Cell Biol* 151, 1169-1178.

Mercer, J.N., Chan, C.S., Tkatch, T., Held, J., and Surmeier, D.J. (2007). Nav1.6 sodium channels are critical to pacemaking and fast spiking in globus pallidus neurons. *J Neurosci* 27, 13552-13566.

Mitchell, K.J. (2011). The genetics of neurodevelopmental disease. *Curr Opin Neurobiol*. 21, 197-203.

Modafferi, E.F., and Black, D.L. (1997). A complex intronic splicing enhancer from the c-src pre-mRNA activates inclusion of a heterologous exon. *Mol Cell Biol* 17, 6537-6545.

Morrow, E.M. (2010). Genomic copy number variation in disorders of cognitive development. *J Am Acad Child Adolesc Psychiatry* 49, 1091-1104.

Munoz-Sanjuan, I., Smallwood, P.M., and Nathans, J. (2000). Isoform diversity among fibroblast growth factor homologous factors is generated by alternative promoter usage and differential splicing. *J Biol Chem* 275, 2589-2597.

NHLBI Exome Sequencing Project (ESP). Seattle, W. (2011). Exome Variant Server.

Nicholson, P., Yepiskoposyan, H., Metze, S., Zamudio Orozco, R., Kleinschmidt, N., and Muhlemann, O. (2010). Nonsense-mediated mRNA decay in human cells: mechanistic insights, functions beyond quality control and the double-life of NMD factors. *Cell Mol Life Sci* 67, 677-700.

Noda, M., Ikeda, T., Kayano, T., Suzuki, H., Takeshima, H., Kurasaki, M., Takahashi, H., and Numa, S. (1986). Existence of distinct sodium channel messenger RNAs in rat brain. *Nature* 320, 188-192.

Noujaim, S.F., Kaur, K., Milstein, M., Jones, J.M., Furspan, P., Jiang, D., Auerbach, D.S., Herron, T., Meisler, M.H., and Jalife, J. (2012). A null mutation of the neuronal sodium channel Nav1.6 disrupts action potential propagation and excitation-contraction coupling in the mouse heart. *FASEB J* 26, 63-72.

O'Brien, J.E., Drews, V.L., Jones, J.M., Dugas, J.C., Barres, B.A., and Meisler, M.H. (2012a). Rbfox proteins regulate alternative splicing of neuronal sodium channel SCN8A. *Mol Cell Neurosci* 49, 120-126.

O'Brien, J.E., Sharkey, L.M., Vallianatos, C.N., Han, C., Blossom, J.C., Yu, T., Waxman, S.G., Dib-Hajj, S.D., and Meisler, M.H. (2012b). Interaction of voltage-gated sodium channel Nav1.6 (SCN8A) with microtubule-associated protein Map1b. *J Biol Chem* 287, 18459-18466.

O'Roak, B.J., Deriziotis, P., Lee, C., Vives, L., Schwartz, J.J., Girirajan, S., Karakoc, E., Mackenzie, A.P., Ng, S.B., Baker, C., Rieder, M.J., Nickerson, D.A., Bernier, R., Fisher, S.E., Shendure, J., and Eichler, E.E. (2011). Exome sequencing in sporadic autism spectrum disorders identifies severe de novo mutations. *Nature* **43**, 585-589.

Oh, Y., and Waxman, S.G. (1998). Novel splice variants of the voltage-sensitive sodium channel alpha subunit. *Neuroreport* **9**, 1267-1272.

Okuse, K., Malik-Hall, M., Baker, M.D., Poon, W.Y., Kong, H., Chao, M.V., and Wood, J.N. (2002). Annexin II light chain regulates sensory neuron-specific sodium channel expression. *Nature* **417**, 653-656.

Onkal, R., Mattis, J.H., Fraser, S.P., Diss, J.K., Shao, D., Okuse, K., and Djamgoz, M.B. (2008). Alternative splicing of Nav1.5: an electrophysiological comparison of 'neonatal' and 'adult' isoforms and critical involvement of a lysine residue. *J Cell Physiol* **216**, 716-726.

Osorio, N., Cathala, L., Meisler, M.H., Crest, M., Magistretti, J., and Delmas, P. (2010). Persistent Nav1.6 current at axon initial segments tunes spike timing of cerebellar granule cells. *J Physiol* **588**, 651-670.

Papale, L.A., Beyer, B., Jones, J.M., Sharkey, L.M., Tufik, S., Epstein, M., Letts, V.A., Meisler, M.H., Frankel, W.N., and Escayg, A. (2009). Heterozygous mutations of the voltage-gated sodium channel SCN8A are associated with spike-wave discharges and absence epilepsy in mice. *Hum Mol Genet* **18**, 1633-1641.

Papale, L.A., Paul, K.N., Sawyer, N.T., Manns, J.R., Tufik, S., and Escayg, A. (2010). Dysfunction of the Scn8a voltage-gated sodium channel alters sleep architecture, reduces diurnal corticosterone levels, and enhances spatial memory. *J Biol Chem* **285**, 16553-16561.

Patino, G.A., and Isom, L.L. (2010). Electrophysiology and beyond: multiple roles of Na⁺ channel beta subunits in development and disease. *Neurosci Lett* **486**, 53-59.

Pavone, P., Spalice, A., Polizzi, A., Parisi, P., and Ruggieri, M. (2011). Ohtahara syndrome with emphasis on recent genetic discovery. *Brain Dev* *in press*.

Payandeh, J., Scheuer, T., Zheng, N., and Catterall, W.A. (2011). The crystal structure of a voltage-gated sodium channel. *Nature* **475**, 353-358.

Payandeh, J., Gamal El-Din, T.M., Scheuer, T., Zheng, N., and Catterall, W.A. (2012). Crystal structure of a voltage-gated sodium channel in two potentially inactivated states. *Nature* **486**, 135-139.

Pellet-Many, C., Frankel, P., Jia, H., and Zachary, I. (2008). Neuropilins: structure, function and role in disease. *Biochem J* **411**, 211-226.

Plummer, N.W., McBurney, M.W., and Meisler, M.H. (1997). Alternative splicing of the sodium channel SCN8A predicts a truncated two-domain protein in fetal brain and non-neuronal cells. *J Biol Chem* 272, 24008-24015.

Plummer, N.W., Galt, J., Jones, J.M., Burgess, D.L., Sprunger, L.K., Kohrman, D.C., and Meisler, M.H. (1998). Exon organization, coding sequence, physical mapping, and polymorphic intragenic markers for the human neuronal sodium channel gene SCN8A. *Genomics* 54, 287-296.

Plummer, N.W., and Meisler, M.H. (1999). Evolution and diversity of mammalian sodium channel genes. *Genomics* 57, 323-331.

Poduri, A., and Lowenstein, D. (2011). Epilepsy genetics--past, present, and future. *Curr Opin Genet Dev* 21, 325-332.

Poon, W.Y., Malik-Hall, M., Wood, J.N., and Okuse, K. (2004). Identification of binding domains in the sodium channel Na(V)1.8 intracellular N-terminal region and annexin II light chain p11. *FEBS letters* 558, 114-118.

Raman, I.M., and Bean, B.P. (1997). Resurgent sodium current and action potential formation in dissociated cerebellar Purkinje neurons. *J Neurosci* 17, 4517-4526.

Raman, I.M., Sprunger, L.K., Meisler, M.H., and Bean, B.P. (1997). Altered subthreshold sodium currents and disrupted firing patterns in Purkinje neurons of Scn8a mutant mice. *Neuron* 19, 881-891.

Raman, I.M., and Bean, B.P. (2001). Inactivation and recovery of sodium currents in cerebellar Purkinje neurons: evidence for two mechanisms. *Biophys J* 80, 729-737.

Ratnapriya, R., Vijai, J., Kadandale, J.S., Iyer, R.S., Radhakrishnan, K., and Anand, A. (2010). A locus for juvenile myoclonic epilepsy maps to 2q33-q36. *Hum Genet* 128, 123-130.

Rauch, A., Wieczorek, D., Graf, E., Wieland, T., Ende, S., Schwarzmayr, T., Albrecht, B., Bartholdi, D., Beygo, J., Di Donato, N., Dufke, A., Cremer, K., Hempel, M., Horn, D., Hoyer, J., Joset, P., Ropke, A., Moog, U., Riess, A., Thiel, C.T., Tzschach, A., Wiesener, A., Wohlleber, E., Zweier, C., Ekici, A.B., Zink, A.M., Rump, A., Meisinger, C., Grallert, H., Sticht, H., Schenck, A., Engels, H., Rappold, G., Schrock, E., Wieacker, P., Riess, O., Meitinger, T., Reis, A., and Strom, T.M. (2012). Range of genetic mutations associated with severe non-syndromic sporadic intellectual disability: an exome sequencing study. *Lancet* 380, 1674-1682.

Riederer, B.M. (2007). Microtubule-associated protein 1B, a growth-associated and phosphorylated scaffold protein. *Brain Res Bull* 71, 541-558.

Roach, J.C., Glusman, G., Smit, A.F.A., Huff, C.D., Hubley, R., Shannon, P.T., Rowen, L., Pant, K.P., Goodman, N., Bamshad, M., Shendure, J., Drmanac, R.,

Jorde, L.B., Hood, L., and Galas, D.J. (2010). Analysis of Genetic Inheritance in a Family Quartet by Whole-Genome Sequencing. *Science* 328, 636-639.

Robinson, P., Krawitz, P., and Mundlos, M. (2011). Strategies for exome and genome sequence data analysis in disease-gene discovery projects. *Clin Genet* 80, 127-132.

Rosenmund, C., Sigler, A., Augustin, I., Reim, K., Brose, N., and Rhee, J.S. (2002). Differential control of vesicle priming and short-term plasticity by Munc13 isoforms. *Neuron* 33, 411-424.

Rougier, J.S., van Bemmelen, M.X., Bruce, M.C., Jespersen, T., Gavillet, B., Apotheloz, F., Cordonier, S., Staub, O., Rotin, D., and Abriel, H. (2005). Molecular determinants of voltage-gated sodium channel regulation by the Nedd4/Nedd4-like proteins. *Am J Physiol Cell Physiol* 288, C692-701.

Royeck, M., Horstmann, M.T., Remy, S., Reitze, M., Yaari, Y., and Beck, H. (2008). Role of axonal Nav1.6 sodium channels in action potential initiation of CA1 pyramidal neurons. *J Neurophysiol* 100, 2361-2380.

Rush, A.M., Dib-Hajj, S.D., and Waxman, S.G. (2005). Electrophysiological properties of two axonal sodium channels, Nav1.2 and Nav1.6, expressed in mouse spinal sensory neurones. *J Physiol* 564, 803-815.

Rush, A.M., Wittmack, E.K., Tyrrell, L., Black, J.A., Dib-Hajj, S.D., and Waxman, S.G. (2006). Differential modulation of sodium channel Na(v)1.6 by two members of the fibroblast growth factor homologous factor 2 subfamily. *Eur J Neurosci* 23, 2551-2562.

Schaller, K.L., Krzemien, D.M., Yarowsky, P.J., Krueger, B.K., and Caldwell, J.H. (1995). A novel, abundant sodium channel expressed in neurons and glia. *J Neurosci* 15, 3231-3242.

Schaller, K.L., and Caldwell, J.H. (2000). Developmental and regional expression of sodium channel isoform NaCh6 in the rat central nervous system. *J Comp Neurol* 420, 84-97.

Schiavon, E., Sacco, T., Cassulini, R.R., Gurrola, G., Tempia, F., Possani, L.D., and Wanke, E. (2006). Resurgent current and voltage sensor trapping enhanced activation by a beta-scorpion toxin solely in Nav1.6 channel. Significance in mice Purkinje neurons. *J Biol Chem* 281, 20326-20337.

Sebat, J., Lakshmi, B., Malhotra, D., Troge, J., Lese-Martin, C., Walsh, T., Yamrom, B., Yoon, S., Krasnitz, A., Kendall, J., Leotta, A., Pai, D., Zhang, R., Lee, Y.H., Hicks, J., Spence, S.J., Lee, A.T., Puura, K., Lehtimaki, T., Ledbetter, D., Gregersen, P.K., Bregman, J., Sutcliffe, J.S., Jobanputra, V., Chung, W., Warburton, D., King, M.C., Skuse, D., Geschwind, D.H., Gilliam, T.C., Ye, K., and Wigler, M.

(2007). Strong association of de novo copy number mutations with autism. *Science* **316**, 445-449.

Sepp, K.J., Hong, P., Lizarraga, S.B., Liu, J.S., Mejia, L.A., Walsh, C.A., and Perrimon, N. (2008). Identification of neural outgrowth genes using genome-wide RNAi. *PLoS Genetics* **4**, e1000111.

Shakkottai, V.G., Xiao, M., Xu, L., Wong, M., Nerbonne, J.M., Ornitz, D.M., and Yamada, K.A. (2009). FGF14 regulates the intrinsic excitability of cerebellar Purkinje neurons. *Neurobiol Dis* **33**, 81-88.

Sharkey, L.M., Cheng, X., Drews, V., Buchner, D.A., Jones, J.M., Justice, M.J., Waxman, S.G., Dib-Hajj, S.D., and Meisler, M.H. (2009a). The ataxia3 mutation in the N-terminal cytoplasmic domain of sodium channel Na(v)1.6 disrupts intracellular trafficking. *J Neurosci* **29**, 2733-2741.

Sharkey, L.M., Jones, J.M., Hedera, P., and Meisler, M.H. (2009b). Evaluation of SCN8A as a candidate gene for autosomal dominant essential tremor. *Parkinsonism Relat Disord* **15**, 321-323.

Shibata, H., Huynh, D.P., and Pulst, S.M. (2000). A novel protein with RNA-binding motifs interacts with ataxin-2. *Hum Mol Genet* **9**, 1303-1313.

Smith, M.R., Smith, R.D., Plummer, N.W., Meisler, M.H., and Goldin, A.L. (1998). Functional analysis of the mouse Scn8a sodium channel. *J Neurosci* **18**, 6093-6102.

Smith, M.R., and Goldin, A.L. (1999). A mutation that causes ataxia shifts the voltage-dependence of the Scn8a sodium channel. *Neuroreport* **10**, 3027-3031.

Spampanato, J., Escayg, A., Meisler, M.H., and Goldin, A.L. (2001). Functional effects of two voltage-gated sodium channel mutations that cause generalized epilepsy with febrile seizures plus type 2. *J Neurosci* **21**, 7481-7490.

Srinivasan, Y., Elmer, L., Davis, J., Bennett, V., and Angelides, K. (1988). Ankyrin and spectrin associate with voltage-dependent sodium channels in brain. *Nature* **333**, 177-180.

Stuhmer, W., Conti, F., Suzuki, H., Wang, X.D., Noda, M., Yahagi, N., Kubo, H., and Numa, S. (1989). Structural parts involved in activation and inactivation of the sodium channel. *Nature* **339**, 597-603.

Sudol, M., and Hunter, T. (2000). NeW wrinkles for an old domain. *Cell* **103**, 1001-1004.

Sun, H., Hu, X.Q., Emerit, M.B., Schoenebeck, J.C., Kimmel, C.E., Peoples, R.W., Miko, A., and Zhang, L. (2008). Modulation of 5-HT₃ receptor desensitization by the light chain of microtubule-associated protein 1B expressed in HEK 293 cells. *J Physiol* **586**, 751-762.

Sun, W., Wagnon, J.L., Mahaffey, C.L., Briese, M., Ule, J., and Frankel, W.N. (2013). Aberrant sodium channel activity in the complex seizure disorder of *Celf4* mutant mice. *J Physiol* 591, 241-255.

Sung, Y.H., Baek, I.J., Kim, D.H., Jeon, J., Lee, J., Lee, K., Jeong, D., Kim, J.S., and Lee, H.W. (2013). Knockout mice created by TALEN-mediated gene targeting. *Nat Biotechnol* 31, 23-24.

Tamkun, M.M., and Catterall, W.A. (1981). Reconstitution of the voltage-sensitive sodium channel of rat brain from solubilized components. *J Biol Chem* 256, 11457-11463.

Tan, J., Liu, Z., Nomura, Y., Goldin, A.L., and Dong, K. (2002). Alternative splicing of an insect sodium channel gene generates pharmacologically distinct sodium channels. *J Neurosci* 22, 5300-5309.

Tang, Z.Z., Zheng, S., Nikolic, J., and Black, D.L. (2009). Developmental control of *CaV1.2* L-type calcium channel splicing by Fox proteins. *Mol Cell Biol* 29, 4757-4765.

Teramoto, N., Zhu, H.L., Yotsu-Yamashita, M., Inai, T., and Cunnane, T.C. (2012). Resurgent-like currents in mouse vas deferens myocytes are mediated by *Nav1.6* voltage-gated sodium channels. *Pflugers Arch* 464, 493-502.

Tran, T.S., Rubio, M.E., Clem, R.L., Johnson, D., Case, L., Tessier-Lavigne, M., Haganir, R.L., Ginty, D.D., and Kolodkin, A.L. (2009). Secreted semaphorins control spine distribution and morphogenesis in the postnatal CNS. *Nature* 462, 1065-1069.

Trudeau, M.M. (2006). Heterozygosity for a protein truncation mutation of sodium channel *SCN8A* in a patient with cerebellar atrophy, ataxia, and mental retardation. *J Med Genet* 43, 527-530.

Trudeau, M.M., Dalton, J.C., Day, J.W., Ranum, L.P., and Meisler, M.H. (2006). Heterozygosity for a protein truncation mutation of sodium channel *SCN8A* in a patient with cerebellar atrophy, ataxia, and mental retardation. *J Med Genet* 43, 527-530.

Ulbricht, W. (2005). Sodium channel inactivation: molecular determinants and modulation. *Physiol Rev* 85, 1271-1301.

Underwood, J.G., Boutz, P.L., Dougherty, J.D., Stoilov, P., and Black, D.L. (2005). Homologues of the *Caenorhabditis elegans* Fox-1 protein are neuronal splicing regulators in mammals. *Mol Cell Biol* 25, 10005-10016.

van Bemmelen, M.X., Rougier, J.S., Gavillet, B., Apotheloz, F., Daidie, D., Tateyama, M., Rivolta, I., Thomas, M.A., Kass, R.S., Staub, O., and Abriel, H. (2004). Cardiac voltage-gated sodium channel *Nav1.5* is regulated by *Nedd4-2* mediated ubiquitination. *Circ Res* 95, 284-291.

- Van Wart, A., and Matthews, G. (2006). Impaired firing and cell-specific compensation in neurons lacking nav1.6 sodium channels. *J Neurosci* 26, 7172-7180.
- Van Wart, A., Trimmer, J.S., and Matthews, G. (2007). Polarized distribution of ion channels within microdomains of the axon initial segment. *J Comp Neurol* 500, 339-352.
- Vanoye, C.G., Lossin, C., Rhodes, T.H., and George, A.L., Jr. (2006). Single-channel properties of human NaV1.1 and mechanism of channel dysfunction in SCN1A-associated epilepsy. *J Gen Physiol* 127, 1-14.
- Veeramah, K.R., O'Brien, J.E., Meisler, M.H., Cheng, X., Dib-Hajj, S.D., Waxman, S.G., Talwar, D., Girirajan, S., Eichler, E.E., Restifo, L.L., Erickson, R.P., and Hammer, M.F. (2012). De Novo Pathogenic SCN8A Mutation Identified by Whole-Genome Sequencing of a Family Quartet Affected by Infantile Epileptic Encephalopathy and SUDEP. *Am J Hum Genet* 90, 502-510.
- Vissers, L.E.L.M., Ligt, J.d., Gilissen, C., Janssen, I., Steehouwer, M., Vries, P.d., Lier, B.v., Arts, P., Wieskamp, N., Rosario, M.d., Bon, B.W.M.v., Hoischen, A., Vries, B.B.A.d., Brunner, H.G., and Veltman, J.A. (2010). A de novo paradigm for mental retardation. *Nature* 42, 1109-1112.
- Volkers, L., Kahlig, K.M., Verbeek, N.E., Das, J.H., van Kempen, M.J., Stroink, H., Augustijn, P., van Nieuwenhuizen, O., Lindhout, D., George, A.L., Jr., Koeleman, B.P., and Rook, M.B. (2011). Na(v) 1.1 dysfunction in genetic epilepsy with febrile seizures-plus or Dravet syndrome. *Eur J Neurosci* 34, 1268-1275.
- Wang, K., Li, M., and Hakonarson, H. (2010). ANNOVAR: functional annotation of genetic variants from high-throughput sequencing data. *Nucleic Acids Res* 38, e164.
- Wefers, B., Meyer, M., Ortiz, O., Hrabe de Angelis, M., Hansen, J., Wurst, W., and Kuhn, R. (2013). Direct production of mouse disease models by embryo microinjection of TALENs and oligodeoxynucleotides. *Proc Natl Acad Sci U S A* 110, 3782-3787.
- Weiss, L.A., Escayg, A., Kearney, J.A., Trudeau, M., MacDonald, B.T., Mori, M., Reichert, J., Buxbaum, J.D., and Meisler, M.H. (2003). Sodium channels SCN1A, SCN2A and SCN3A in familial autism. *Mol Psychiatry* 8, 186-194.
- Widmark, J., Sundstrom, G., Ocampo Daza, D., and Larhammar, D. (2011). Differential evolution of voltage-gated sodium channels in tetrapods and teleost fishes. *Mol Biol Evol* 28, 859-871.
- Williams, J.A. (1970). Origin of transmembrane potentials in non-excitabile cells. *J Theor Biol* 28, 287-296.

- Wittmack, E.K., Rush, A.M., Craner, M.J., Goldfarb, M., Waxman, S.G., and Dib-Hajj, S.D. (2004). Fibroblast growth factor homologous factor 2B: association with Nav1.6 and selective colocalization at nodes of Ranvier of dorsal root axons. *J Neurosci* *24*, 6765-6775.
- Wittmack, E.K., Rush, A.M., Hudmon, A., Waxman, S.G., and Dib-Hajj, S.D. (2005). Voltage-gated sodium channel Nav1.6 is modulated by p38 mitogen-activated protein kinase. *J Neurosci* *25*, 6621-6630.
- Wood, J.N., Bevan, S.J., Coote, P.R., Dunn, P.M., Harmar, A., Hogan, P., Latchman, D.S., Morrison, C., Rougon, G., Theveniau, M., and et al. (1990). Novel cell lines display properties of nociceptive sensory neurons. *Proc Biol Sci* *241*, 187-194.
- Wu, S., Yue, W., Jia, M., Ruan, Y., Lu, T., Gong, X., Shuang, M., Liu, J., Yang, X., and Zhang, D. (2007). Association of the neuropilin-2 (NRP2) gene polymorphisms with autism in Chinese Han population. *Am J Med Genet Part B Neuropsychiatr Genet* *144B*, 492-495.
- Yarov-Yarovoy, V., DeCaen, P.G., Westenbroek, R.E., Pan, C.Y., Scheuer, T., Baker, D., and Catterall, W.A. (2012). Structural basis for gating charge movement in the voltage sensor of a sodium channel. *Proc Natl Acad Sci U S A* *109*, E93-102.
- Yu, F.H., and Catterall, W.A. (2003). Overview of the voltage-gated sodium channel family. *Genome Biol* *4*, 207.
- Yu, F.H., Mantegazza, M., Westenbroek, R.E., Robbins, C.A., Kalume, F., Burton, K.A., Spain, W.J., McKnight, G.S., Scheuer, T., and Catterall, W.A. (2006). Reduced sodium current in GABAergic interneurons in a mouse model of severe myoclonic epilepsy in infancy. *Nature neuroscience* *9*, 1142-1149.
- Zakon, H.H., Jost, M.C., and Lu, Y. (2011). Expansion of voltage-dependent Na⁺ channel gene family in early tetrapods coincided with the emergence of terrestriality and increased brain complexity. *Mol Biol Evol* *28*, 1415-1424.
- Zakon, H.H. (2012). Adaptive evolution of voltage-gated sodium channels: the first 800 million years. *Proc Natl Acad Sci U S A* *109 Suppl 1*, 10619-10625.
- Zarrinpar, A., and Lim, W.A. (2000). Converging on proline: the mechanism of WW domain peptide recognition. *Nat Struct Biol* *7*, 611-613.
- Zhang, Y., Bekku, Y., Dzhashiashvili, Y., Armenti, S., Meng, X., Sasaki, Y., Milbrandt, J., and Salzer, J.L. (2012). Assembly and maintenance of nodes of ranvier rely on distinct sources of proteins and targeting mechanisms. *Neuron* *73*, 92-107.
- Zhu, H.L., Aishima, M., Morinaga, H., Wassall, R.D., Shibata, A., Iwasa, K., Nomura, M., Nagao, M., Sueishi, K., Cunnane, T.C., and Teramoto, N. (2008). Molecular and

biophysical properties of voltage-gated Na⁺ channels in murine vas deferens. *Biophys J* 94, 3340-3351.

Zhu, H.L., Shibata, A., Inai, T., Nomura, M., Shibata, Y., Brock, J.A., and Teramoto, N. (2010). Characterization of NaV1.6-mediated Na⁺ currents in smooth muscle cells isolated from mouse vas deferens. *J Cell Physiol* 223, 234-243.

Zubovic, L., Baralle, M., and Baralle, F.E. (2012). Mutually exclusive splicing regulates the Nav 1.6 sodium channel function through a combinatorial mechanism that involves three distinct splicing regulatory elements and their ligands. *Nucleic Acids Res* 40, 6255-6269.

Zuzarte, M., Heusser, K., Renigunta, V., Schlichthorl, G., Rinne, S., Wischmeyer, E., Daut, J., Schwappach, B., and Preisig-Muller, R. (2009). Intracellular traffic of the K⁺ channels TASK-1 and TASK-3: role of N- and C-terminal sorting signals and interaction with 14-3-3 proteins. *J Physiol* 587, 929-952.